I.O.S.

AN EXPERIMENTAL COMPARISON OF A SHIPBORNE WAVE RECORDER AND A WAVERIDER BUOY CONDUCTED AT THE CHANNEL LIGHTVESSEL

BY
G.N. CRISP

REPORT NO. 235
1987

INSTITUTE OF OCEANOGRAPHIC SCIENCES
NATURAL ENVIRONMENT RESEARCH COUNCIL

INSTITUTE OF OCEANOGRAPHIC SCIENCES

Wormley, Godalming, Surrey, GU8 5UB.

(042 - 879 - 4141)

(Director: Dr A.S. Laughton FRS)

Bidston Observatory,

Birkenhead, Merseyside, L43 7RA.

(051 - 653 - 8633)

When citing this document in a bibliography the reference should be given as follows:-

CRISP, G.N. 1987 An experimental comparison of a shipborne wave recorder and a waverider buoy conducted at the Channel Lightvessel. *Institute of Oceanographic Sciences, Report,* No. 235, 181pp.

INSTITUTE OF OCEANOGRAPHIC SCIENCES

WORMLEY

An experimental comparison of a shipborne wave recorder and a waverider buoy conducted at the Channel Lightvessel

by

G.N. Crisp*

I.O.S. Report No. 235

March 1987

Present address:

R2175
Royal Signals & Radar Establishment
St Andrews Road
Great Malvern
WORCS. WR14 3PS

Page No.

CONTENTS

ABSTRACT

This report describes the analysis of an experiment conducted with a view to comparing wave measurements made with a Shipborne Wave Recorder to measurements made with a Waverider buoy. The practical details of the experiment are given in Appendices 1, 2 and 3.

The ship used in the experiment was equipped with motion sensors which allowed some checks to me made on the calibration of the SBWR using field data. These are described in section 2 and showed that within reasonable limits, the transducers and electronics were accurately calibrated.

Chapter 3 describes the comparison of the data obtained from the two instruments. It is shown that the relative frequency response of the Shipborne Wave Recorder and Waverider buoy (Figure 3.5) differs markedly from the form which is usually assumed to correct SBWR data. If the usual formula is used to correct the SBWR spectra the significant wave height H_s would be overestimated by about 40%. However, the usual correction formula is normally applied to data which are recorded on paper charts and analysed using the Tucker/Draper analysis method which gives H_s and the zero crossing period T_z. H_s is corrected by the function appropriate to T_z. This analysis procedure is very sensitive to errors in the estimation of the record's zero upcross period (T_z) and it is shown that in practice systematic errors in the estimation of T_z largely compensate the errors arising from the standard correction formula. Thus when the Tucker/Draper analysis method is used, the data measured in this experiment are consistent with those which have been reported previously.

Frequency response measurements made previously involved a number of ships of different sizes, equipped with recorders whose transducers were located at various depths. Section 4 describes an analysis of these data together with those measured in the present experiment. It is shown that both the ship's length and the transducer's mean depth influence the instrument's frequency response characteristics. An empirical scaling law is developed and it is suggested that this could provide a basis for correcting digitally recorded and analysed SBWR data. An attempt to provide a theoretical explanation for the observed frequency responses is then described. Various shortcomings in the existing theory are identified, but none of these on their own can explain the observations. However a simple interference theory shows some qualitative similarity to the observations.

1. INTRODUCTION

The Shipborne Wave Recorder (referred to hereafter as the SBWR), is a rugged instrument which has been used for many years to make routine wave measurements. Some of the most useful wave climate information has been measured using this instrument, and valuable wave data continue to be recorded at stations equipped with it. This is because, provided a suitable ship of opportunity can be found in an area of interest, the SBWR is cheap to operate, and gives high data returns. It is often the case that such ships can be found in those areas where moored buoys are difficult to maintain. Thus, although wave measuring buoys have been commercially available for some time, the SBWR continues to be of considerable practical interest and it is therefore important to understand its capabilities and limitations.

During the period 1973-1977 a series of wave measurements were made on behalf of the United Kingdom Offshore Operators' Association. The measurements were conducted at three locations and at each site simultaneous measurements were made using a SBWR and a Waverider buoy. A total of eight site-years of data was recorded, and a comparison of the results from the two instrument systems was reported by Graham, Verboom and Shaw (1978). Their results, which are summarised in Table 1, indicated that systematic errors existed in one of the instruments. In general the SBWR measurements indicated larger wave heights than did the Waverider, and the difference between the instruments was more pronounced under calm conditions than in severe sea states. The present author has examined some of the data analysed by Graham et al, and was unable to explain their results.

Other workers (Darbyshire (1961), Cartwright (1963) and van Aken and Bouws (1974)) have conducted comparisons between wave measuring buoys and the SBWR and their results are at variance with those of Graham et al. It is therefore tempting to attribute Graham's results to simple calibration errors of some kind. This explanation is not satisfactory as it is most unlikely that all of the data would be affected in the same way, as they were obtained using a number of different buoys and ships.

Thus a new investigation was required so that the magnitude and cause of the reported errors could be established. In this report the results obtained in such an experiment are described. The measurements were conducted aboard a Trinity House lightvessel (No 23), which was moored in the Western English Channel

at a position 49° 54.5' N, 2° 55.5' W. At this position the seabed is reasonably flat so that the wave conditions in the area are expected to be spatially uniform. The water depth in the area is approximately 60 m. The experiment extended over a period of one month during the Autumn of 1980.

The ship was equipped with a Shipborne Wave Recorder which was modified so that outputs from all of the sensors were available, as well as the conventional wave recorder output. In addition a ship motion sensor capable of measuring the ship's pitch, roll and heave was mounted on the light vessel. Waverider buoy wave measurements were made using a standard buoy moored approximately 1 km to the East of the lightvessel. The data were telemetered by radio to the light vessel where they were received and recorded together with the information derived from the ship-mounted instruments. The experimental arrangements are described in greater detail in Appendix 1 and details of the instrument calibrations are given in Appendix 2. Details of the data analysis scheme used to calculate the various spectra described below are given in Appendix 3.

Table 1 Comparison of wave heights measured by SBWR and Waverider buoy, taken from Graham, Verboom and Shaw (1978)

WRB	Percentage Increase H_s SBWR over WRB			
H_s Threshold Wave Height	Station A	Station B	Station C	All Stations
metres	%	%	%	%
1.0	+18.0	+17.0	+10.0	+14.0
1.5	+17.3	+11.3	+4.7	+10.0
2.0	+11.0	+10.5	+7.5	+10.0
2.5	+11.2	+8.0	+6.8	+8.0
3.0	+9.3	+8.3	+9.0	+7.3
3.5	+8.6	+7.1	+8.6	+7.1
4.0	+7.5	+8.0	+7.5	+8.3
4.5	+6.9	+7.1	+11.3	+8.9
5.0	+6.2	+6.0	+10.0	+6.0
5.5	+5.6	+7.3	+9.1	+5.5
6.0	+3.5	+8.3	+8.3	+8.3
6.5	+4.6	+9.2	+4.6	+6.2
7.0	+6.3	+7.1	+1.4	+7.1
7.5	+3.7	+5.3	-1.3	+5.3
8.0	+6.3	+6.3	-3.8	+5.0
8.5	+7.9	+2.9	0.0	+5.9
9.0	+8.9	+7.8	0.0	+5.6
9.5	+7.9	+6.3	*	+5.3
10.0	*	+5.0	*	+3.0
Return Period				
1 year	+3.4	+4.4	+1.7	+5.1
10 years	+3.2	+3.7	+0.8	+4.6
50 years	+3.6	+3.2	+0.2	+4.3
100 years	+2.8	+2.9	-0.1	+4.2

2. ANALYSIS OF THE INTERNAL CONSISTENCY OF THE DATA SET

2.1 Introduction

The instruments mounted upon the light vessel, which are described in Appendix 3, included a ship motion sensor and a shipborne wave recorder. As the signals derived from each of the SBWR's transducers were recorded independently it is possible to compare the ship's heave measured by the SBWR accelerometers, with the same measurement made using the ship motion sensor. Similarly a measure of the ship's roll may be obtained from the SBWR data and this can also be compared with measurements derived from the ship motion sensor. In both cases such a comparison is valuable as a test of the internal consistency of the data set. The results, which are presented below, show that within reasonable limits the calibration procedures used in the experiment were successful.

The spectral analysis procedure which was used in the data analysis is described in detail in Appendix 3. Nevertheless it is helpful to remark here that the spectra used in sections 2 and 3 of this report were calculated as follows. Time series of data values sampled at 2 Hz were assembled into records of 1024 seconds duration. These records were Fourier transformed without the use of a window function. Then the raw Fourier transforms were corrected for the known electronic frequency responses and, after correction, smoothed power spectra were calculated by averaging sets of 10 adjacent harmonics in the corrected periodogram. Thus each smoothed estimate is statistically independent and has 20 degrees of freedom.

2.2 Heave Measurements

The sum of the SBWR double integrated accelerometer signals provides an estimate of the ship's vertical displacement at the centre of the ship's tranverse section which includes the accelerometers. The vertical motion of the ship at a position somewhat forward of that section was obtained from the double integral of the accelerometer signal derived from the ship motion sensor. It is a simple matter, using the measured pitch angle of the ship, to correct these data so that both sets of heave information then refer to the same position on the ship's hull.

It can easily be seen from Figure 2.1(a) that

$$h_b(t)-h_a(t) = \ell\sin(\alpha(t)) \qquad (2.2.1)$$

As the pitch angle α is small, the sine of α in 2.2.1 may be replaced by $\alpha(t)$ so that, after applying a Fourier transformation, we obtain an expression for $H_a(f)$ given by

$$H_a(f) = H_b(f) - \ell A(f) \tag{2.2.2}$$

where $H_a(f)$, $H_b(f)$ and $A(f)$ are the complex Fourier transforms of $h_a(t)$, $h_b(t)$ and $\alpha(t)$. (The computation was performed in this way rather than using 2.2.1 directly for reasons of computer efficiency.)

The corresponding quantity measured using the SBWR accelerometers is given by

$$H(f) = \frac{H_p(f) + H_s(f)}{2} \tag{2.2.3}$$

where H_p and H_s are the complex Fourier transforms of the double integrated port and starboard accelerations, corrected for the equivalent frequency response of the double integrators. Obviously, for an ideal set of measurements, H_a and H would be identical and so any discrepancy between H_a and H must reflect systematic instrumental errors. While H_a and H are coherent and can therefore be compared directly, the data reduction which is achieved by forming a smoothed energy spectrum reduces the number of calculations which need to be performed. We have therefore compared the smoothed energy spectra $|H_a|^2$ and $|H|^2$.

In order to conduct such a comparison, a set of 87 pairs of corresponding corrected smoothed spectra were used. The relative magnitudes of the heave spectral estimates at each frequency were obtained by calculating the average ratio of the spectral estimates at each frequency. At each frequency also, the standard error in the mean ratio of the spectral estimates was calculated.

Figure 2.2 shows the average ratio of the spectral estimates described above, together with the 95% confidence limits. The overall behaviour of the plot shows that the ratio is close to unity over the range 0.07 Hz-0.3 Hz, with a slight dip at 0.2 Hz. This corresponds to the maximum of the pitch response of the ship, and therefore is probably caused by some error in the corrections which were applied in order to refer both sets of measurements to the same point on the ship. A simple error in the sign of the correction term in 2.2.2 would have this effect.

Consequently we carried out a check in which the sign of the correction term was reversed. This introduced clearly identifiable errors into the corrected heave spectrum and we therefore conclude that the corrections which we have applied to the data were of the correct polarity.

At frequencies above 0.3 Hz, the ratios increase with frequency, an effect which is explained in part by the influence of a low pass filter in the ship motion sensor heave channel, which was not allowed for when correcting the complex spectra. However, as may be seen from Figures 2.3 and 2.4, above 0.3 Hz the heave spectral densities are small because the ship does not respond to waves of these frequencies. Thus errors in the heave channel in this frequency range are of little importance.

Below 0.08 Hz the SBWR heave spectral estimates are significantly larger than the corresponding ship motion sensor spectral estimates. Such an effect might be expected because the SBWR accelerometers are mounted on short pendula while the ship motion sensor's accelerometer was gyro stabilised. Tucker (1959) has shown theoretically that the errors which arise as a result of mounting an accelerometer on a short pendulum correspond to low frequency noise in the heave spectrum. The magnitude of the spectrum of this noise may be calculated if the form of the heave spectrum is known. We have calculated the noise spectrum assuming a Pierson Moskowitz spectral shape which may be written in terms of a dimensionless frequency, x, as follows:

$$G(x) = Ax^{-5}\, e^{-5/4x^{-4}} \qquad (2.2.4)$$

where x is the frequency normalised by the frequency at the peak of the spectrum. In Figure 2.5 the function G(x) and the corresponding noise spectrum f(x) are shown. Assuming that the ship motion sensor is noiseless, the ratio of the spectral densities plotted in Figure 2.2 should be given by

$$R(x) = \frac{f(x) + G(x)}{G(x)} \qquad (2.2.5)$$

Figure 2.6 shows the function R(x) plotted on logarithmic scales, together with the measured ratios. The value of x associated with each experimental point was

calculated assuming that the heave spectra correspond to a Pierson Moskowitz spectrum with a peak frequency of 0.098 Hz, and the uncertainty in the x values indicated reflects the uncertainty in identifying the location of the maximum in the average heave spectrum. In view of the crude assumption made that the heave data can be adequately described by a single average spectrum of the assumed form, the agreement is remarkably good. It is not surprising that, at the lowest value of x, the experimental value of R(x) falls below the theoretical curve. This is probably caused by some residual noise in the data derived from the gyro stabilised sensor.

2.3 Roll measurements

As is evident from Figure 2.1(b), for small roll angles the difference in displacement on either side of the ship is proportional to the roll angle θ.

$$H_p - H_s = c\theta \qquad (2.3.1)$$

where c is the separation of the SBWR sensors. Thus the magnitude of the roll sensor signal may be used to check the calibration of the SBWR accelerometers by comparing the spectrum of $(H_p - H_s)$ with the spectrum of θ.

It was found that a proportion of the roll sensor spectra contained high frequency noise which was of such a character that the relevant records were not identified as faulty when subjected to the validation procedures described in Appendix 3. However, the corrupt data could be easily identified because these spectra showed excessively large spectral densities at high frequencies. The data were therefore subjected to an additional test in which the magnitude of the spectral density at the peak of the spectrum was compared with the spectral density averaged between 0.54 and 0.64 Hz. If the dynamic range of a spectrum calculated in this way was less than 10^3, that spectrum was discarded. The average spectrum of the remaining data, shown in Figure 2.7, is very narrow, which is a typical feature of roll spectra. Corresponding spectra were calculated from the SBWR accelerometer data using Equation 2.3.1.

The relative magnitudes of the two sets of spectra were determined at each frequency by performing a reduced major axis analysis on the population of estimate pairs. The slope of the line which passed through the origin, and which minimised the sum of the squares of the perpendicular distance of the data from it, was

calculated. In addition the 95% confidence limits on the calculated slope were determined. The results of the analysis is shown in Figure 2.8. The plot shows that over the range of frequencies for which the roll spectrum has an appreciable magnitude, the two sets of data are in reasonable agreement. A similar analysis using pressure sensor derived roll measurements could not be carried out because of difficulties associated with wave reflection from the hull.

2.4 Consistency of the data

The data analysed above show that the calibration procedures adopted result in consistent measures derived from the SBWR accelerometer data and the ship motion sensor data. This increases the confidence which may be placed in the SBWR data, which in the next section are used in a comparison between the SBWR and the Waverider.

Nomenclature

h_a	vertical displacement
h_b	vertical displacement
c	separation of SBWR heave sensors
ℓ	fore and aft separation of centre of SBWR heave sensors and ship motion sensor
α	angle of pitch
H_a	Fourier transform of h_a
H_b	Fourier transform of h_b
A	Fourier transform of α and constant in PM spectrum
f	frequency
t	time
G(x)	Pierson Moskowitz spectral density
x	non dimensional wave frequency
f(x)	noise spectral density
R(x)	function of G(x) and f(x)
θ	angle of roll

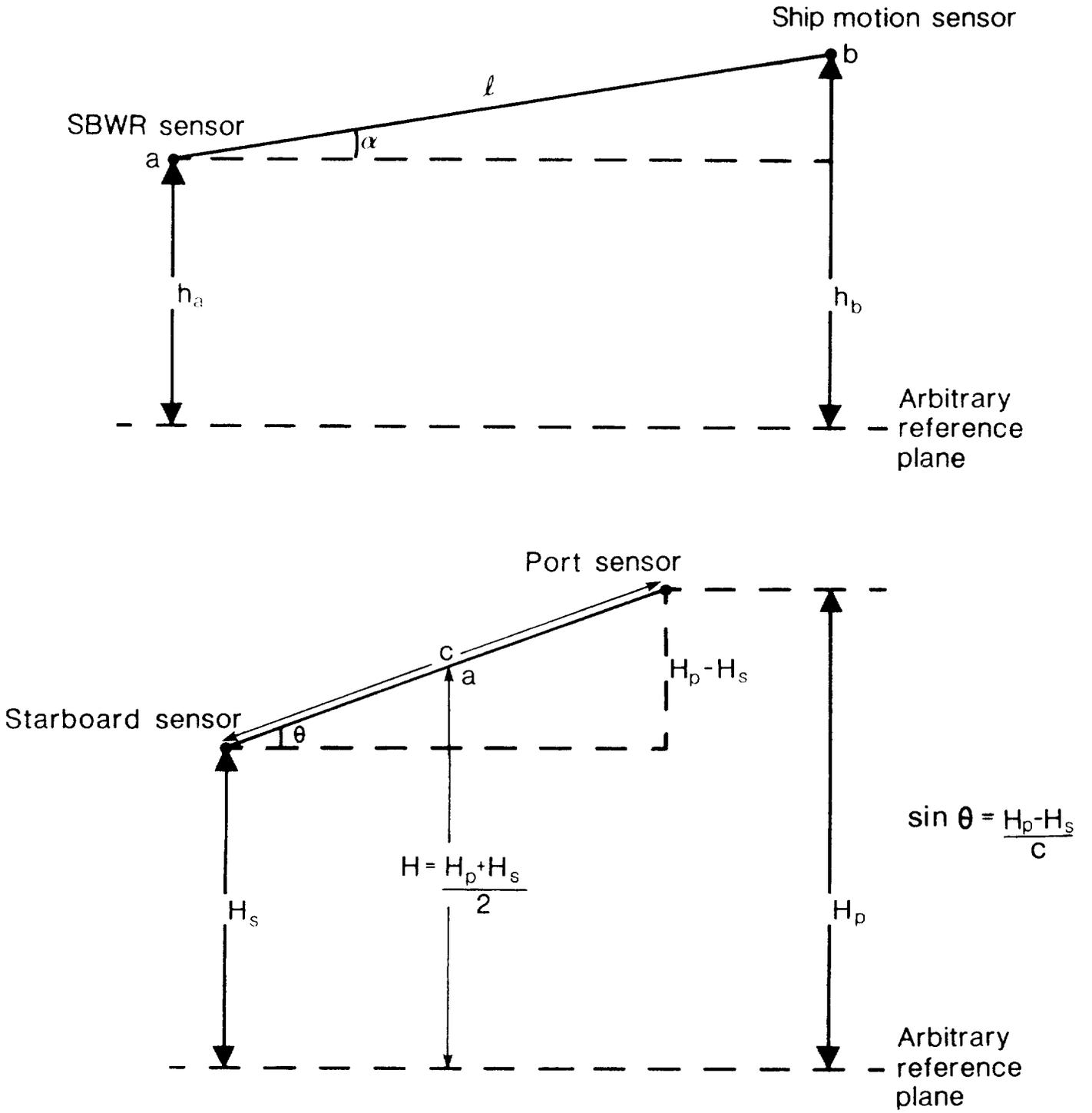

Fig 2.1 Geometry of SBWR and ship motion sensors.

a) Shows a longitudinal section through the ship, the point (a) lies on a line joining the two SBWR accelerometers.

b) Shows a transverse Section at the station at which the SBWR sensors were located.

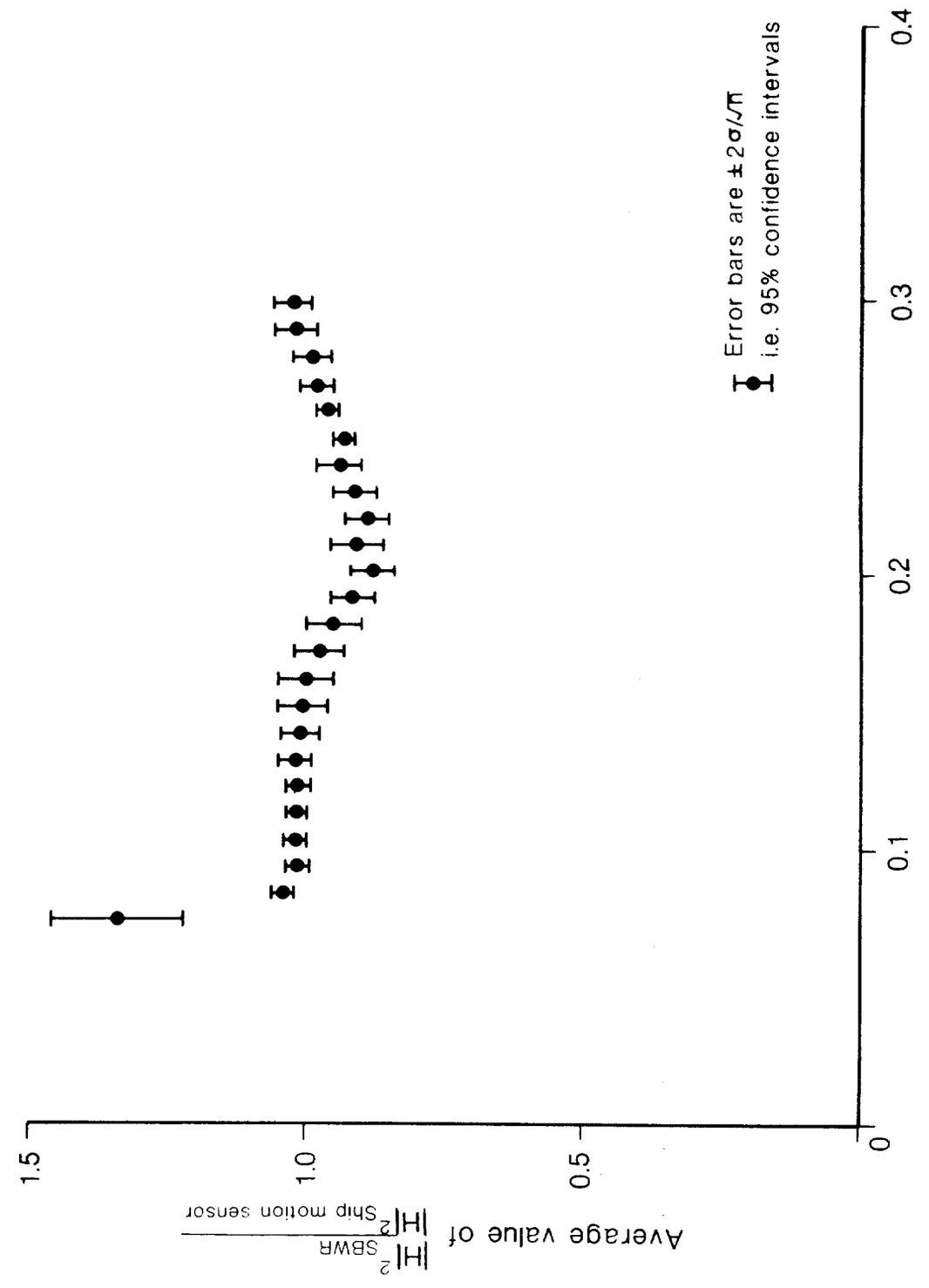

Fig 2.2 Comparison of heave measurements derived from SBWR with heave measurements from ship motion sensor. The anomalously high point at 0.074 Hz is attributable to low frequency noise in the SBWR accelerometer channel. This is caused by the accelerometers' short pendulum mounting.

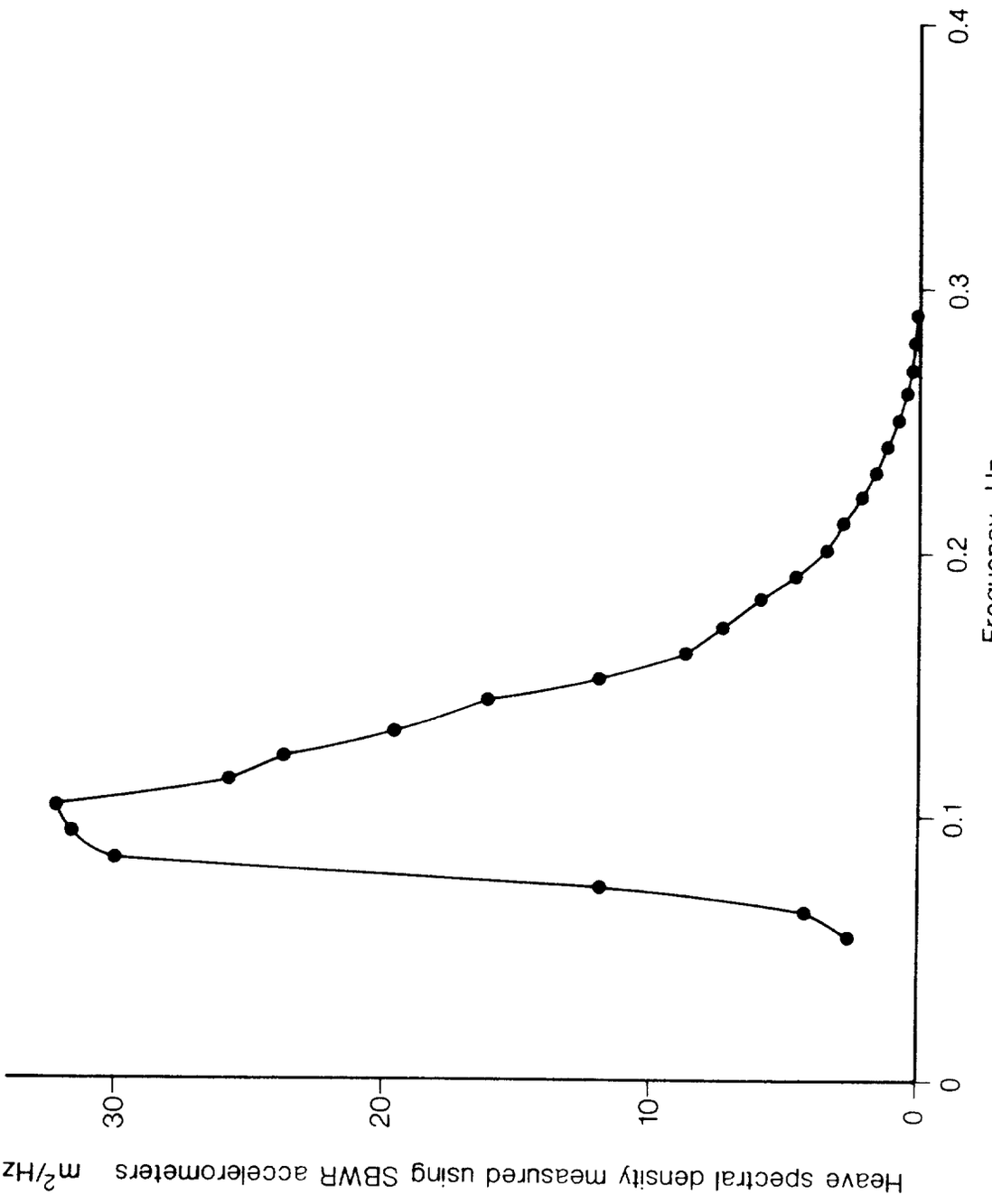

Fig 2.3 Average SBWR Heave spectrum derived using 87 records

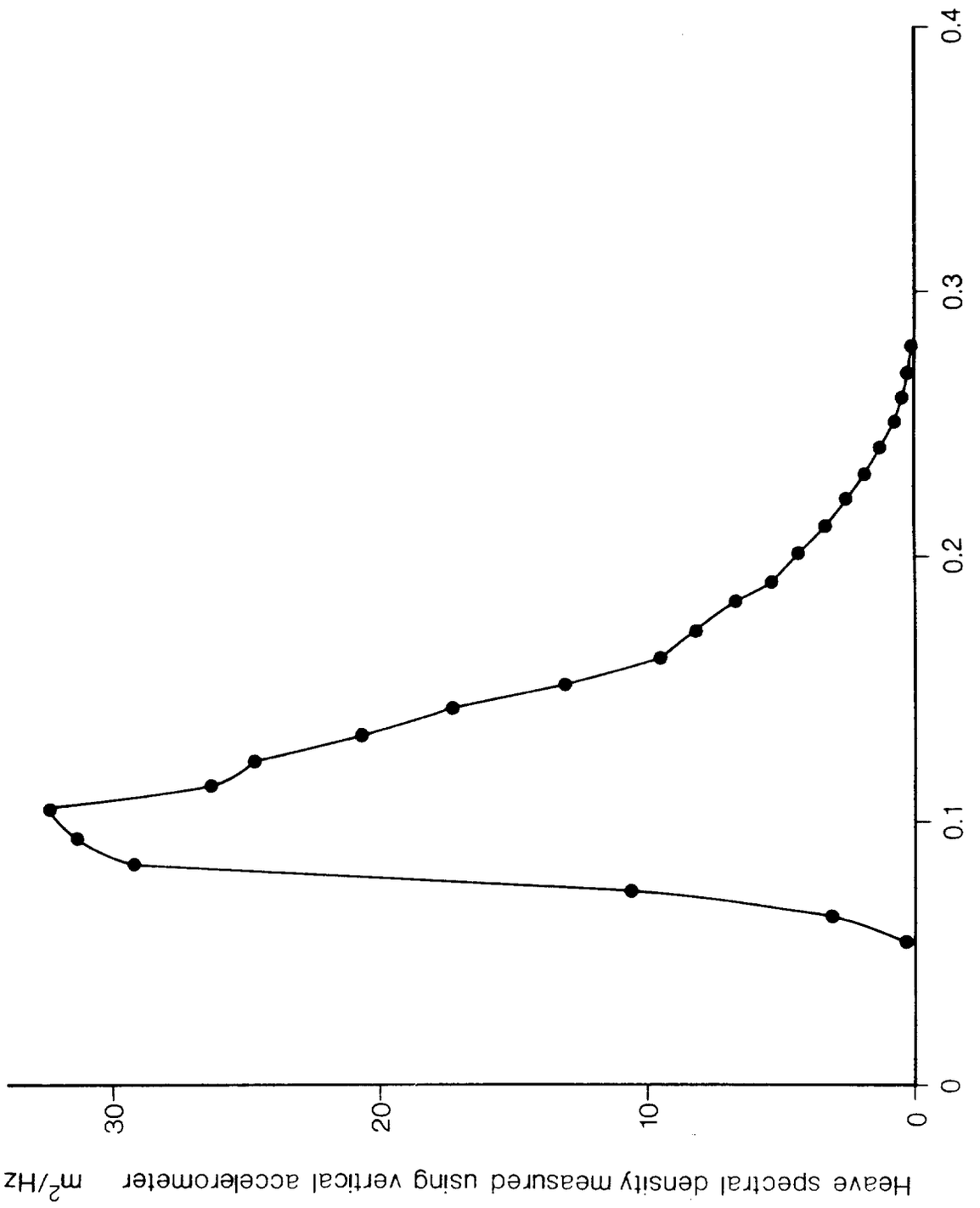

Fig 2.4 Average ship motion sensor Heave spectrum derived using 87 records.

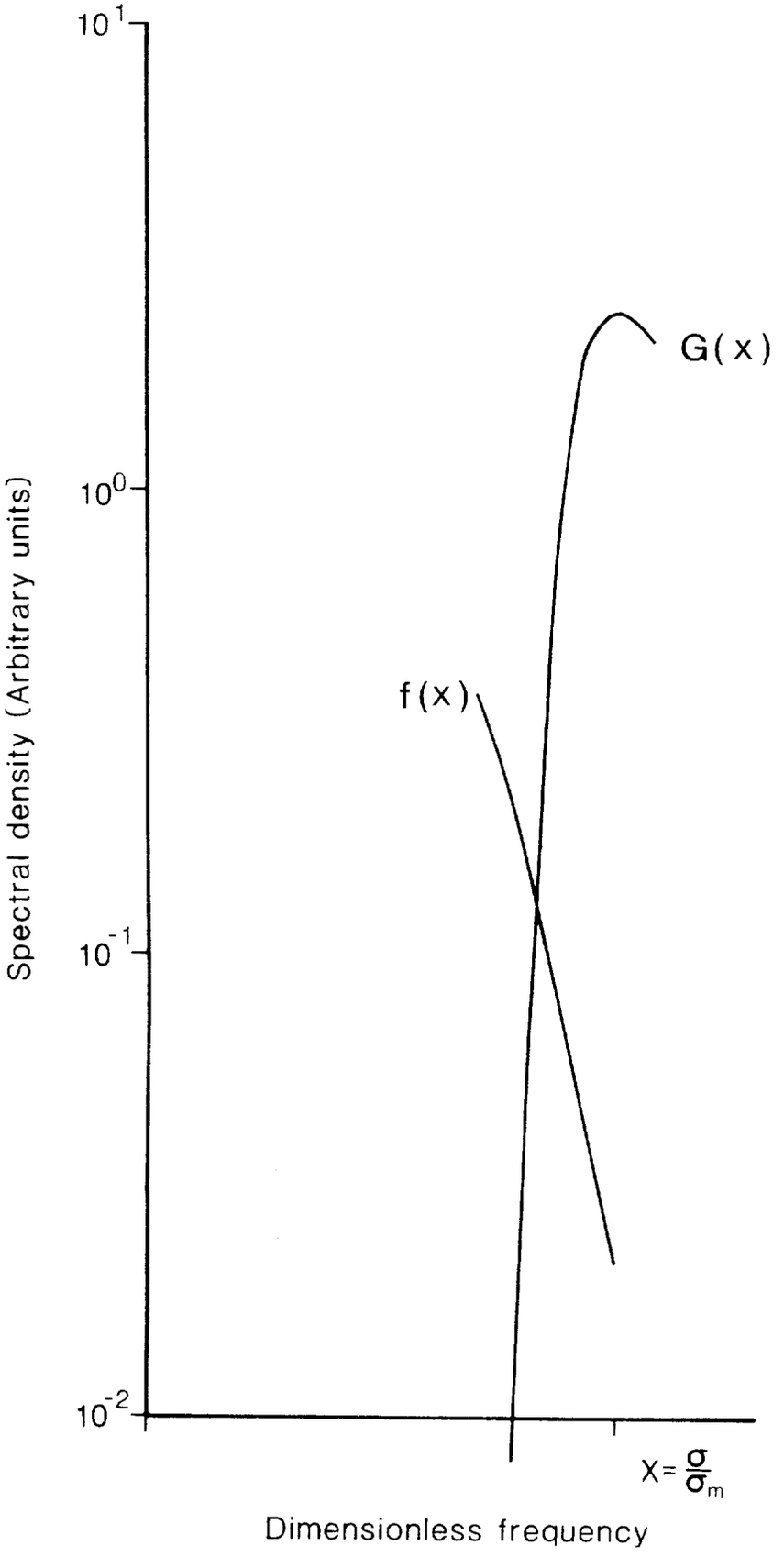

Fig 2.5 ERROR spectrum, f(x), for pendulum mounted accelerometer, compared with Pierson Moskowitz wave spectrum, G(x)

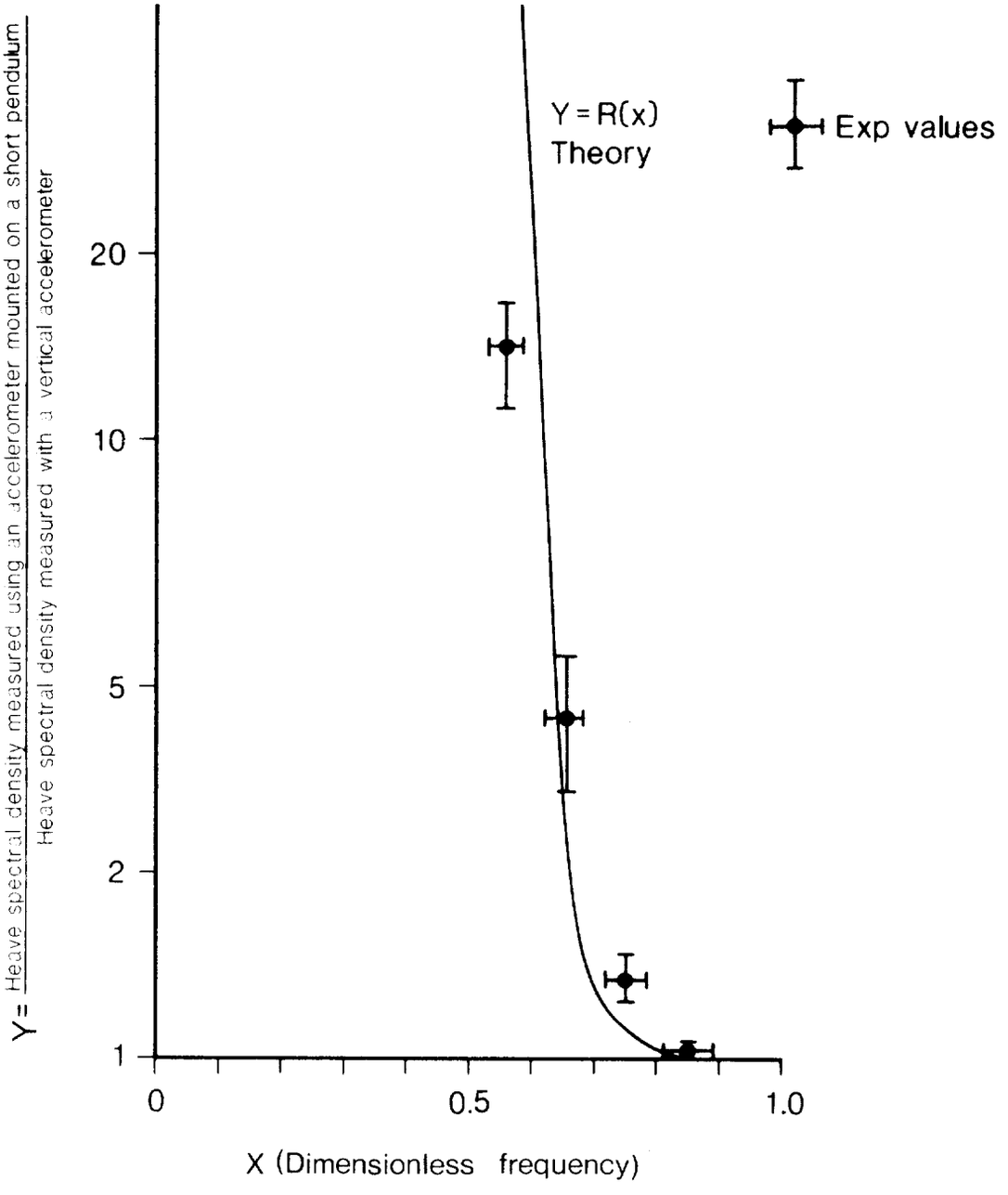

Fig 2.6 Comparison of the ratio of the heave measurements from two sensors with the theory due to Tucker (1959)

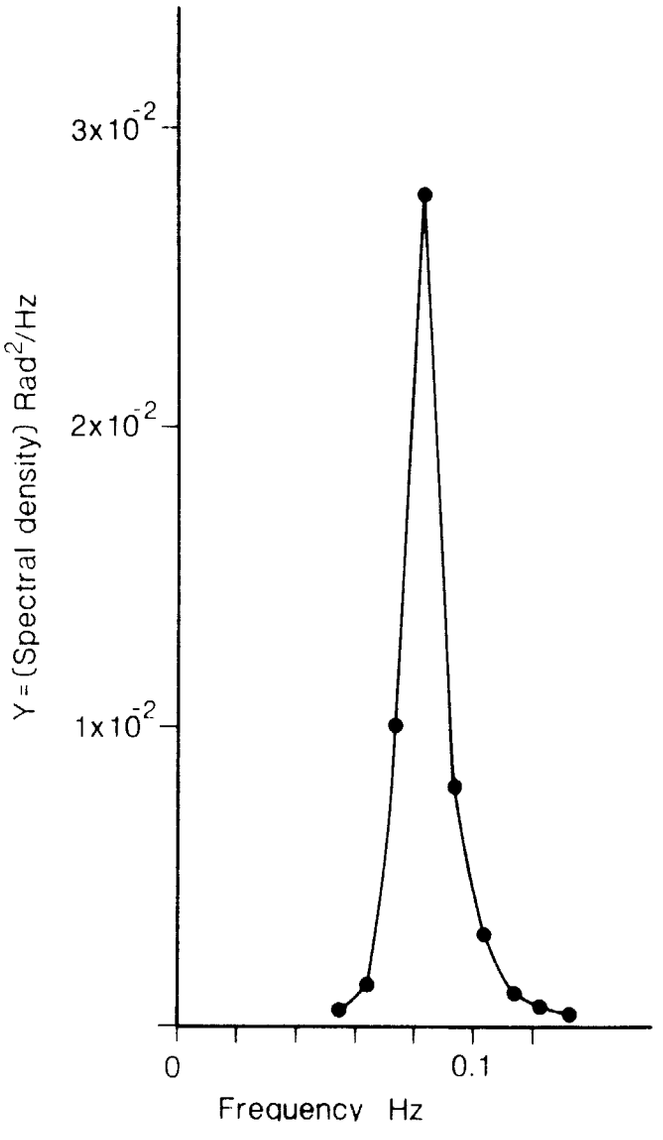

Fig 2.7 Average roll spectrum obtained from 38 records.

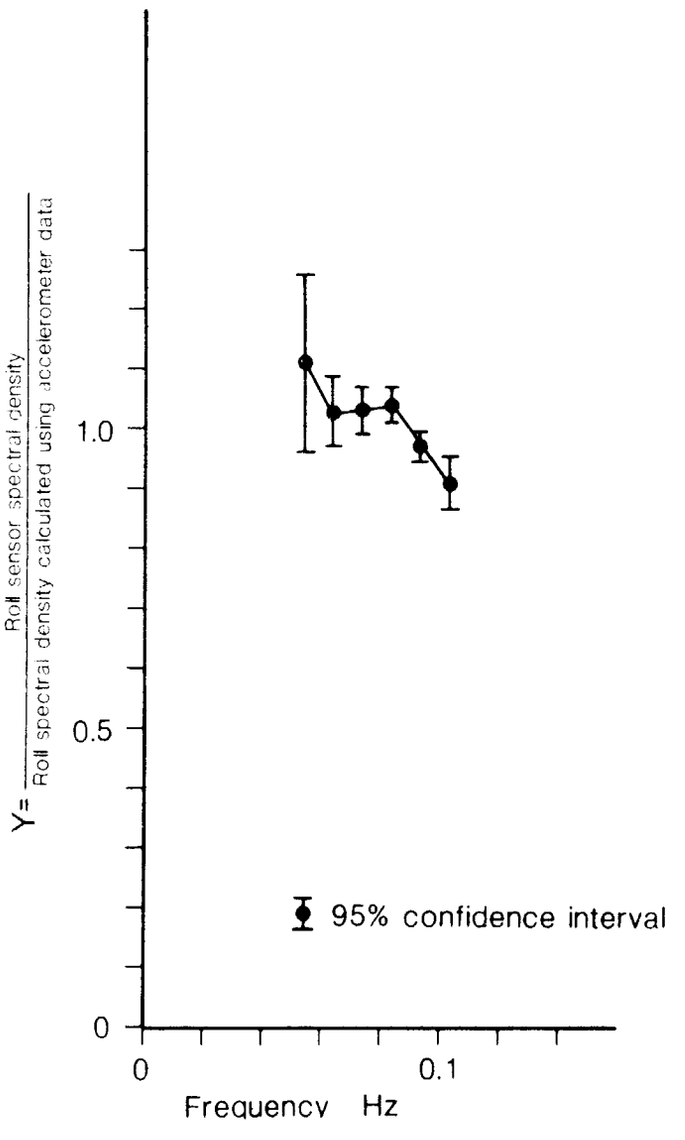

Fig 2.8 Comparison of roll measurements obtained using roll sensor with roll measurements obtained from SBWR.

3. COMPARISON OF SBWR AND WAVERIDER DATA

3.1 Introduction

In this section the Waverider and Shipborne Wave Recorder results are compared. Such comparisons can be carried out in a variety of ways, but those chosen here are intended to address the following questions:

1) How does the empirically determined relative response of the two instruments compare with that conventionally used to analyse shipborne wave recorder data?

2) What procedure should be used to analyse digitally recorded SBWR data?

3) Are the data presented here consistent with the findings of Graham et al?

As we shall show later, the empirically determined relative frequency response of the two instruments is not in good agreement with the conventionally assumed SBWR response function. This indicates that there are shortcomings in the assumptions embodied in the simplified hydrodynamic theory on which the conventional response function is based. A rigorous analysis of the instrument's behaviour would have to incorporate a calculation of the velocity field close to the ship's hull. Such a calculation is difficult and beyond the scope of this report. Consequently we present below the simplified theory, which is essentially that which has been used for many years, so that the assumptions which it contains can be clearly identified and examined later in the light of the comparisons which are presented below.

3.2 The SBWR - a simplified theory

In order to construct as simple a theory as possible for the SBWR it is assumed that the pressure signals and accelerometer signals are corrected for the appropriate electronic responses. Thus each corrected signal corresponds to the output from an ideal pressure or heave (vertical displacement) sensor. If the outputs from corresponding port and starboard sensors are summed and divided by 2, then the differential component in each signal caused by the ship's roll is eliminated. Some compensation is also achieved for the partial reflection of waves incident abeam of the ship. It is also assumed that the pressure distribution in the vicinity of the ship is not influenced by the presence of the ship's hull. In ship motion theory this assumption is known as the Froude-Krylov hypothesis. Thus using the simplified mathematical model, the SBWR may be thought of as a

single pressure sensor and a single displacement sensor mounted upon a thin spar whose displacement response to the waves will be specified later

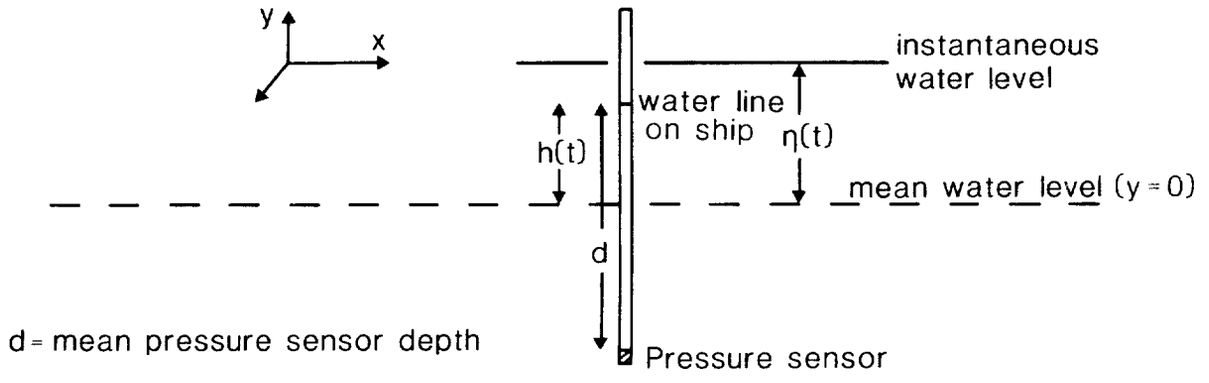

Fig 3.1 Idealised model of SBWR

Provided the surface waves are not too steep, they may be treated using linear theory so that the pressure in the fluid surrounding the pressure sensor may be calculated using Equation A4.24 from Appendix 4.

$$p = \rho g(d-h(t)) + \rho g \sum_n \eta_n e^{k_n(h(t)-\eta(y)-d)} \qquad (3.2.1)$$

Where a_n is a component wave amplitude defined by the relation

$$\eta(t) = \sum_n a_n \cos(\omega_n t + \phi_n) = \sum_n \eta_n e^{-k_n d}$$

and ϕ_n is a random phase.

The pressure may be measured in units of water head in which case the factors of ρg may be dropped in 3.2.1 and, as the instrument is designed to respond only to varying pressures, the static term $\rho g d$ in 3.2.1 may be ignored so that 3.2.1 may be rewritten as

$$p(t) = -h(t) + \sum \eta_n e^{-k_n d} e^{k_n(h(t)-\eta(t))} \qquad (3.2.2)$$

Thus if the displacement signal obtained from the heave sensors is added to p, the first term on the right hand side of 3.2.2 is eliminated and the resulting total signal V(t) is given by

$$V(t) = p(t) + h(t) = \sum_n \eta_n e^{-k_n d} e^{k_n (h(t)-\eta(t))} \qquad (3.2.3)$$

If the argument of the second exponential is small, which is the case when the wave height at the ship measured with respect to a ship mounted reference frame, is small in comparison with the wave length $2\pi/k_n$,

$$S(t) \simeq \sum_n \eta_n e^{-k_n d} \qquad (3.2.4)$$

Thus the output of the instrument treated in this way is equivalent to the output which would be obtained using a fixed pressure sensor located at a depth d below the free surface. Historically SBWR data have been treated using corrections based upon a modified version of Equation 3.2.4, namely

$$S(t) = \sum_n \eta_n e^{-\alpha k_n d} \qquad (3.2.5)$$

Thus the instrument's amplitude response is given by

$$R(k) = \frac{S(k)}{\eta(k)} = e^{-\alpha k d}$$

(Usually the multiplying constant, α, is written as k, we use α here to avoid confusion with the wave numbers k_n.)

The constant α in Equation 3.2.5 was incorporated into the formula on an empirical basis as a result of a rather limited series of comparisons between SBWR spectra and corresponding buoy measured spectra. Various values of α have been reported, varying from 2 to 3.5 (Canham et al (1962), Cartwright (1963), Darbyshire (1961)) and most standard analyses conducted within IOS assume a value of 2.5.
Figure 3.2 shows the function R(k) plotted as a function of frequency for the sensor geometry used in the work reported here. It is usually the case that

routine analyses of SBWR data are carried out using the so-called Tucker-Draper analysis scheme (Tucker (1961), Draper (1966)), so that an average correction based upon a measured value of the record's zero upcross period has to be used. All of the data used by Graham et al (1978) were analysed in this way.

At first sight it might be thought that the pressure signal should be corrected in isolation using the usual response function appropriate for fixed pressure sensors, and that the wave signal would then be obtained by summing the corrected pressure signal with the accelerometer signal. This argument is false as it does not take account of the unattenuated static term in the pressure equation. If such a correction scheme is used, the wave heights derived from the analysis are underestimated. This is because at low frequencies, where the ship's heave response transfer function is close to unity, the hydrostatic term in Equation 3.2.2 is 180° out of phase with the corresponding dynamic pressures.

3.3 Comparison of SBWR and Waverider Spectra

The frequency domain comparisons described below were based upon a primary data set of 84 records from each sensor, each record being of 17 minutes duration. The records were validated and spectrally analysed using the methods described in Appendix 3. Figure 3.3 shows the average Waverider spectrum and the average SBWR spectrum calculated using these data. The spectra were corrected only for the electronic part of the frequency responses and the SBWR spectra were obtained from the sum of the signals derived from the four SBWR sensor channels. The hydrodynamic attenuation of the SBWR signal is evident at high frequencies and it is interesting to see how effective is the conventional hydrodynamic frequency response correction. Figure 3.4 shows the average SBWR spectra obtained when each spectrum is corrected using the classical and modified hydrodynamic formulae. The spectra, corrected with the classical formula, give general agreement with the corresponding Waverider spectra at the lower frequencies, though there are some significant differences, particularly above 0.4 Hz, where it is obvious that the corrections applied to the data are too large. The modified formula is worse in this respect and unreasonable behaviour is observed above 0.25 Hz.

In order to allow a more detailed analysis of the SBWR response, the average transfer function relating the SBWR spectrum to the Waverider spectrum was calculated using the set of SBWR spectra which had been corrected for electronic response only. The transfer function at a given frequency was obtained from the slope of

a plot of the SBWR smoothed spectral densities at that frequency against the corresponding Waverider spectral densities. This was done using a reduced major axis fit, constrained to pass through the origin. Such a transfer function should vary as the square of the corresponding amplitude response, thus using the simple SBWR model described above it should vary as $e^{-2\alpha k(f)d}$ where $k(f)$ is given by the deepwater dispersion relation:

$$k(f) = \frac{(2\pi f)^2}{g} \qquad (3.3.1)$$

Figure 3.5 shows the empirically determined transfer function together with the theoretical response based upon the classical hydrodynamic formula. It is evident that relatively good agreement occurs for frequencies below 0.18 Hz, but that for frequencies in the range 0.2-0.3 Hz the classical formula underestimates the attenuation factor and above 0.33 Hz the SBWR output exceeds the value given by the classical formula. This behaviour explains the minimum at about 0.45 Hz which may be seen in the average spectrum computed using the classically corrected data (Figure 3.4). In view of this, spectral corrections using the modified hydrodynamic formula are expected to give rise to errors. The impact of these upon integral properties of the spectrum is evaluated in section 3.4.

Figure 3.6 shows the energy transfer functions computed using the pressure and accelerometer data in isolation. It can be seen that in the frequency range 0.2-0.3 Hz where the classical correction formula fails, the pressure and accelerometer channels make contributions to the total signal which are of comparable magnitude. This suggests that the failure of the classical formula is related to relative motions between the ship upon which the recorder is mounted, and the surrounding water.

In this region up to about 0.25 Hz, the attenuation of the wave signal increases rapidly with frequency, and it is probable that the high values for α, reported by other workers, were obtained by fitting data in this part of the spectrum.

3.4 Comparison of Integral properties of the spectrum

3.4.1 Calculation Method

The empirical transfer function differs significantly from the formula used to correct SBWR data, and consequently errors are to be expected when SBWR data are

corrected using the usual formula. Most historical SBWR data have been analysed to give Hs and Tz values directly from the time series, using the Tucker/Draper analysis method. In spectral terms, Hs is defined as $4\sqrt{m_o}$ and Tz is theoretically given by $\sqrt{\frac{m_o}{m_2}}$ where m_n are the moments of the spectrum of order n, defined by

$$m_n = \int_0^\infty f^n S(f) df$$

Thus the effect of the different frequency responses upon Hs and Tz obtained from spectral analysis of digital data may be examined by investigating the influence of the frequency response upon the spectral moments. Measures of wave period other than Tz may also be defined in terms of spectral moments, so we examine the effect of the frequency response on the spectral moments of various orders.

The influence of errors in the SBWR transfer function upon the spectral moment of a given order will depend upon the particular form of the wave spectrum considered. Although, as in section 3.5.2, the effect of the empirical transfer function can be evaluated for a set of spectra prescribed in analytical terms, it is computationally simpler to evaluate these effects using the experimental spectra. This assumes that the conditions under which the experiment was conducted were in some way typical. Each of the SBWR spectra used to calculate the transfer function described in section 3.3 was corrected using Equation 3.2.5 with the parameter α set to 0, 1 and 2.5. The first of these values corresponds to no hydrodynamic correction, $\alpha = 1$ corresponds to the classical hydrodynamic formula and $\alpha = 2.5$ is a typical value used for the correction of Tucker/Draper analysed chart records. It is evident from Figure 3.2 that large corrections are applied to the high frequency spectral estimates. It is not surprising that when the spectral moments are evaluated over the usual frequency range (0.04-0.64 Hz), the errors in the correction formula result in wide differences between SBWR and Waverider spectral moments. However the empirical transfer function is reasonably close to the classical formula for frequencies below 0.35 Hz, so that it is possible that reasonably consistent results may be obtained by summing the spectral moments over a restricted range of frequencies; this is of interest as it may suggest a suitable means of analysing digital SBWR data.

Consequently the moments of the SBWR and the Waverider spectra were evaluated over a restricted frequency range from 0.04 Hz to 0.34 Hz. For each value of α the

best linear relationship between the SBWR and Waverider moments was obtained using a least squares fit. The fit was constrained to pass through the origin and gave symmetrical weight to the two sets of moments (reduced major axis fit). Tables 3.1-3.3 summarise the results of these comparisons.

3.4.2 Comparisons with $\alpha = 0$

Table 3.1 shows comparisons obtained without hydrodynamic correction ($\alpha = 0$). The first column gives the results obtained for the SBWR's normal output and the second column gives the results for the sum of the SBWR's individual outputs. The systematic difference between the two sets of results is only 2% which is consistent with the accuracy to which the electronics were calibrated. As expected, the uncorrected SBWR data give an underestimate of the energy in the high frequency wave components, and consequently the SBWR moments are smaller than the corresponding Waverider moments. Naturally the disagreement becomes worse for the higher order moments as these give more weight to high frequency components than do the lower order moments.

3.4.3 Comparisons with $\alpha = 1$

The results obtained by comparing the moments for SBWR spectra which were corrected using the classical formula ($\alpha = 1$) are shown in Table 3.2. The agreement between the Waverider and SBWR moments is remarkably good; the differences in m_o correspond to errors of less than $\frac{1}{2}\%$ in wave height and the errors in m_o and m_2, combined, correspond to errors of about 5% in Tz. In view of the calibration uncertainties these figures must be fortuitiously good; nevertheless they suggest the basis for an analysis scheme for digitally recorded SBWR data. The agreement amongst the moments of order greater than 2 becomes progressively less good, and it is possible that a value of α slightly in excess of unity would give a more accurate correction factor. However in view of the difficulties discussed later in transferring results from one ship to another, it is not considered worthwhile to pursue this point any further.

Unfortunately although the restricted range of summation used above allows consistent results for Waverider and SBWR spectral moments, when they are evaluated in this way, both sets of moments are biased by the restricted frequency range. A comprehensive investigation of the degree of bias should be based upon a data set which includes sea states covering a complete range of wave heights and periods and is beyond the scope of this report. An indication of the bias produced by

the restricted range of integration is presented in Tables 3.4-3.10. The low order moments are, as expected, insensitive to the high frequency limit of integration used to evaluate the moments while the high order moments are seriously biased. The bias in m_0 is approximately 4% corresponding to an underestimate of Hs by 2%, which is probably acceptable. m_2 is reduced by 34%, though the short period sea states used in these comparisons probably represent the most severe biases which will occur. The combined effect of the biases in m_0 and m_2 correspond to a 17% increase in Tz. Thus when the effect of the truncation of the moments is combined with the errors associated with using the classical hydrodynamic correction formula, Tz is increased overall by 22%. This is a significant error, but is no worse than the errors in Tz which arise from the analysis of zero crossings using analogue paper charts.

3.4.4 Comparisons with $\alpha = 2.5$

Table 3.3 shows the SBWR moments, calculated from spectra which were corrected using the modified hydrodynamic formula. It is evident that this procedure overcorrects the SBWR spectra, and that this gives errors in the resulting moments. Even the zero order moment is seriously affected, and the m_0 values obtained for $\alpha = 2.5$ correspond to an overestimate in Hs by 34%. This discrepancy is disturbingly large as Graham et al concluded that, for wave conditions of comparable height, the SBWR overestimated Hs by a much smaller percentage.

However Graham et al obtained their data by Tucker/Draper analysis of analogue chart records, and consequently their results are not directly comparable with those discussed here. In order to investigate the possible influence of the recording and analysis method upon the measured Hs values, a set of analogue chart recordings were made using both the SBWR and the Waverider systems. The analysis of these records is described in the next section.

3.5 Tucker/Draper Analysis of Analogue Charts

3.5.1 Comparison of Analogue Chart Records

In order to establish whether or not the behaviour of the instruments reported here was consistent with the results reported by Graham et al, a number of chart records from each instrument were analysed by the Tucker/Draper method. These were corrected for the instrument's frequency response using the same method as was adopted in previous work, thus a single correction factor was determined for each record on the basis of the modified hydrodynamic formula ($\alpha = 2.5$) evaluated

at a single frequency corresponding to the reciprocal of the record's zero upcross period. The results of this analysis for 37 corresponding SBWR and Waverider chart records is shown in Figure 3.7. The straight line shown is constrained to pass through the origin and represents the maximum likelihood estimator of the functional relationship between the two measures of wave height. The slope of the line is 1.075 ± 0.022 at 95% confidence. This figure is close to the SBWR error reported by Graham et al for sea states with H_S less than 4 m. However, not all of the chart records used in this analysis were recorded during those periods for which the digital data were analysed. For comparison between analogue and corresponding digital records, a subset was used which comprised of only 17 records. When a similar fit was applied using the corresponding analogue SBWR H_S values for this subset against $4\sqrt{m_o}$ for the Waverider, the gradient of the best fit line was 1.04 ± 0.07 at 95% confidence. Thus the subset also shows a small increase in Hs values for the SBWR compared with the Waverider, though the significance of the result is not high. Nevertheless both fits indicate that the Tucker/Draper analysis method is quite insensitive to the transfer function errors which were demonstrated previously in section 3. It is curious that the Tucker/Draper analysis gives good agreement with α set to a value of 2.5, and it is fruitful to attempt to calculate the errors associated with the Tucker/Draper correction method as this may help to identify the reason for good agreement with $\alpha = 2.5$.

3.5.2 Theoretical Behaviour of the Tucker/Draper Correction Procedure

The Tucker/Draper analysis method allows H_S to be estimated directly from an analogue chart record. This is then corrected using the attenuation factor corresponding to the zero upcross period T_z', measured from the chart record: the original concept for this effectively assumed that the waves have a narrow frequency band centred at $1/T_z'$. This procedure may undercorrect high frequency components more than it overcorrects low frequency components. In addition, the zero upcross period measured from the chart, T_z', will be longer than the true sea state T_z because of high frequency attenuation due both to the hydrodynamics of the SBWR's operation, and to the indefinite frequency response of the analogue chart recorder. (This is difficult to quantify because the effect of friction between pen and paper leads to a highly nonlinear response, which tends to damp the high frequency "wiggles" in the chart record.)

In order to calculate the theoretical accuracy of the Tucker/Draper correction

procedure we shall ignore the effect of pen friction and assume that the waves are adequately described by a Pierson-Moskowitz spectrum. This has only one independant variable which can be wind speed, H_S or T_Z. For the present purpose, the relationship between wave height and sea state period, which the Pierson-Moskowitz spectrum embodies is unimportant, so we use a sea state spectrum of the form

$$S(f) = af^{-5}e^{-\frac{1}{\pi}(fT_z)^{-4}} \tag{3.5.1}$$

where a is regarded as a constant given by

$$a = H_S^2/4\pi T_Z^4$$

When measured by a SBWR, the observed spectrum is attenuated at high frequencies, and, as we neglect the pen recorder's response, we assume that the spectrum is attenuated according to the modified hydrodynamic formula 3.2.5. This assumes that the waves are observed in deep water and gives for the SBWR spectrum, S'(f):

$$S'(f) = S(f)e^{-\beta\sqrt{\pi}(fT_Z)^2} \tag{3.5.2}$$

where the parameter β, given by

$$\beta = 2(2\pi)^2\alpha d/gT_Z^2\sqrt{\pi} \tag{3.5.3}$$

describes the response of a particular recorder in relation to the sea state period. For the Channel lightvessel the empirically determined response was fairly close to the classical hydrodynamic formula, so we set α to unity, in which case β is given numerically by

$$\beta = 9.42/T_Z^2 \qquad \text{where } T_Z \text{ is in seconds.}$$

The variance of the SBWR record, m_o', may be calculated from 3.5.1 and 3.5.2 from which

$$m_o' = \int_0^\infty af^{-5}\, e^{-\frac{1}{\pi}(fT_Z)^{-4}}\, e^{-\beta\sqrt{\pi}(fT_Z)^2}\, df \tag{3.5.4}$$

which simplifies, using the substitution $\frac{1}{u} = \sqrt{\pi}(fT_z)^2$ to:

$$m_o' = m_o I_1(\beta) \tag{3.5.5}$$

where

$$I_1(\beta) = \int_0^\infty 2ue^{-u^2} e^{-\beta/u} du \tag{3.5.6}$$

The second moment of the SBWR spectrum, m_2', may be evaluated in a similar way giving

$$m_2' = \frac{m_o \; I_2(\beta)}{\sqrt{\pi}\; T_z^2} \tag{3.5.7}$$

where

$$I_2(\beta) = \int_0^\infty 2e^{-u^2} e^{-\beta/u} du$$

and consequently the theoretical relationship $T_z' = \sqrt{m_o'/m_2'}$ gives the zero upcross period of the SBWR record as

$$T_z'^2 = \sqrt{\pi}\; T_z^2 \; I_1(\beta)/I_2(\beta) \tag{3.5.8}$$

In the Tucker/Draper analysis procedure, m_o' is estimated from the chart record and a single correction is applied, based upon setting $f = 1/T_z'$ in Equation 3.5.2. This renders the corrected value of m_o' given by

$$m_o' \text{ corrected} = m_o' \; e^{\beta\sqrt{\pi}\,\frac{T_z^2}{T_z'^2}} \tag{3.5.9}$$

Using Equations 3.5.8 and 3.5.5 this expression may be rewritten in the following form:

$$\frac{m_o' \text{ corrected}}{m_o} = I_1(\beta) \; e^{\beta I_2(\beta)/I_1(\beta)} \tag{3.5.10}$$

which gives the fractional error in m_o as a result of the correction procedure. As $H_s \propto \sqrt{m_o}$, the fractional error in H_s is given by

$$\frac{H_s'}{H_s} = \sqrt{\frac{m_o' \text{ corrected}}{m_o}} \qquad (3.5.11)$$

The integrals $I_1(\beta)$ and $I_2(\beta)$ were evaluated numerically for a range of values of β which were chosen so that, for the Channel lightvessel geometry and $\alpha = 1$, the range of sea state periods given in Table 3.11 was included.

Evidently the theory predicts that for $\alpha = 1$ the Tucker/Draper analysis method should give rise to errors in wave height of less than 5% for sea states with $T_Z > 4.5$ seconds. It follows that when $\alpha = 2.5$, the Tucker/Draper method should overestimate wave height by $C^{1.5}$, where C is the amplitude correction factor in Table 3.11. For sea states of about 5-6 seconds period, which were used in the comparison of Waverider and SBWR analogue chart data this would give overestimates of SBWR Hs values of about 30%. As we have only observed overestimates which are on average about 8%, it must be concluded that the theory presented here is inadequate.

In order to investigate in detail how the observations differ from the theory, a set of 20 records was selected. For each record the digital data were analysed as described previously, and the corresponding analogue chart records were also analysed using the Tucker/Draper method. Three of the analogue records were of poor stylographic quality and were discarded, leaving the data set summarised in Table 3.12.

A number of features of these data are worth noting.

1) The uncorrected SBWR H_s values obtained from the analogue charts agree well with the H_s values obtained from the uncorrected SBWR digital time series; the mean $\frac{H_s \text{ chart}}{H_s \text{ digital}}$ being 1.02. This shows that the SBWR chart recorder calibration was adequate.

2) The mean ratio $\frac{H_s \text{ Waverider}}{H_s \text{ SBWR}}$ from the analogue charts is 1.18. This agrees well with the relationship based upon a larger body of digital data which was described in the previous section. These gave m_o SBWR = 0.71 m_o Waverider, which corresponds to $\frac{H_s \text{ Waverider}}{H_s \text{ SBWR}} = 1.20$.
Thus we may also have confidence in the accuracy of the Waverider

chart recorder's calibration.

3) The mean ratio $\frac{T_z \text{ SBWR}}{T_z \text{ Waverider}}$ evaluated using spectra truncated at 0.347 Hz was 1.21. The corresponding result from the pervious section, based on the relationships for spectral moments gives a value of 1.17 for this ratio.

4) The mean ratio $\frac{T_z \text{ SBWR}}{T_z \text{ Waverider}}$, evaluated using Waverider spectra truncated at 0.64 Hz and SBWR data truncated at 0.347 Hz is 1.34. This ratio should correspond to T'_z/T_z in the theory presented above, as the full bandwidth Waverider spectrum should give a value of T_z which is close to that of the sea state, while the SBWR T_z value should be only slightly affected by truncating the uncorrected spectrum at 0.347 Hz because this spectrum is attenuated at high frequencies. The value of T'_z/T_z given by the theory is not very good at predicting this ratio. This is not too surprising as the empirical transfer function for the SBWR shows significant departures from the classical attenuation formula for wave frequencies between 0.2 and 0.3 Hz.

5) The mean ratio $\frac{T_z \text{ SBWR}}{T_z \text{ Waverider}}$ evaluated using spectral Waverider data truncated at 0.347 Hz and SBWR analogue chart data, is 1.43.

Thus the analogue charts give longer zero upcross wave periods than corresponding digital data. In view of the fact that the measured frequency response of SBWR chart recorders (shown in Figures 3.8 and 3.9) is rather good, it is probable that the long chart T_z values arise because it is difficult, in hand analysis, to identify the smaller zero upcross waves. There may also be some effect from static friction in the chart recorders, which tends to reduce small "wiggles", but is very non-linear and difficult to analyse.

The discrepancy between the value of α appropriate to the analysis of digital data and the value of α appropriate for the correction of Tucker/Draper analysed data may be resolved using these results. As the analogue charts give values of T'_z/T_z of about 1.44 when the theory predicts a ratio of 1.15, we conclude that the Tucker/Draper T_z values are too high by a factor 1.24. The Tucker/Draper H_s correction factor is of the form $\exp(a\alpha/T'^2_z)$ where a is a constant and α is the factor introduced into the modified hydrodynamic formula. Thus the overestimation of T'_z would be exactly compensated by choosing a value of $(1.24)^2$ for α. In practice a rather larger value for α is used in which case the data will be over-corrected and the SBWR Hs values will be too high. The size of this effect may be calculated from the data in Table 3.11 as follows.

We consider first an idealised SBWR with the Channel lightvessel geometry and which obeyed the frequency response relationships embodied in the previous theory. If this were used to measure a sea state of 6 seconds period, then when the data were corrected using the Tucker/Draper procedure and $\alpha = 1$, a correction factor of 1.19 would be applied to the data. A corresponding normalised corrected amplitude of about 0.975 would be obtained so that Hs would be underestimated by 2.5%. In practice, with a real SBWR, the T_Z value measured from the chart record is greater than the idealised recorder would observe by a factor 1.24. In this case the correction factor applied to the data would be

$$C' = (e^{1.54\sqrt{\pi}\beta\ T_z^2/T_z'^2})^{\frac{1}{2}}$$

rather than

$$C = (e^{\beta\sqrt{\pi}T_z^2/T_z'^2})^{\frac{1}{2}}$$

In both of these formulae β is evaluated with $\alpha = 1$ and T_z' refers to the value which would be observed by the idealised SBWR.

Thus

$$C' = C^{0.8}$$

on substituting $C = 1.19$, C' has a value 1.15. We now recall that the idealised recorder underestimated Hs by 2.5% so that the real instrument overestimates Hs by 12.5%. This result is of the correct order of magnitude, but rather larger than the experimentally observed enhancement of Hs. The difference is likely to arise because the real SBWR transfer function does not follow the classical attenuation formula well between 0.2 and 0.3 Hz. Nevertheless it is reasonable, on the basis of the analysis presented above to attribute the successful use of $\alpha = 2.5$ with the Tucker/Draper method to compensating errors in the estimation of Tz from chart records.

Nomenclature

p	pressure
ρ	density of sea water
g	acceleration due to gravity
d	mean depth of SBWR pressure sensor
$h(t)$	displacement of ship relative to sea surface
η	sea surface elevation above mean level
k	wave number, defined as 2π/wave length
$V(t)$	SBWR output signal
$R(k)$	SBWR transfer function
α	empirical constant
f	wave frequency
Hs	significant wave height
Tz	zero upcross period
$S(f)$	spectral density of sea state
$S'(f)$	spectral density measured by SBWR
β	dimensionless function of SBWR sensor depth and sea state period
$m_{o,2}$	moments of sea state spectrum
$m'_{o,2}$	moments of spectrum measured by SBWR
I_1	$2\int_o^\infty u\, e^{-u^2}\, e^{-\beta/u}\, du$
I_2	$2\int_o^\infty e^{-u^2}\, e^{-\beta/u}\, du$

Table 3.1 Slope of best fit line relating SBWR spectral moments to corresponding Waverider spectral moments - no hydrodynamic correction

Moment	A Normal SBWR Output	B Sum of individual SBWR sensor signals
m_{-2}	0.82 ± 0.04	0.85 ± 0.04
m_{-1}	0.76 ± 0.03	0.78 ± 0.03
m_o	0.69 ± 0.03	0.71 ± 0.03
m_1	0.61 ± 0.02	0.63 ± 0.02
m_2	0.52 ± 0.02	0.53 ± 0.02
m_3	0.42 ± 0.02	0.43 ± 0.02
m_4	0.34 ± 0.02	0.35 ± 0.02

In each case spectral moments were evaluated over the frequency range 0.04-0.347 Hz

Table 3.2 Slope of best fit lines relating SBWR spectral moments to corresponding Waverider moments calculated using spectra which were corrected according to the classical hydrodynamic formula

Moment	Sum of individual sensor signals
m_{-2}	1.04 ± 0.05
m_{-1}	1.02 ± 0.02
m_o	0.99 ± 0.03
m_1	0.94 ± 0.03
m_2	0.89 ± 0.03
m_3	0.85 ± 0.03
m_4	0.82 ± 0.03

In each case spectral moments were evaluated over the frequency range 0.04-0.347 Hz

Table 3.3 Slope lines relating SBWR spectral moments to corresponding Waverider spectral moments calculated using spectra which were corrected according to the modified hydrodynamic formula with $\alpha = 2.5$

Moment order	Sum of individual sensor signals
-2	1.54 ± 0.07
-1	1.70 ± 0.07
0	1.99 ± 0.07
1	2.45 ± 0.08
2	3.15 ± 0.12
3	4.10 ± 0.18
4	5.23 ± 0.24

In each case spectral moments were evaluated over the frequency range 0.04-0.347 Hz

Table 3.4 Comparison of m_{-2} calculated over two frequency ranges using the same Waverider spectra

H_S(m)	T_Z(s)	m_{-2} (m^2Hz^{-2}) calculated from 0.044-0.64 Hz	m_{-2} (m^2Hz^{-2}) calculated from 0.06-0.347 Hz
1.84	5.33	15.1	15.0
1.78	5.29	13.9	13.8
1.71	5.16	12.4	12.4
1.79	6.07	18.4	18.4
1.65	5.73	14.1	14.1
1.46	5.39	10.2	10.1
1.52	5.83	11.4	11.4
1.66	6.08	14.0	14.0
1.57	5.86	11.8	11.8
1.69	5.62	13.4	13.3
1.85	6.20	17.8	17.9
1.84	5.87	15.3	15.2

Mean ratio 1.002

Standard deviation 0.005

Table 3.5 Comparison of m_{-1} calculated over two frequency ranges using the same Waverider spectra

H_s (m)	T_z (s)	m_{-1} ($m^2 Hz^{-1}$) calculated from 0.044-0.64 Hz	m_{-1} ($m^2 Hz^{-1}$) calculated from 0.06-0.347 Hz
1.84	5.33	1.64	1.62
1.78	5.29	1.52	1.50
1.71	5.16	1.38	1.36
1.79	6.07	1.80	1.78
1.65	5.73	1.44	1.43
1.46	5.39	1.07	1.05
1.52	5.83	1.20	1.19
1.66	6.08	1.46	1.45
1.57	5.86	1.26	1.25
1.69	5.62	1.44	1.42
1.85	6.20	1.84	1.83
1.84	5.87	1.70	1.68

Mean ratio 1.01 Standard deviation 0.004

Table 3.6 Comparison of m_o calculated over two frequency ranges using the same Waverider spectra

H_s (m)	T_z (s)	m_o (m^2) calculated from 0.044-0.64 Hz	m_o (m^2) calculated from 0.06-0.347 Hz
1.84	5.33	0.212	0.202
1.78	5.29	0.197	0.187
1.71	5.16	0.183	0.183
1.79	6.07	0.201	0.194
1.65	5.73	0.171	0.164
1.46	5.39	0.134	0.127
1.52	5.83	0.145	0.140
1.66	6.08	0.172	0.167
1.57	5.86	0.154	0.149
1.69	5.62	0.178	0.170
1.85	6.20	0.215	0.207
1.84	5.87	0.212	0.204

Mean ratio 1.043 Standard deviation 0.009

Table 3.7 Comparison of m_1 calculated over two frequency ranges using the same Waverider spectra

H_S(m)	T_Z(s)	$m_1 \times 10^2$ (m^2/Hz) calculated from 0.044-0.64 Hz	$m_1 \times 10^2$ (m^2/Hz) calculated from 0.06-0.347 Hz
1.84	5.33	3.46	3.02
1.78	5.29	3.25	2.81
1.71	5.16	3.09	2.68
1.79	6.07	2.83	2.52
1.65	5.73	2.57	2.28
1.46	5.39	2.15	1.88
1.52	5.83	2.17	1.97
1.66	6.08	2.48	2.27
1.57	5.86	2.30	2.08
1.69	5.62	2.74	2.37
1.85	6.20	3.08	2.72
1.84	5.87	3.18	2.83

Mean ratio 1.13 Standard deviation 0.022

Table 3.8 Comparison of m_2 calculated over two frequency ranges using the same Waverider spectra

H_S(m)	T_Z(s)	$m_2 \times 10^3$ (m^2/Hz^2) calculated from 0.044-0.64 Hz	$m_2 \times 10^3$ (m^2/Hz^2) calculated from 0.06-0.347 Hz
1.84	5.33	7.45	5.46
1.78	5.29	7.05	5.09
1.71	5.16	6.86	5.02
1.79	6.07	5.46	4.07
1.65	5.73	5.20	3.92
1.46	5.39	4.61	3.39
1.52	5.83	4.27	3.35
1.66	6.08	4.68	3.71
1.57	5.86	4.49	3.52
1.69	5.62	5.64	4.01
1.85	6.20	5.93	4.34
1.84	5.87	6.18	4.57

Mean ratio 1.34 Standard deviation 0.046

Table 3.9 Comparison of m_3 calculated over two frequency ranges using the same Waverider spectra

H_s (m)	T_z (s)	$m_3 \times 10^3$ (m^2/Hz^3) calculated from 0.044-0.64 Hz	$m_3 \times 10^3$ (m^2/Hz^3) calculated from 0.06-0.347 Hz
1.84	5.33	2.09	1.14
1.78	5.29	1.98	1.07
1.71	5.16	1.94	1.09
1.79	6.07	1.44	0.81
1.65	5.73	1.41	0.81
1.46	5.39	1.28	0.73
1.52	5.83	1.10	0.68
1.66	6.08	1.15	0.72
1.57	5.86	1.14	0.70
1.69	5.62	1.56	0.81
1.85	6.20	1.56	0.84
1.84	5.87	1.62	0.87

Mean ratio 1.77 Standard deviation 0.106

Table 3.10 Comparison of m_4 calculated over two frequency ranges using the same Waverider spectra

H_s (m)	T_z (s)	$m_4 \times 10^4$ (m^2/Hz^4) calculated from 0.044-0.64 Hz	$m_4 \times 10^4$ (m^2/Hz^4) calculated from 0.06-0.347 Hz
1.84	5.33	7.30	2.69
1.78	5.29	6.89	2.52
1.71	5.16	6.75	2.62
1.79	6.07	4.90	1.86
1.65	5.73	4.80	1.91
1.46	5.39	4.39	1.73
1.52	5.83	3.64	1.56
1.66	6.08	3.67	1.59
1.57	5.86	3.68	1.59
1.69	5.62	5.49	1.86
1.85	6.20	5.27	1.88
1.84	5.87	5.53	1.89

Mean ratio 2.61 Standard deviation 0.22

Table 3.11

Accuracy of the Tucker/Draper correction procedure

T_z	Beta	Normalised Period (T'_z/T_z)	Correction Factor	Normalised Amplitude (H'_s/H_s)
2.00	2.35	1.459	2.666	0.77706
2.50	1.51	1.380	2.017	0.85298
3.00	1.05	1.323	1.700	0.89853
3.50	0.77	1.279	1.517	0.92732
4.00	0.59	1.245	1.400	0.94634
4.50	0.47	1.218	1.321	0.95938
5.00	0.38	1.195	1.263	0.96859
5.50	0.31	1.176	1.221	0.97527
6.00	0.26	1.160	1.188	0.98023
6.50	0.22	1.147	1.162	0.98397
7.00	0.19	1.135	1.141	0.98685
7.50	0.17	1.124	1.125	0.98910
8.00	0.15	1.115	1.111	0.99087
8.50	0.13	1.107	1.099	0.99230
9.00	0.12	1.100	1.089	0.99345
9.50	0.10	1.094	1.080	0.99438
10.00	0.09	1.088	1.073	0.99515
10.50	0.09	1.083	1.067	0.99580
11.00	0.08	1.078	1.061	0.99634
11.50	0.07	1.074	1.056	0.99679
12.00	0.07	1.070	1.052	0.99717

Table 3.12

Record No.	Hs WRB from spectrum f max = 0.64 Hz	Tz WRB from spectrum f max = 0.64 Hz	Hs WRB from analogue chart	Tz WRB from analogue chart	Hs WRB from spectrum f max = 0.35 Hz	Tz WRB from spectrum f max = 0.35 Hz	Hs SBWR from spectrum. No hydrodynamic correction f max = 0.35 Hz	Tz SBWR from spectrum. No hydrodynamic correction f max = 0.35 Hz	Hs SBWR from chart. No correction	Tz SBWR from chart	Hs SBWR from chart. Corrected using $\alpha = 2.5$
1	2.05	6.4	1.82	8.50	2.03	7.17	1.61	8.25	1.48	8.2	2.04
2	1.77	5.9	1.80	8.16	1.73	6.99	1.56	8.99	1.50	9.1	1.92
3	1.87	6.0	1.90	8.16	1.83	7.00	1.72	9.44	1.61	9.7	2.01
4	1.88	5.9	1.71	7.22	1.85	6.82	1.50	9.16	1.48	10.0	1.82
5	2.02	6.7	1.77	8.67	2.00	7.34	1.70	9.23	1.91	9.8	2.37
6	1.80	6.3	1.87	7.43	1.78	6.89	1.53	8.98	1.67	9.5	2.10
7	1.88	6.6	1.78	7.67	1.87	7.13	1.56	8.80	1.29	10.0	1.59
8	2.09	5.5	1.78	7.23	2.04	6.44	1.86	8.32	1.76	8.9	2.28
9	2.07	5.4	1.92	7.34	2.02	6.18	1.67	8.22	1.60	9.2	2.04
10	2.25	5.8	2.29	7.29	2.21	6.39	1.56	7.72	1.64	8.8	2.14
11	2.15	5.9	1.92	6.89	2.12	6.52	1.76	7.72	1.93	8.5	2.59
12	2.05	5.7	1.83	6.72	2.02	6.19	1.56	7.72	1.81	8.2	2.37
13	2.96	6.0	3.42	6.45	2.94	6.33	2.42	7.14	2.46	7.7	3.50
14	3.02	5.9	3.75	6.49	2.99	6.26	2.65	7.27	2.59	7.6	3.72
15	3.23	6.0	3.74	6.71	3.20	6.36	2.44	6.82	1.99	7.6	2.85
16	2.99	5.6	3.64	6.54	2.96	6.07	2.55	7.11	2.47	7.4	3.61
17	3.16	6.0	3.31	6.62	3.13	6.41	2.81	7.24	2.47	7.6	3.55
18	3.06	6.1	-	-	3.02	6.55	2.56	7.86	2.52	7.2	3.75
19	2.75	6.1	-	-	2.72	6.49	2.86	7.35	2.79	7.9	3.90
20	2.88	6.1	-	-	2.86	6.50	2.38	7.16	2.80	8.1	3.84

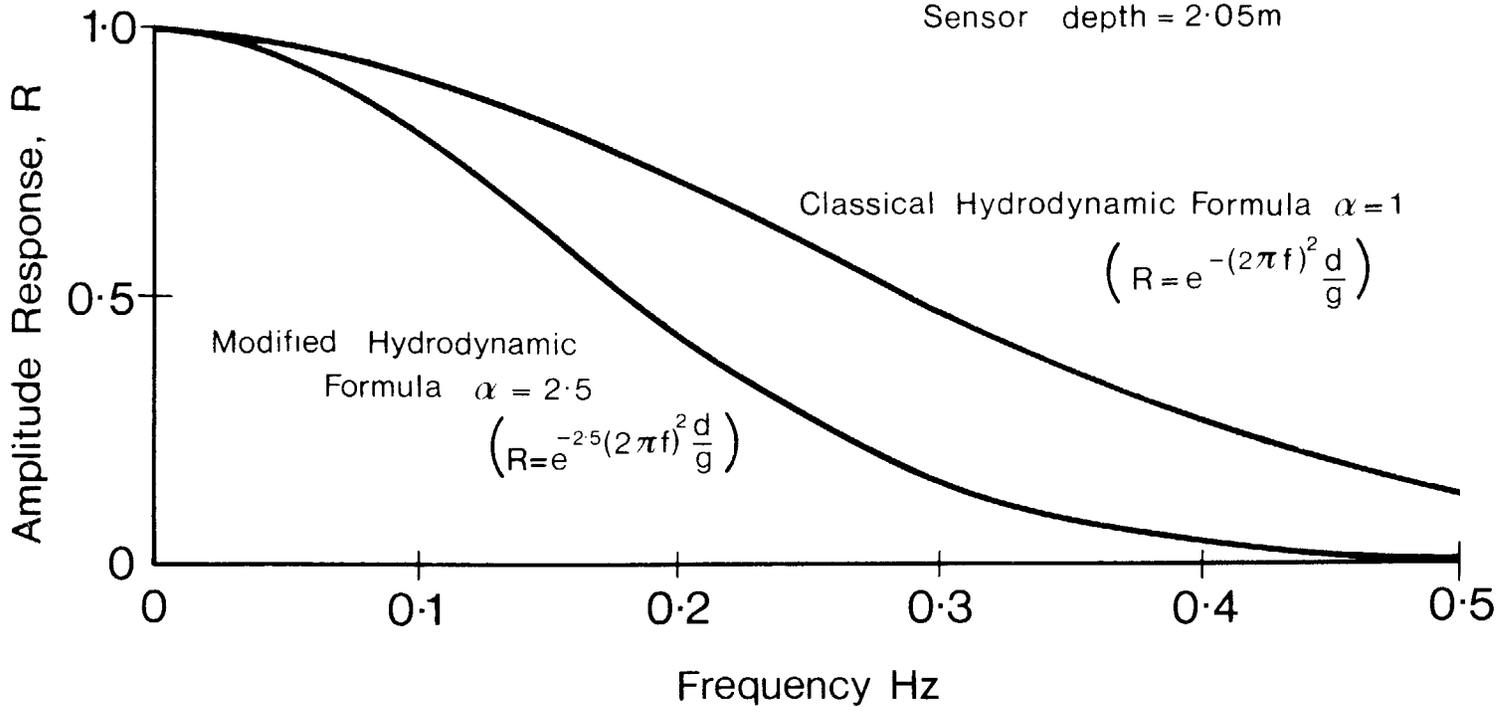

Fig 3.2 The hydrodynamic response functions used to correct the Channel Lightvessel data.

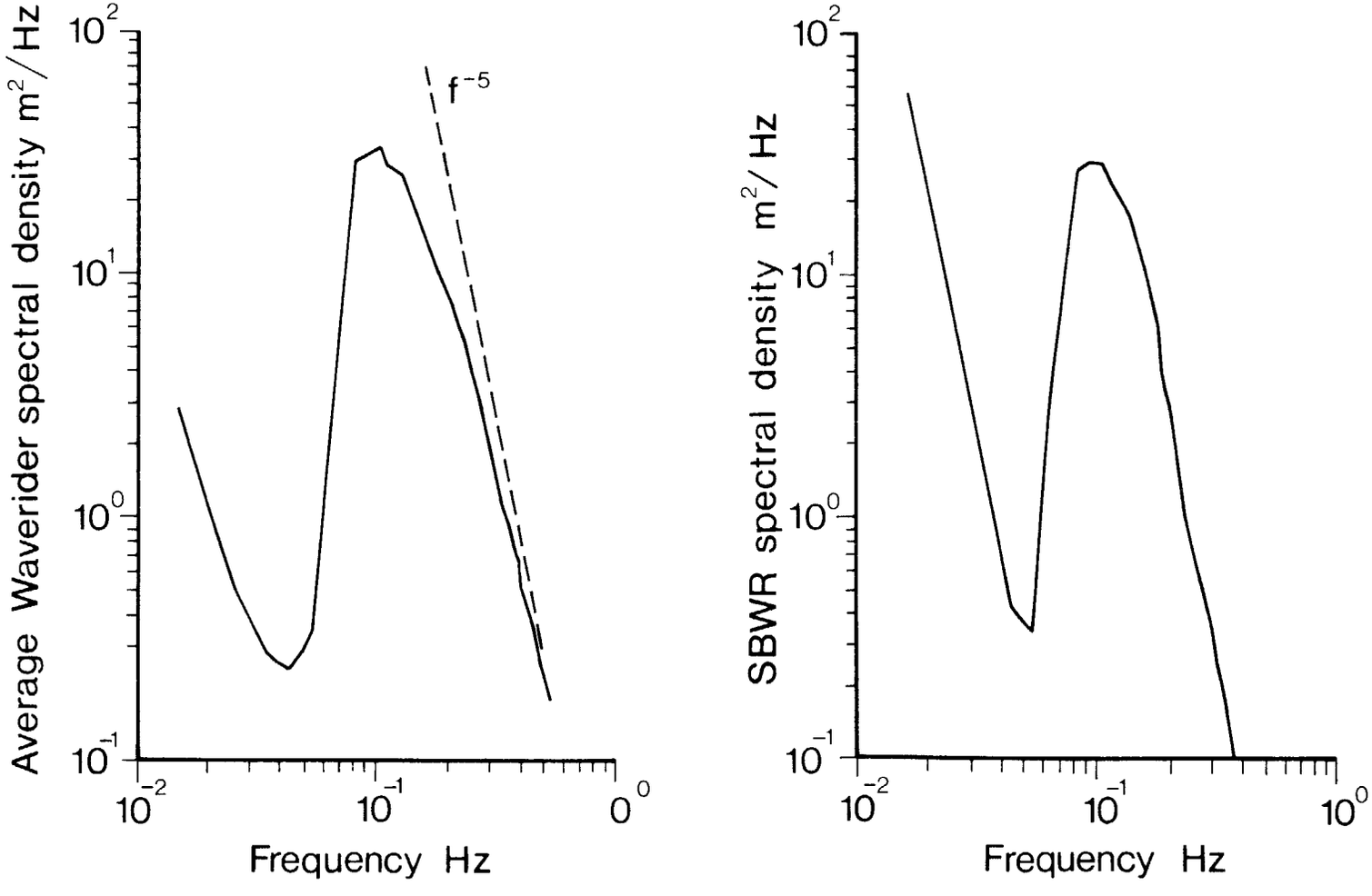

Waverider

SBWR - No hydrodynamic correction

Fig 3.3 Average of 87 spectra which comprised the selected data set

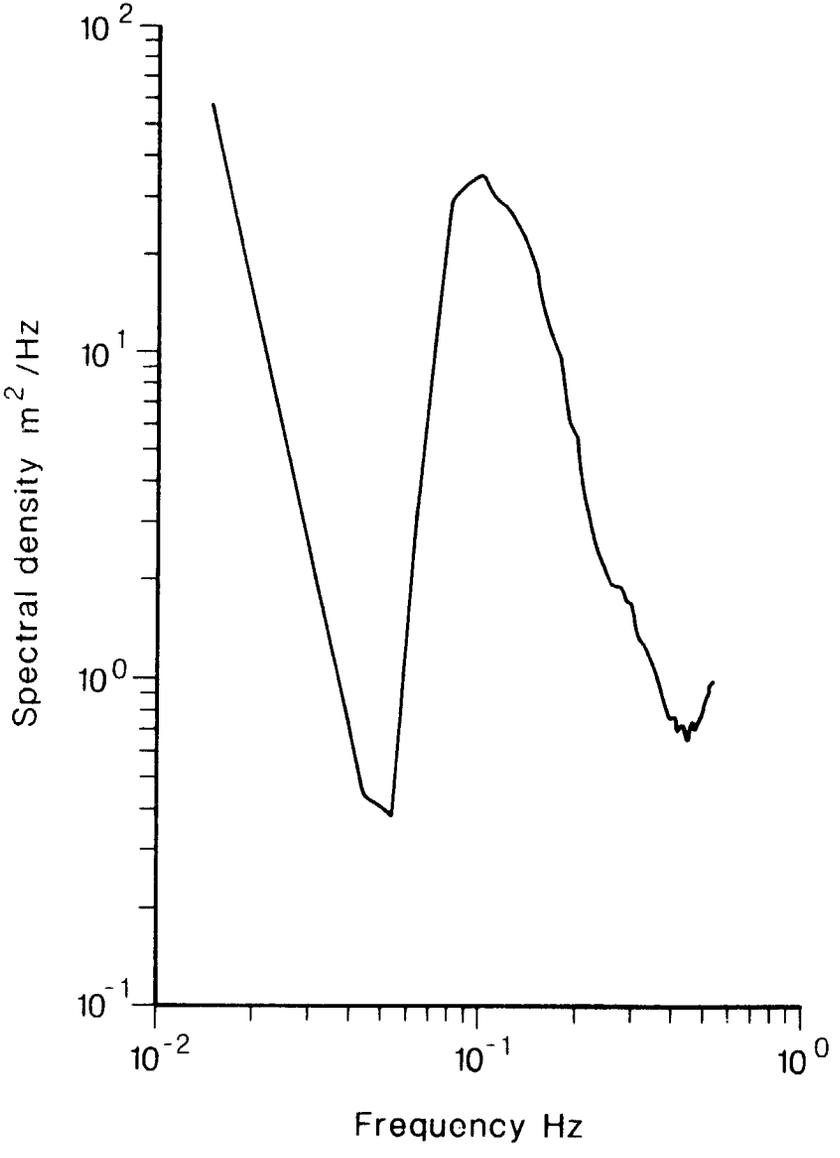

Classical correction (α = 1)

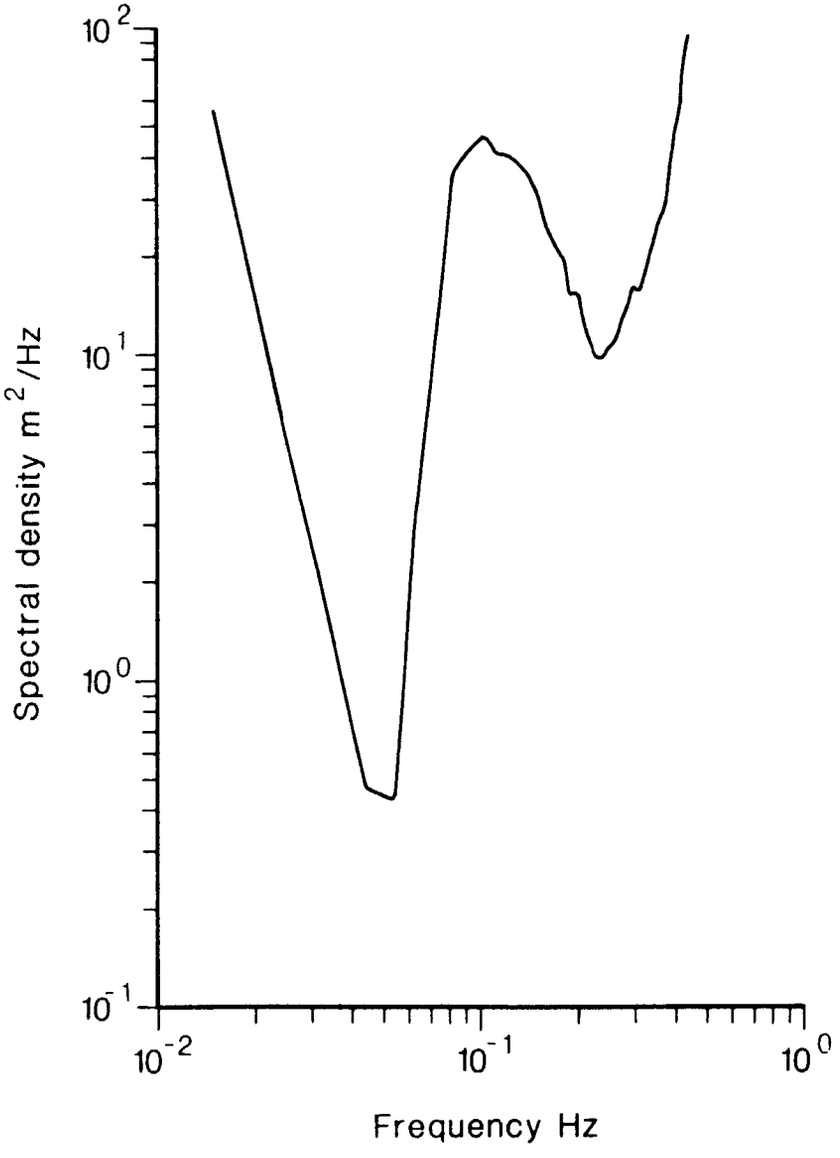

Modified correction (α = 2.5)

Fig 3.4 SBWR average spectra corrected for hydrodynamic attenuation

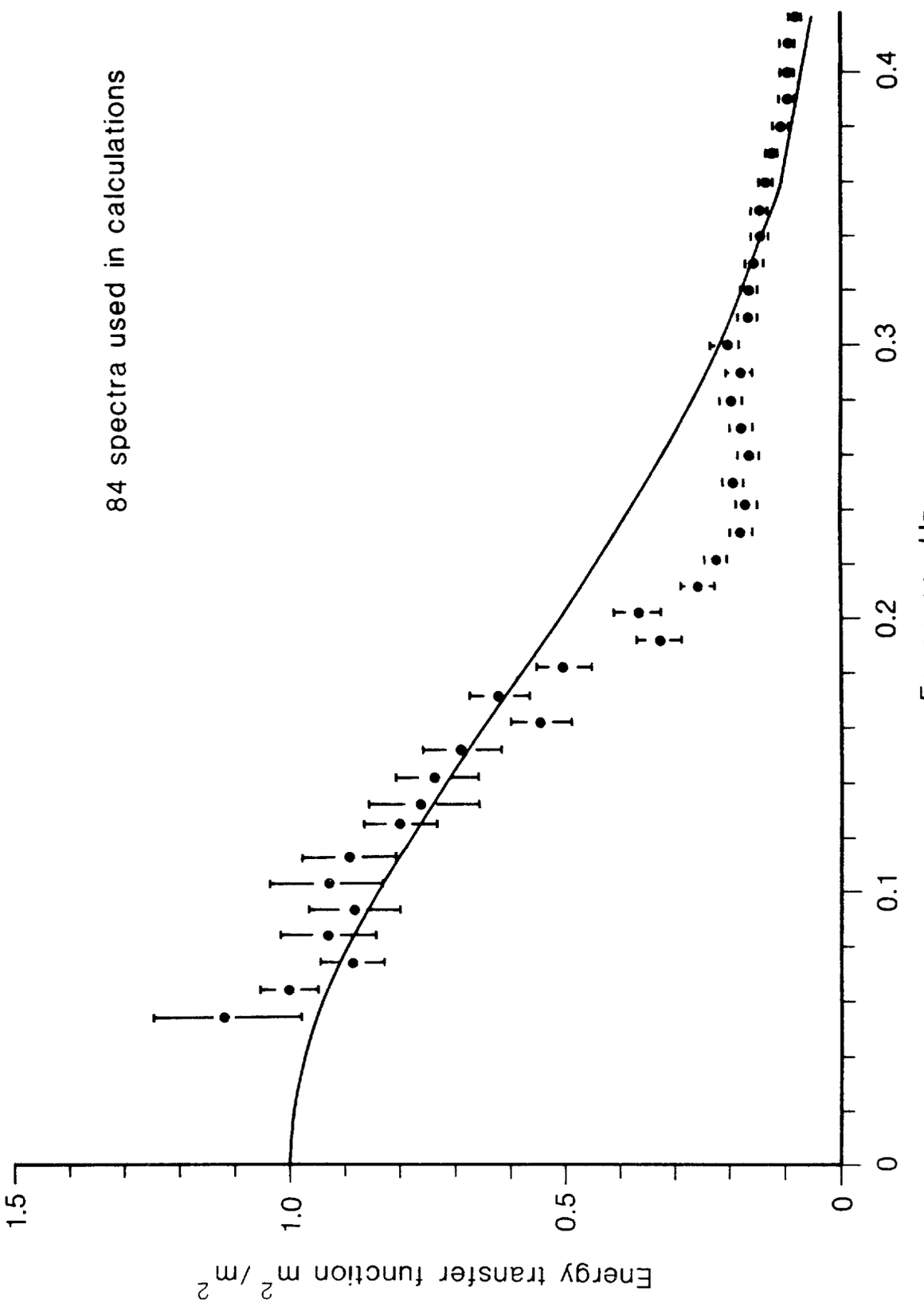

Fig 3.5 Energy transfer function for SBWR compared with classical hydrodynamic attenuation

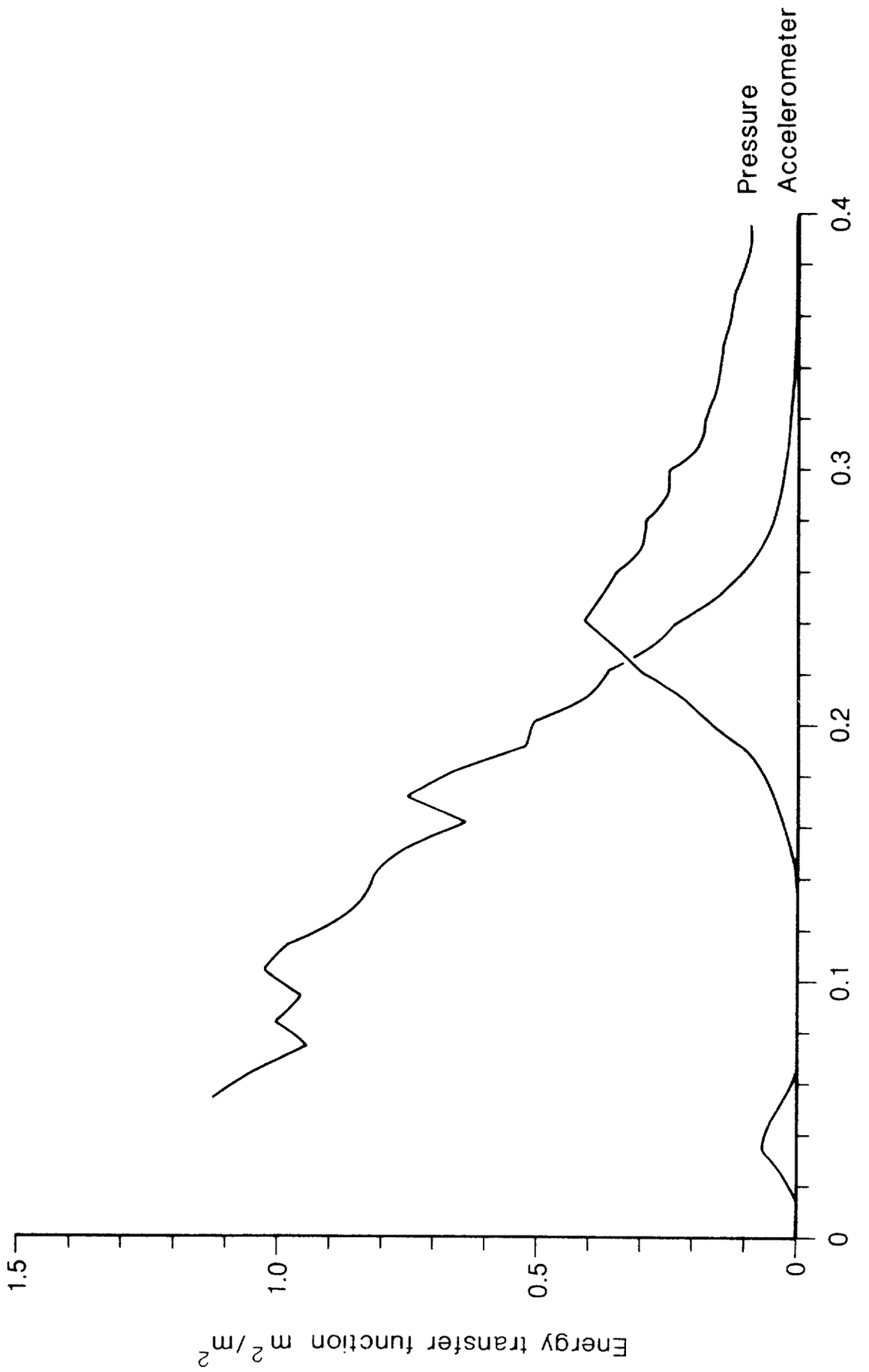

Fig 3.6 Energy Transfer Functions for SBWR. Pressure and Accelerometer signals obtained from Channel Lightvessel Data.

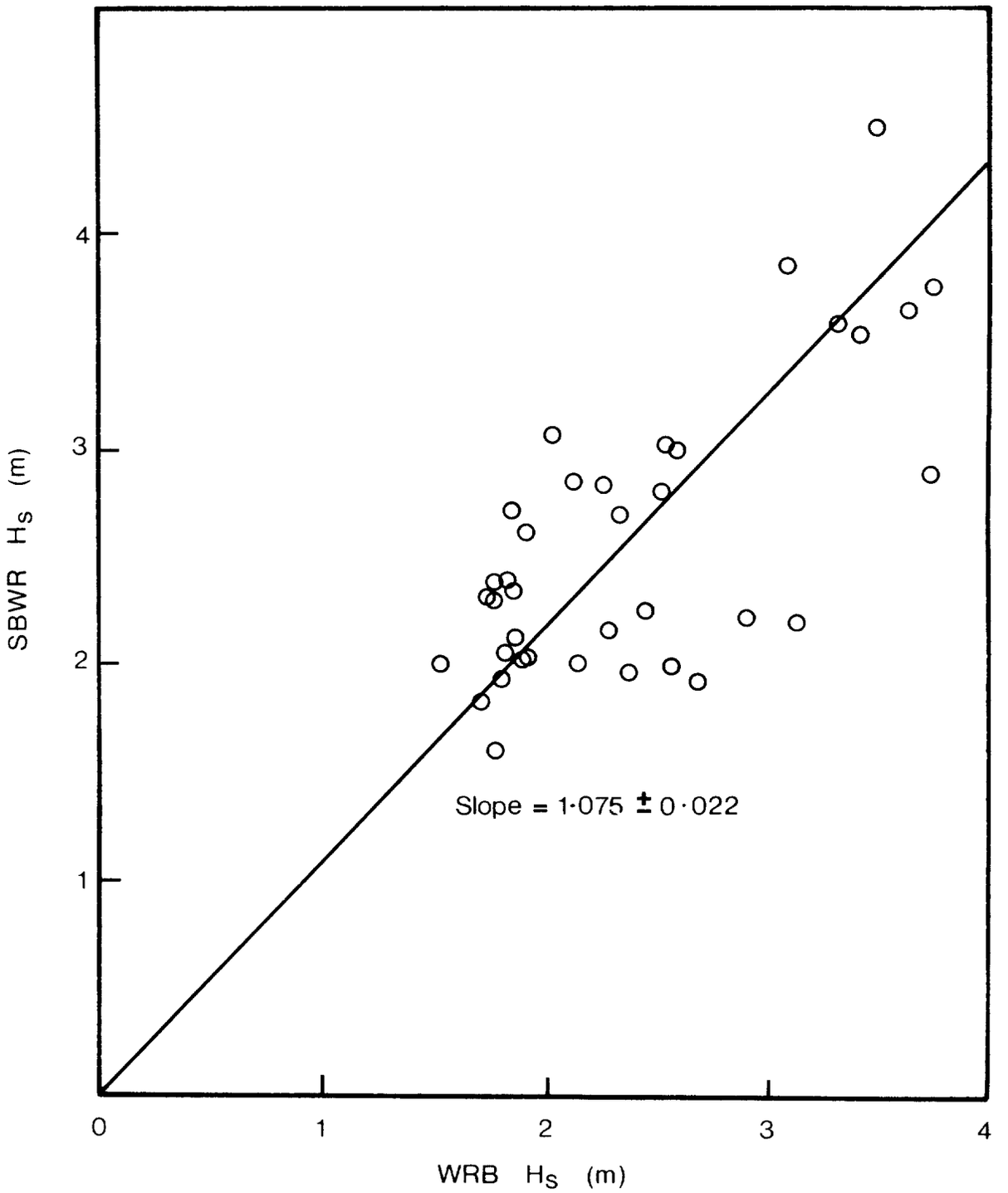

Fig 3.7 SBWR H_S v$_S$ WRB H_S for Tucker/Draper analysed chart records. The SBWR values were corrected using the modified hydrodynamic formula (α = 2.5).

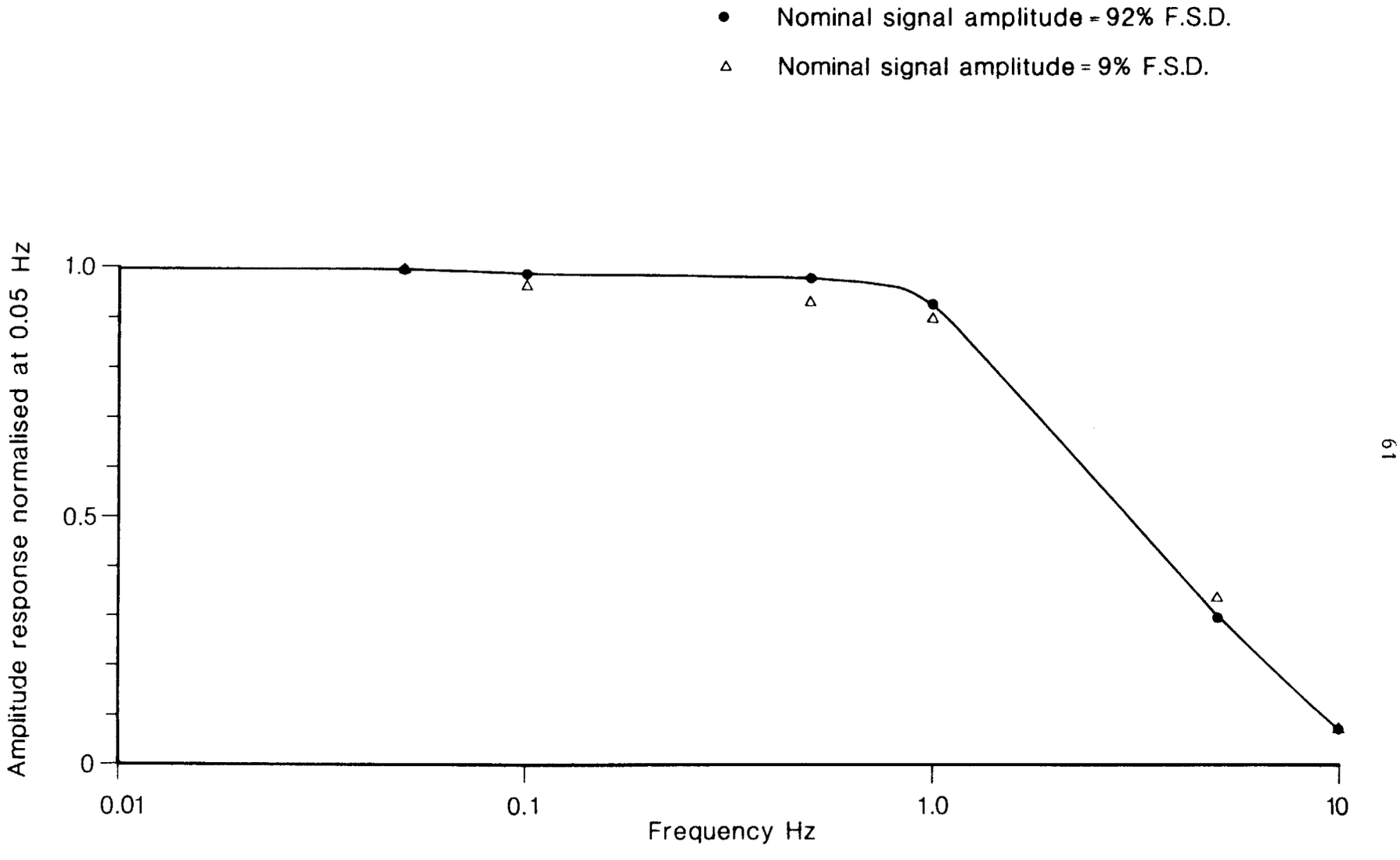

Fig 3.8 Frequency Response of Chessel chart recorder Type 301 used in MK 2 SBWR

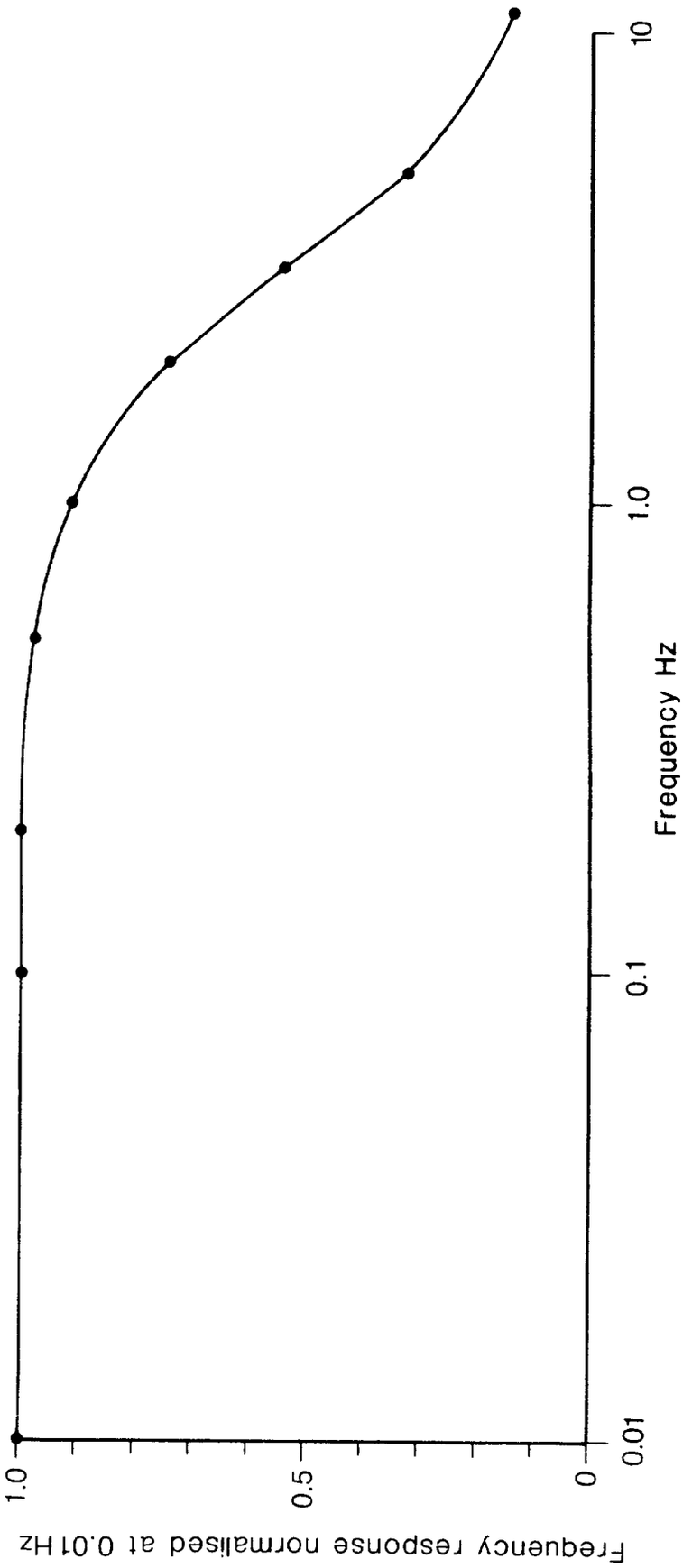

Fig 3.9 Frequency Response of MK 1 SBWR Galvanometer Type chart recorder

4 INTERPRETATION OF SBWR TRANSFER FUNCTIONS

4.1 Introduction

The form of the SBWR transfer function shown in section 3 differs from that which is conventionally used to interpret SBWR data. It is reasonable to enquire if the behaviour observed in this experiment may be expected for recorders mounted upon other ships. If a complete theory fitting the data could be constructed, this would allow the behaviour of recorders on other ships to be estimated with a high degree of confidence. As will be shown in section 4.4, we can at present go only a short distance down this path. In the absence of a sufficiently accurate theory, a second approach to the problem is to attempt to construct empirical scaling laws based upon measurements made aboard different ships. In sections 4.2 and 4.3 this possibility is explored.

4.2 Observations of SBWR Transfer Functions for Recorders on Other Ships.

There have been three detailed series of measurements reported in the literature, in which comparisons were made between accelerometer buoys and SBWR spectra. In each case frequency by frequency comparisons were made between SBWR spectra and corresponding spectra derived from an accelerometer buoy which was located in the vicinity of the recording vessel.

The first of these comparisons is described by Cartwright (1963) and further details are given in Canham, Cartwright, Goodrich, and Hogben (1962). In this series of measurements comparisons were made between spectra from an accelerometer buoy and spectra from a SBWR on the Ocean Weather Ship "Weather Reporter". Some of the comparisons were made with the ship under way so that corrections had to be made in order to allow for the resulting Doppler shifts. These corrections introduce additional uncertainties into the analysis so we examine those comparisons which were made with the ship held stationary. Only a limited amount of data was gathered under these conditions; Canham et al give three sets of results obtained from a spectral analysis of only 50 minutes of data. Their results, which are shown in Figure 4.1(b) agree quite well with the modified hydrodynamic formula. The results obtained from the analysis of spectra recorded when the ship was under way show similar behaviour.

Darbyshire (1961) compared spectra obtained from an accelerometer buoy with ship-borne wave recorder spectra obtained using two recorders; one mounted upon a lightvessel (Figure 4.1(a)) and one mounted upon a research ship (Discovery II)

(Figure 4.1(c)). The buoy spectra showed high levels of noise at low frequencies so that only data corresponding to frequencies in excess of 0.1 Hz were analysed. The modified hydrodynamic formula was fitted to each set of data although this could be achieved with only a moderate degree of success: particularly in the case of data recorded on "Discovery II". Both sets of data were analysed using an analogue harmonic analyser which must have introduced additional calibration problems into the experiment. Thus, although it is obvious that the responses measured on both ships fell well below the values predicted using the classical hydrodynamic formula, this experiment gives no clear indication that the modified formula is universally applicable. The lightvessel data have some qualitative features which are comparable with the results reported here, with a rapid increase in attenuation occuring above 0.18 Hz. A calibration error of 5-10% in amplitude would allow reasonable agreement between the data and the classical formula over the frequency range 0.12-0.18 Hz - outside this range the response would fall below the classical curve in the same manner as we have measured. The Discovery data shows a maximum at 0.22 Hz, whose origin is not understood and consequently only three data points were used to fit this data to the modified formula. As was pointed out by Darbyshire, the Discovery data showed a number of curious features which may have been caused by the strong tidal currents which occurred in the area where the experiment was conducted.

The most recent comparison, carried out by van Aken and Bouws (1971), used an instrument mounted upon Ocean Weather Ship Cumulus. The instrument was calibrated in an unusual way, but fortunately responses were measured for the accelerometers and pressure sensors in isolation as well as for the whole instrument. The data which they present can be recalculated using this information to give the response of the instrument referred to the usual calibration constants. The procedure for doing this is described in Appendix 5.

Figure 4.2 shows the original data, converted into an energy response curve, together with the corrected energy response and the hydrodynamic response functions corresponding to the sensor depth which was 1.5 m. As in the case of the data shown in Figure 4.1, neither of the experimental curves fits the theoretical responses well, though the general shape of the corrected response is similar to that found with the recorder mounted upon the Channel lightvessel(LV).

It is obvious that there is a high degree of scatter amongst the published data

and that no universal response function applies to all of the measured data. However there is one common feature which may be identified in the data recorded on OWS Weather Reporter, OWS Cumulus and the Channel lightvessel. In each case the transfer function falls off slowly at low frequencies, corresponding to attenuation values close to the classical formula, then in each case, at some higher frequency, the response falls away very rapidly, and then either continues to decay more slowly or may even show a small hump at approximately 0.25 Hz. It is not possible to tell if the data given by Darbyshire have the same features because of the restricted frequency range of those measurements, but in the case of both ships it is possible that the data may correspond to a portion of a curve with similar features.

4.3 Empirical Scaling Laws

The data presented previously have all been compared with the exponential frequency response laws, which correspond to the classical and modified hydrodynamic models. In this section we seek to replot the available data in such a way that the observed transfer functions may be related to characteristics of the ships upon which each recorder was mounted. These are summarised in Table 4.1. It should be noted that the literature contains only a limited amount of data concerning the size of the ships used in these experiments, and consequently the lengths reported in Table 4.1 may not be exact.

In order to construct an empirical scaling law we have taken all of the published SBWR transfer functions, and where necessary corrected the data for the electronic part of the SBWR's response. In the case of the Cumulus data, a correction was also applied to refer these measurements to the usual instrument calibration constants. These data are shown together in Figure 4.3, plotted as a function of wave frequency.

It is noticeable in this graph that the curves for Discovery II and Weather Reporter lie to the left of those for Cumulus and Channel LV. This is indicative of a tendancy for the response of recorders mounted on large vessels to fall more rapidly with frequency than that of recorders mounted on shorter ships. (The curve for Discovery is ambigious in this respect, but this recorder had a particularly deep pressure sensor.) Thus it is likely that a more consistent result may be obtained if the response of each instrument was expressed as a function of ship length as well as frequency. On dimensional grounds alone it would be

sensible to postulate that the transfer function might depend upon the ratio of the ship's length to the wavelength of the waves under observation, and this suggests a scaling law of the form

$$|R|^2 = |R(\xi_1)|^2 \quad \text{where } \xi_1 = \sqrt{\frac{2\pi L}{g}}\ f$$

and L is the ship's length and f is the wave frequency

Figure 4.4 shows a plot of $|R|^2$ Vs ξ. By comparison with Figure 4.3 it is clear that scaling the frequencies in this way reduces the scatter between observations made on different ships. Of course this is not the only scaling which can be used, and a similar law can be constructed by nondimensionalising the wave frequencies with respect to any characteristic length appropriate to a given ship. If all of the ships used in these experiments were geometrically similar, then it would not matter which characteristic length was chosen, but it is evident from the range of values of d/L shown in Table 4.1 that the depth of the recorders' pressure sensors did not vary in proportion to the ships' lengths. While the scaling law proposed above is to some degree successful, it is worth while testing a second scaling law based upon the depth at which each instrument's pressure sensor was mounted. Figure 4.5 shows the data plotted according to the scaling law:

$$|R|^2 = |R(\xi_2)|^2 \quad \text{where } \xi_2 = \sqrt{\frac{2\pi d}{g}}\ f$$

The data in Figure 4.5 are somewhat more scattered than in Figure 4.4 so that in this regard the ship length scaling law would appear to be better.

From the point of view of correcting field data with these empirical curves, the most important region is that which corresponds to the lower frequency waves. We therefore divide the data into two regions, one where $|R|^2$ is clearly frequency dependant, and one where the data indicate that the response is rather insensitive to frequency. In Figure 4.4 the boundary between these two regions occurs at $\sqrt{\frac{2\pi L}{g}}\ f \sim 1$. For $\sqrt{\frac{2\pi L}{g}}\ f > 1$ the data are very scattered and in this region it would be best either to assume a constant response ($|R|^2 \sim 0.25$) or to extrapolate the wave spectrum according to the Phillips' law for a saturated spectrum.

In the region where $\sqrt{\frac{2\pi L}{g}}\ f < 1$ Figure 4.4 shows some residual scatter and it is

fruitful to enquire if some reason for this can be found. In fact it is rather surprising that the ship's length scaling law works as well as it does, as we have already shown that the depth of the pressure sensors used in these experiments varied as a proportion of the ship's length. The upper curve in Figure 4.4 corresponds to the recorder with the shallowest pressure sensor depth, while the lower curve (Discovery II) corresponds to the deepest pressure sensor depth. This suggests that some of the residual spread in the results shown in Figure 4.4 is due to variations in pressure sensor depth. In view of this it is worth while trying a scaling law which takes account of both the ship's length and the depth of the pressure sensor. The construction of such a law is open to a wide choice concerning the way in which d and L may be combined. The author therefore proposed two laws:

$$|R|^2 = |R(\xi_3)|^2 \qquad \text{where } \xi_3 = \sqrt{\frac{2\pi}{g}\,dL}\; f$$

$$|R|^2 = |R(\xi_4)|^2 \qquad \text{where } \xi_4 = \sqrt{\frac{2\pi}{g}\,(dL)^{\frac{1}{2}}}\; f$$

The first of these was chosen because this simple formulation appeared capable of fitting the data rather well; however it has the aesthetic disadvantage that ξ_3 is not dimensionless so that a scaling law based on this variable will only work when f, d and L are expressed in the units used here. In an attempt to overcome this difficulty the scaling law based on ξ_4 was tried; this substitutes the harmonic mean of d and L for dL in the previously discussed formulations. Thus ξ_4 is dimensionless and although the form of ξ_4 is arbitrary, it is at least simple.

Figure 4.6 shows $|R|^2$ plotted as a function of ξ_3 and Figure 4.7 shows $|R|^2$ plotted as a function of ξ_4. As anticipated, for the lower values of ξ at least, both scaling laws are superior to those based on d and L alone. None of the scaling laws present here give complete consistency between the observations, but it should be borne in mind that Darbyshire's data were analysed using an analogue chart recorder, and an analogue spectrum analyser. Consequently these data are more likely to be subject ot systematic errors than the other data sets which were all recorded and analysed by digital methods. For this reason the author prefers the

scaling law shown in Figure 4.6 to that shown in 4.7, as in the case of Figure 4.6 the three digital data sets coincide more closely than they do in Figure 4.7. The fact that the "best" scaling law is obtained by a fit to a dimensional quantity could be regarded as an indication that the set of characteristics used to describe the ships in these experiments is incomplete, and that another quantity (with dimensions of $m^{\frac{1}{2}}$) is relevant. However it appears that in the absence of a physical theory capable of explaining the observations, the scaling law shown in Figure 4.6 provides the best practical indication of how field observations made with the SBWR should be corrected. Of course a correction scheme based upon a sound physical theory would be preferable to this approach, and we investigate in the next section to what degree this is possible.

4.4 Modifications to the simplified SBWR Theory

The simple hydrodynamic model for the SBWR neglects a number of effects which might be responsible for the departures between the simple theory and the experimental data. Four such effects have been identified and are discussed below. These are:

1. The influence of forward motion with respect to the water upon the SBWR response
2. The incomplete compensation which occurs when waves are partially reflected at the ship's hull
3. The broadening of the SBWR spectrum as a result of a variable depth of submergence of the pressure sensors
4. The perturbation of the wave motions in the ship's vicinity caused by the presence of the ship's hull.

The second effect listed above is in fact a special case of the perturbation of the wave motion in the ship's vicinity, but it is convenient to consider wave reflection separately. The influence of each of the effects upon the SBWR's response is discussed below in sections 4.5-4.9.

4.5 Influence of ship's forward motion relative to the water

The water currents relative to the recording vessel will change the frequency of encounter of waves of a prescribed wavelength by virtue of the Doppler effect. As the depth attenuation is dependent on wavelength, the measured response will be affected by the presence of tidal currents in the vicinity of moored vessels or by the forward motion of ships which are under way. Cartwright's results (1963) are corrected for the ship's motion and the resulting corrected responses show no

systematic variation with the ship's speed. It is thus reasonable to suppose that the correction procedure used was successful and that these results include no distortion originating from the ship's forward motion. As this response is of the same general form as the other response curves, it is unlikely that this source of error is responsible for the departures from the classical formula. It is also worth noting that only moderate tidal currents occurred in the vicinity of the Channel lightvessel and that the Cumulus data were measured with the ship hove to so that in both cases only small Doppler shifts should have occurred, except perhaps at the high frequency end of the spectrum.

4.6 Partial wave reflection from the ship's hull

The summation of pressure signals derived from sensors located on either side of the ship's hull compensates for spurious signals caused by the ship's rolling motion, and is also intended to cancel out the effect of partial reflection of waves incident at oblique angles to the ship's side. In the cases where no reflection or total reflection occurs the compensation is complete, but when a wave is partially reflected the sum of the pressure sensor signals bears a more complicated relationship to the amplitude of the incident wave. Provided no dissipation occurs, the amplitudes of the reflected and transmitted waves must be such that they have the same energy as the incident wave train. As the wave's energy is proportional to the square of its amplitude:

$$a_i^2 = a_t^2 + a_r^2 \qquad (4.6.1)$$

where a_i, a_t and a_r are the amplitudes of the incident, transmitted and reflected waves.

If the reflection coefficient, α is defined by $a_r = \alpha a_i$ then

$$a_i^2 (1-\alpha^2) = a_t^2 \qquad (4.6.2)$$

If no phase shifts occur across the width of the ship, the SBWR pressure signal, S, is given by

$$S = \frac{a_i}{2} \left[1 + \alpha + \sqrt{1-\alpha^2}\right] \qquad (4.6.3)$$

the ratio s/a_i has been calculated for various values of α and is shown in Table 4.2.

It can be seen that the SBWR output is increased when waves are partially reflected by the hull. In practice, the incident energy will be spread over a range of directions, thus the resultant effect will be smaller than the maximum indicated in Table 4.2. Such effects will only matter at relatively high frequencies when partial reflection may occur. Thus the overall effect is expected to be relatively small.

4.7 Modulation of SBWR signal as a result of variations in the pressure sensors' depth

In the analysis of data derived from a similar experiment to that described here van Aken and Bouws (1974) suggested that the response of the instrument at frequencies above 0.2 Hz was enhanced by spurious contributions to the SBWR signal. They hypothesised that the non-linear attenuation of pressure with depth would allow mixing between components in the real wave spectrum. This would allow side bands at the sum and difference frequencies between any two components in the original spectrum, which while small might dominate at high frequencies where the wave spectral density is also small.

They used a formulation for the subsurface wave pressure distribution which is discussed in Appendix 6 and which the author believes is incorrect. Consequently their conclusions are open to question, and the author has carried out a limited theoretical investigation of the importance of the effect, using a formulation for the subsurface pressure derived in Appendix 4. The details are given in Appendix 6, but it is relevant to remark here that it would appear that intermodulation effects are unimportant over the range of frequencies considered in this work.

4.8 Modification of the wave field in the ship's vicinity

The most sweeping assumption which is incorporated into the simple SBWR model is that concerning the perturbation of the wave field in the vicinity of the ship. In order to improve the theory some method must be introduced which allows the near field motions of the water to be calculated. The problem is a difficult one because these motions must depend upon the shape and dynamics of the recording ship as well as the directional properties of the sea state. Nevertheless some

Table 4.1

Ship	Length (m) L	Depth of pressure transducer (m) d	Ratio d/L
Weather Reporter[1]	72	2.2	0.031
Hellvick LV[2]	33.5	1.4	0.043
Cumulus[3]	62	1.5	0.024
Discovery II[4]	68	2.9	0.043
Channel LV[5]	35	2.2	0.060

Notes on ship length estimation

1. Measured from published line drawing
2. Information supplied by Trinity House
3. Cumulus length estimated from photograph
4. Discovery length estimated from photograph
5. Length measured from ship's plans

Table 4.2 Variation of amplitude response with reflection coefficient

α	$s/a_i = \frac{1}{2}(1 + \alpha + \sqrt{1 - \alpha^2})$
0	1
.1	1.05
.2	1.09
.3	1.13
.4	1.17
.5	1.18
.6	1.20
.7	1.21
.8	1.20
.9	1.17
1.0	1.00

conclusions may be reached using the approximate theory of Korvin-Kroukovsky and Jacobs (1957). Cartwright (1963) interpreted the modified (double exponential) response which he measured in terms of Korvin-Kroukovsky's work. However the present author is of the opinion that the doubled exponential decay of pressure with depth is not a general property predicted by Korvin-Kroukovsky's theory, but this behaviour is expected in one limit. A more general form for the recorder's response may be inferred from the theory which shows the same qualitative features as the measurements. In this section we describe the theory and then compare its qualitative predictions with the data presented above.

The theory given by Korvin-Kroukovsky et al treats the motion of a ship of idealised, cylindrical, cross-section in head seas. A series of plausible but rather heuristic arguments are used to deduce the pressure distribution upon the hull, and hence, by integration over the surface of the ship, its motions are calculated. As our aim here is to calculate the pressure at a specific location, Korvin-Kroukovsky's theory needs some modification, because the integrations of the pressure distribution over the ship's surface are superfluous in the present context.

Korvin-Kroukovshy assumes that the velocity potential in the vicinity of the ship may be expressed in two terms:

$$\phi = \phi_w + \phi_b \qquad (4.8.1)$$

where ϕ_w is the velocity potential for the waves without the ship's perturbations being taken into account. ϕ_b is the velocity potential, due to the presence of the ship, which allows the boundary conditions at the hull to be satisfied, while leaving $\phi = \phi_w$ at great distances from the ship. It is difficult to calculate ϕ_b analytically, so Korvin-Kroukovsky hypothesises that ϕ_b is approximately given by the velocity potential for uniform flow past a cylinder, in which the velocity is given by the difference between the vertical component of the ship's velocity and the vertical component of the far field wave velocity. As the velocity potential for uniform flow past a circular cylinder of radius R is given by

$$\phi = v \frac{r^2}{R} \cos\alpha$$

where r and α are cylindrical co-ordinates

ϕ_b becomes:

$$\phi_b = -(v-v_w)\frac{r^2}{R}\cos\alpha \qquad 4.8.2$$

where v is the vertical component of the ship's motion and v_w, the vertical component of the velocity of the waves in the far field is given by

$$v_w = \frac{\partial \phi_w}{\partial y} \qquad 4.8.3$$

The two terms in 4.8.2 may be separated so that

$$\phi_b = \phi_{bw} + \phi_{bm} \qquad 4.8.4$$

where

$$\phi_{bw} = v_w \frac{r^2}{R}\cos\alpha \qquad \phi_{bm} = -v\frac{r^2}{R}\cos\alpha$$

Korvin-Kroukovsky evaluates the pressure distribution on the hull due to the waves using ϕ_w and ϕ_{bw}, and integrates over the hull to obtain the exciting force for the ship's motion. The pressure distribution due to ϕ_{bm} is treated in isolation because of its dependence on v and is incorporated into the equations of motion of the ship separately.

If co-ordinates are chosen with y upwards and x parallel to the ship's longitudinal axis then ϕ_w may be specified as

$$\phi_w = h\frac{\omega}{k} e^{ky}\cos(kx-\omega t) \qquad 4.8.5$$

which corresponds to a surface wave given by

$$\eta = h \sin(kx-\omega t) \qquad 4.8.6$$

Thus from 4.8.3

$$v_w = h\omega e^{ky}\cos(kx-\omega t) \qquad 4.8.7$$

so that from 4.8.2 and 4.8.4

$$\phi_{bw} = h\omega e^{ky} \frac{r^2}{R} \cos\alpha\cos(kx-\omega t) \qquad 4.8.8$$

The pressure is calculated from ϕ using the approximation $p = \rho\frac{\partial\phi}{\partial t}$ so that

$$p_w = \rho\frac{\partial\phi w}{\partial t} = \rho ghe^{ky} \sin(kx-\omega t) = \rho g\eta e^{ky} \qquad 4.8.9$$

and

$$p_{bw} = \rho\frac{\partial\phi_{bw}}{\partial t} = \rho ghkye^{ky} \sin(kx-\omega t) = \rho g\eta kye^{ky} \qquad 4.8.10$$

thus the sum of the two pressure distributions is given by:

$$p = p_w + p_{bw} = \rho g\eta\ (e^{ky} + ky\ e^{ky}) \qquad 4.8.11$$

which may be written, upon expanding the exponentials as Taylor series, as

$$p = \rho g\eta(\ 1 + 2ky + \frac{3}{2} k^2y^2 \ldots) \qquad 4.8.12$$

Thus to first order in ky, $p = \rho g\eta e^{2ky}$ which is the squared Smith effect referred to by Korvin-Kroukovsky, and quoted by Cartwright as being in approximate agreement with his results.

There are four fundamental difficulties associated with the formulation described above:

1. The free surface is not included in the formulation for ϕ_b.
2. A steady rather than oscillatory flow is used for ϕ_b.
3. The pressure distribution due to ϕ_{bm} is not included.
4. An idealised hull form of rather unrealistic shape has been used in order to render the calculation tractable.

Ursell (1954) has calculated a series of correction factors which are quoted by Korvin-Kroukovsky and which take account of the proximity of the free surface.

He expresses 4.8.12 in the form

$$p = \rho g \eta (1 + (1 + k_4) ky)$$

where k_4 depends upon k as shown below in Table 4.3.

Table 4.3 Variation of k_4 with kR taken from Ursell (1954)

kR	k_4
0	∞
0.262	0.818
0.524	0.632
0.785	0.592
1.571	0.673
2.094	0.738
2.356	0.762
3.142	0.818
3.927	0.859
4.712	0.883

Thus it may be seen that for $kR > 0.262$ the attenuation factor is raised to a power which is substantially less than 2. For a typical ship of 8 m beam, $kR = 0.262$ corresponds to a frequency of 0.18 Hz. At this frequency the Channel lightvessel's heave response has a value of approximately 0.7 so that it is clear that the ship's vertical motion is important for $kR < 0.262$. However, as the idealised hull shape used in the theory is rather unrealistic, k_4 is not included in the theory which is presented below.

4.9 Interference theory for SBWR

In order to derive a theory for the SBWR which includes the perturbation which the ship imposes upon the wave field we use the same general approach followed by Korvin-Kroukovsky et al. We take as our starting point, equation 4.8.2 for ϕ_b:

$$\phi_b = -(v - v_w) \frac{r^2}{R} \cos\alpha \qquad 4.9.1$$

where v, the ship's vertical velocity must be obtained from calculation or experimentally. We assume that the ship's vertical amplitude at the pressure sensors may be written as

$$a(\omega) = T(\omega)\ h\sin(kx - \omega t + \psi(\omega)) \qquad 4.9.2$$

where $T(\omega)$ is the amplitude response and ψ the corresponding phase shift. Differentiating 4.8.2 with respect to time gives the ship's vertical velocity as

$$v(\omega) = -\omega T(\omega)\ h\cos(kx - \omega t + \psi(\omega)) \qquad 4.9.3$$

so that, using 4.9.3, 4.9.1, 4.8.7, 4.8.5 and 4.8.1 the total velocity potential close to the ship becomes

$$\phi = \frac{h\omega}{k} e^{ky} \cos(kx - \omega t) + \frac{r^2}{R} \cos\alpha\ h\omega e^{ky} \cos(kx - \omega t) - T\omega h\cos(kx - \omega t + \psi(\omega) \qquad 4.9.4$$

so that, using the relation $p = \rho\frac{\partial \phi}{\partial t}$ we obtain

$$p = \rho g h e^{ky} \sin(kx - \omega t) + \frac{r^2}{R} \cos\alpha\ \rho g h k e^{ky} \sin(kx - \omega t) - \rho g T h k \sin(kx - \omega t + \psi(\omega) \qquad 4.9.5$$

as on the ship's hull r = R and R cos α is the depth of submergence of the point, (r,α) p may be expressed in the form

$$\frac{p}{\rho g h} = e^{ky} \sin(kx - \omega t) - Tky\sin(kx - \omega t + \psi(\omega)) + kye^{ky} \sin(kx - \omega t) \qquad 4.9.6$$

The first term is the Smith effect term which may be obtained from the Froude - Krylov hypothesis and the last term corresponds to the interference between the ship and the wave field. The second term, which was neglected by Cartwright, takes account of the ship's vertical motion.

On expanding the second term 4.9.6 becomes:

$$\frac{p}{\rho g h} = e^{ky}(1 + ky) \sin(kx - \omega t) - Tky \sin(kx - \omega t) \cos\psi(\omega) - Tky \cos(kx - \omega t) \sin\psi(\omega) \qquad 4.9.7$$

so that the measured instrument response is given by

$$\frac{|p|^2}{(\rho g|h|)^2} = (e^{ky}\,[1 + ky])^2 - 2Tkycos\psi(\omega)\; e^{ky}[1 + ky] + T^2k^2y^2 \qquad 4.9.8$$

Canham et al (1962) gives plots of the ship's heave response from which both the magnitude and phase of T may be deduced as a function of encounter frequency with the ship under way. The author has replotted these data, converting the frequency of encounter into wave frequency using graphs which Canham et al supply for this purpose. The resulting heave responses for head seas are shown in Figure 4.8 A. These show some scatter, so for the purpose of evaluating Equation 4.9.8, the response shown in Figure 4.8 B was used. As the phase shifts given by Canham et al (1962) show no consistent variation according to the ship's speed, it was assumed that these depend upon the frequency of oscillation of the ship rather than the frequency of the exciting forces upon the ship; consequently no frequency corrections were applied to the phase shifts. The phase shift variation with frequency is shown in Figure 4.0 C. Figure 4.8 D shows the measured SBWR response together with the response calculated from Equation 4.9.8, using the data shown. It should be noted that Canham et al deduced the phase of the waves in the ship's vicinity using the SBWR itself so that the validity of the assumed phase variation with frequency is questionable and significant phase shifts may occur at frequencies below 0.2 Hz.

Figure 4.9 shows similar comparison between measured SBWR responses and Equation 4.9.8. In both cases, $\cos(\psi)$ was set to unity over the whole frequency range as no data were conveniently available.

In all three cases the modelled response falls more slowly than the experimental data at intermediate frequencies in the range .15-.2 Hz.

This behaviour may occur either because of the influence of phase shifts which were not included in the calculation, or because of the inadequacy of a model based upon a cylindrical hull shape. Nevertheless the calculated response functions have the desirable qualitative feature that at low frequency the response is approximately that given by the classical attenuation formula while at higher frequency the calculated response of the SBWR falls more rapidly than this. In the high frequency limit the ship must behave as a fixed obstacle so that, with head seas

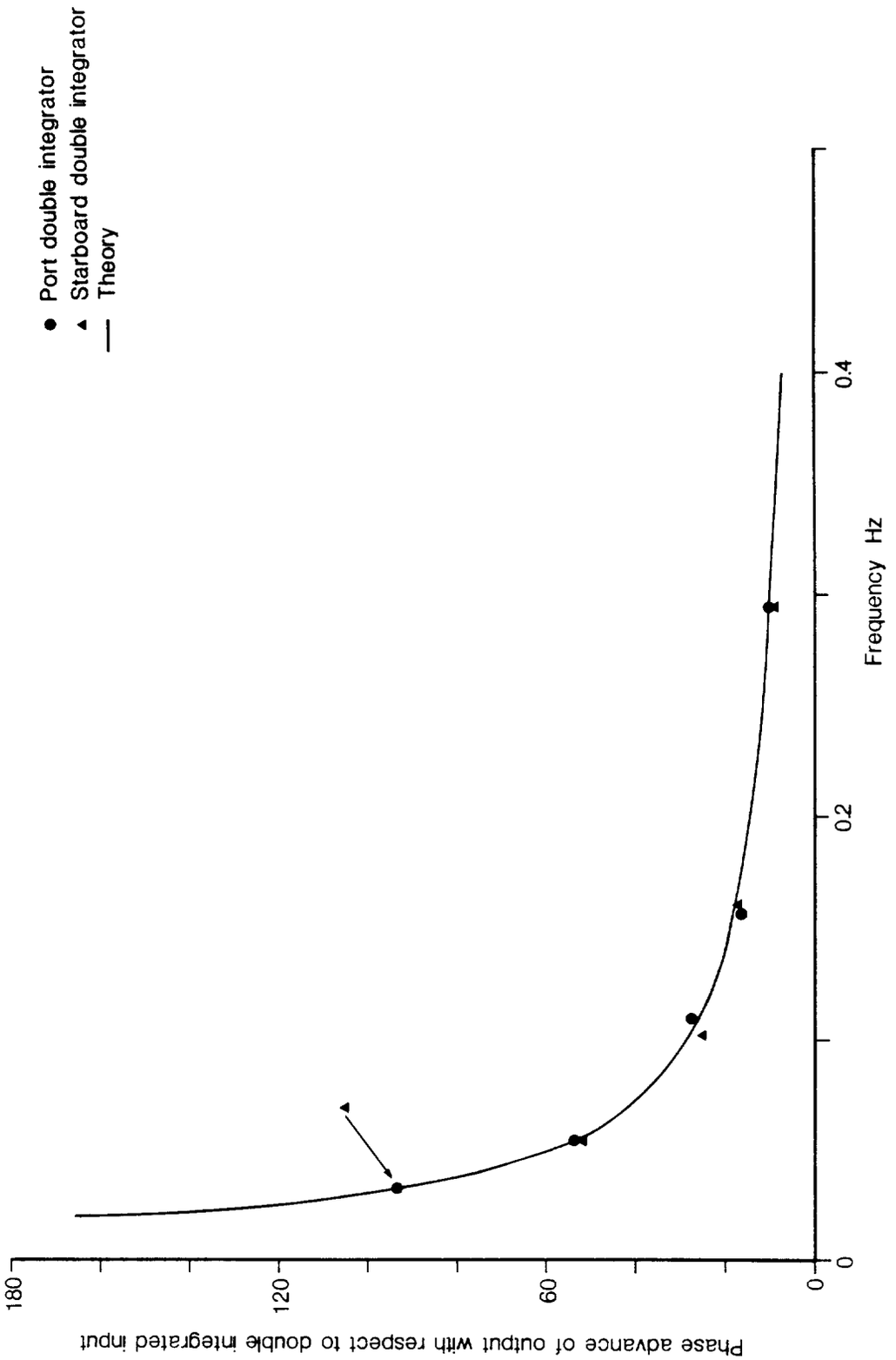

Fig A2.10 Equivalent phase response of SBWR interface double integrators

These double integrators were used to condition those signals derived from the SBWR accelerometers which were recorded separately and which corresponded to the heave displacement at each side of the ship

Nomenclature

L	ship length
d	mean depth of SBWR pressure sensors
ξ_1	nondimensional frequency
$\|R\|^2$	SBWR spectral density transfer function
g	acceleration due to gravity
f	frequency
ξ_2	nondimensional wave frequency
ξ_3	scaled wave frequency
ξ_4	nondimensional wave frequency
a_i	incident wave amplitude
a_t	transmitted wave amplitude
a_r	reflected wave amplitude
α	reflection coefficient
s	SBWR signal
ϕ, ϕ_w, ϕ_b	velocity potentials
r, α	cyclindrical co-ordinates
v	vertical component of ship's velocity
v_w	vertical component of water velocity
y	vertical co-ordinate
R	radius of cylindrical ship's hull
h	wave amplitude
ω	wave angular frequency
t	time
x	horizontal co-ordinate
k	wave number ($k = 2\pi$/wavelength)
η	surface elevation
p, p_w, p_{bw}	pressures
ρ	density of sea water
k_4	variable calculated by Ursell
T	ship heave response transfer function
ψ	phase angle

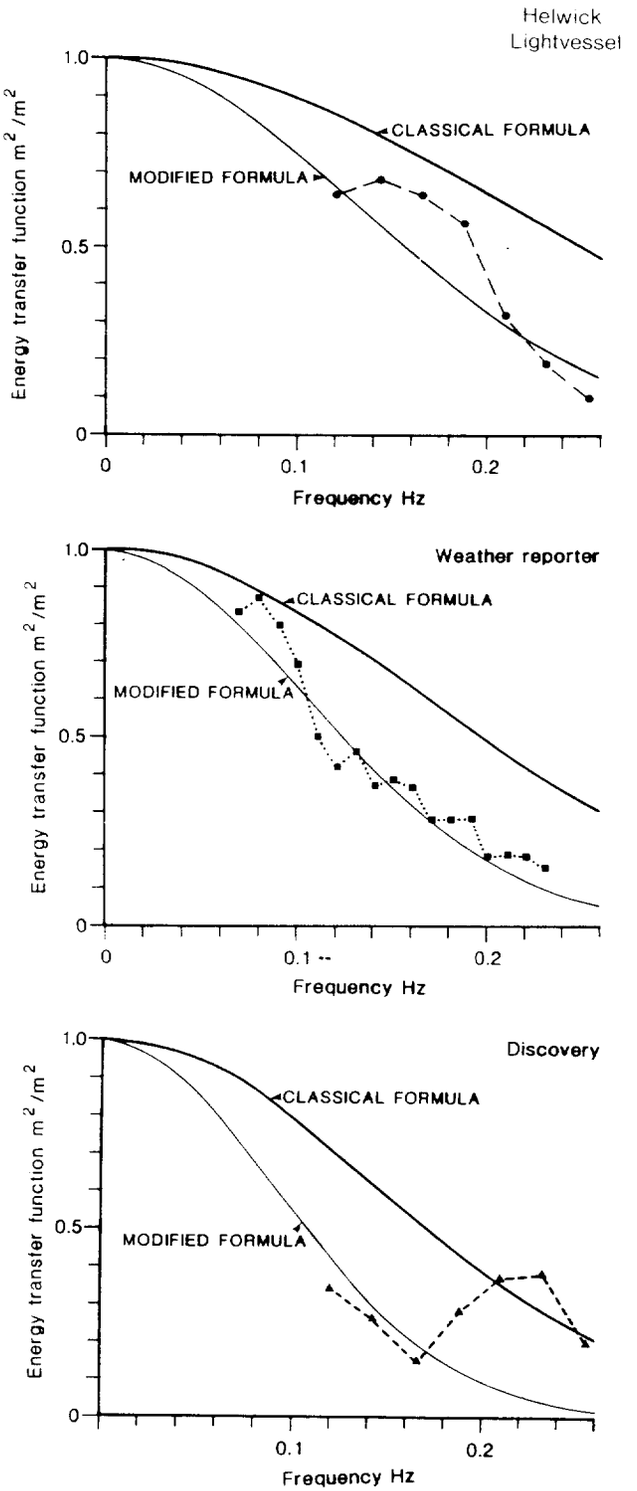

Fig 4.1 Three earlier determinations of frequency response compared with the classical and modified formulae

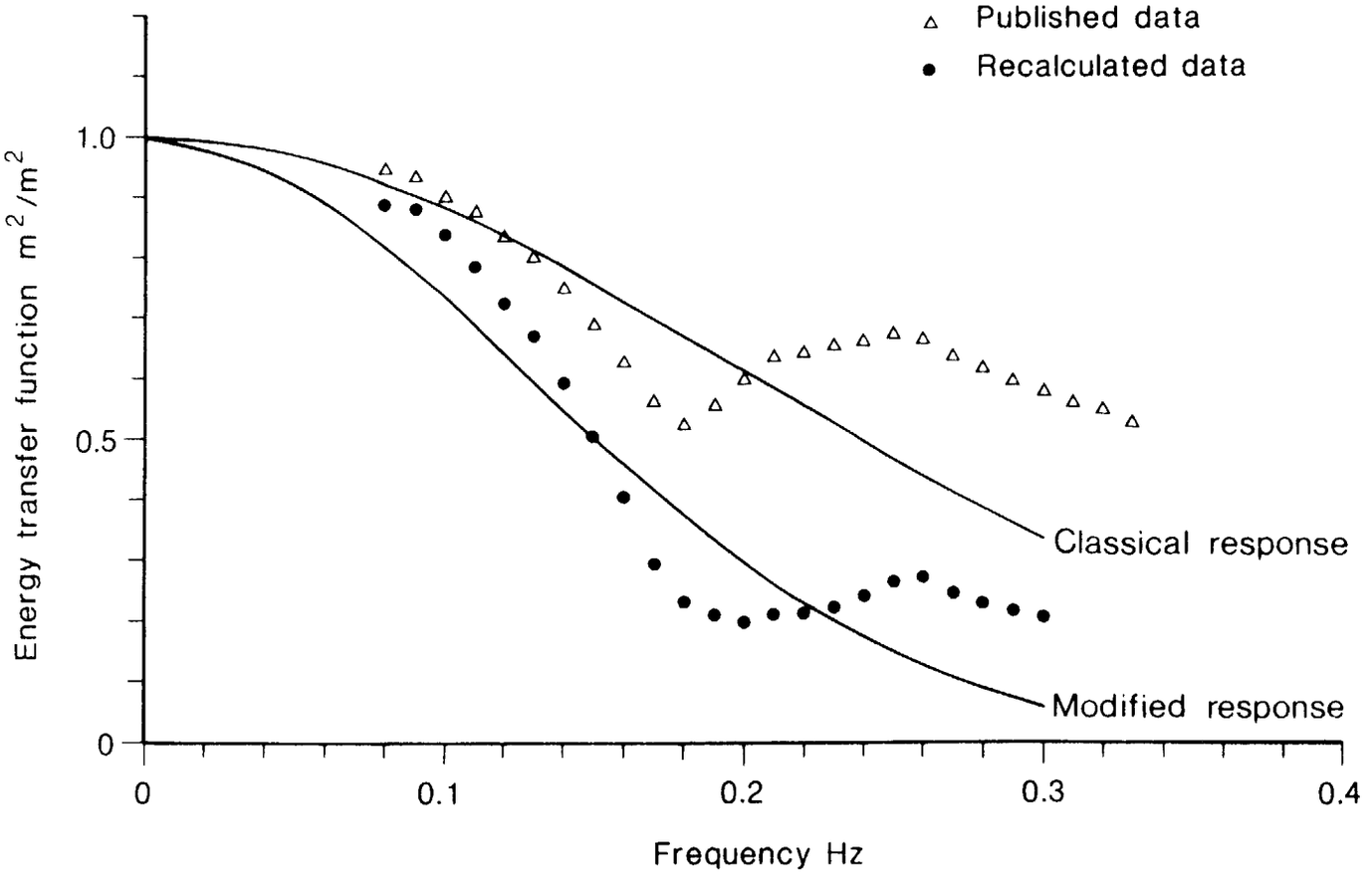

Fig 4.2 Measured response data for O.W.S. Cumulus compared with the classical and modified formulae

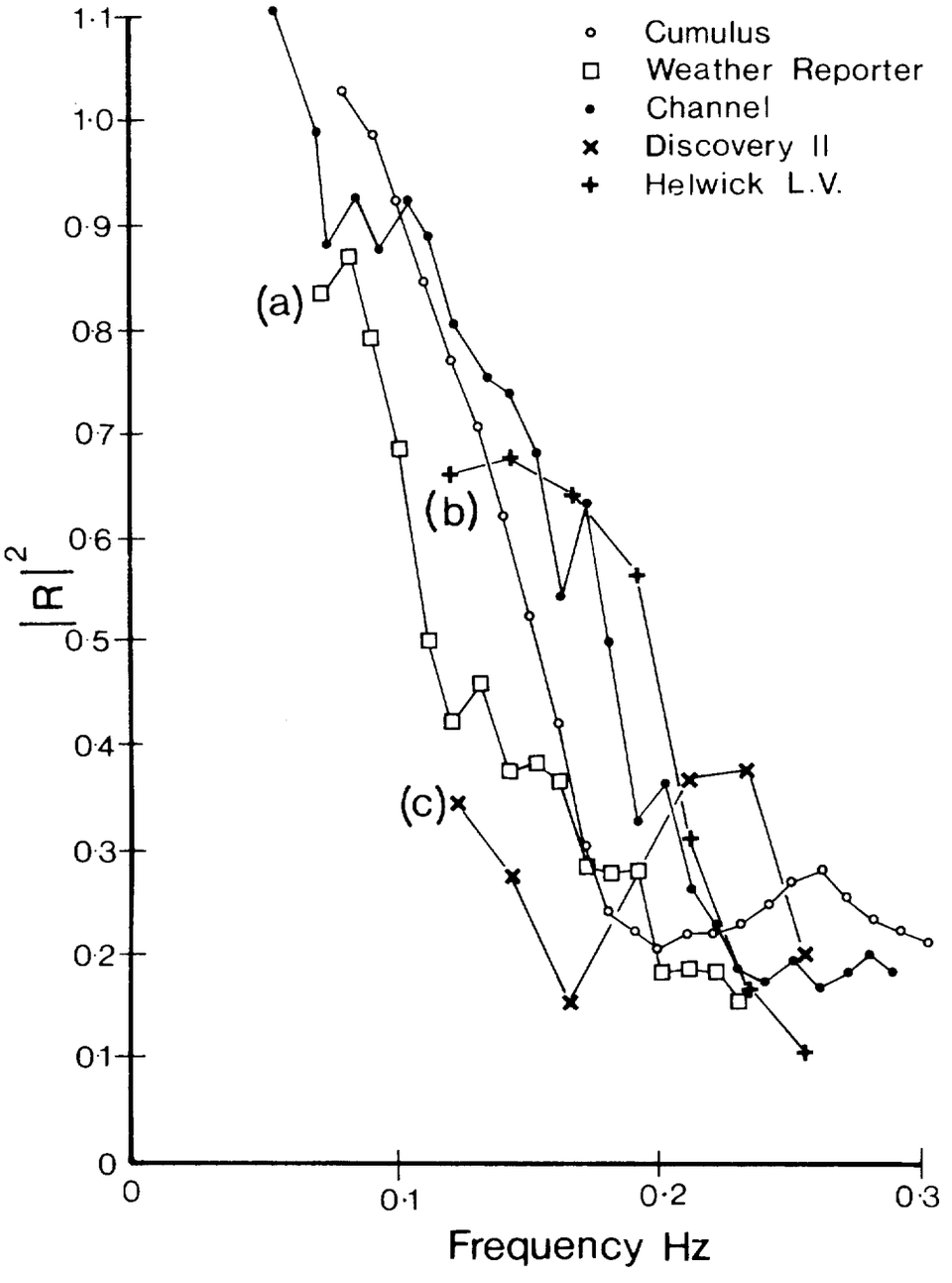

Fig 4.3 $|R|^2$ v_s frequency various ships.

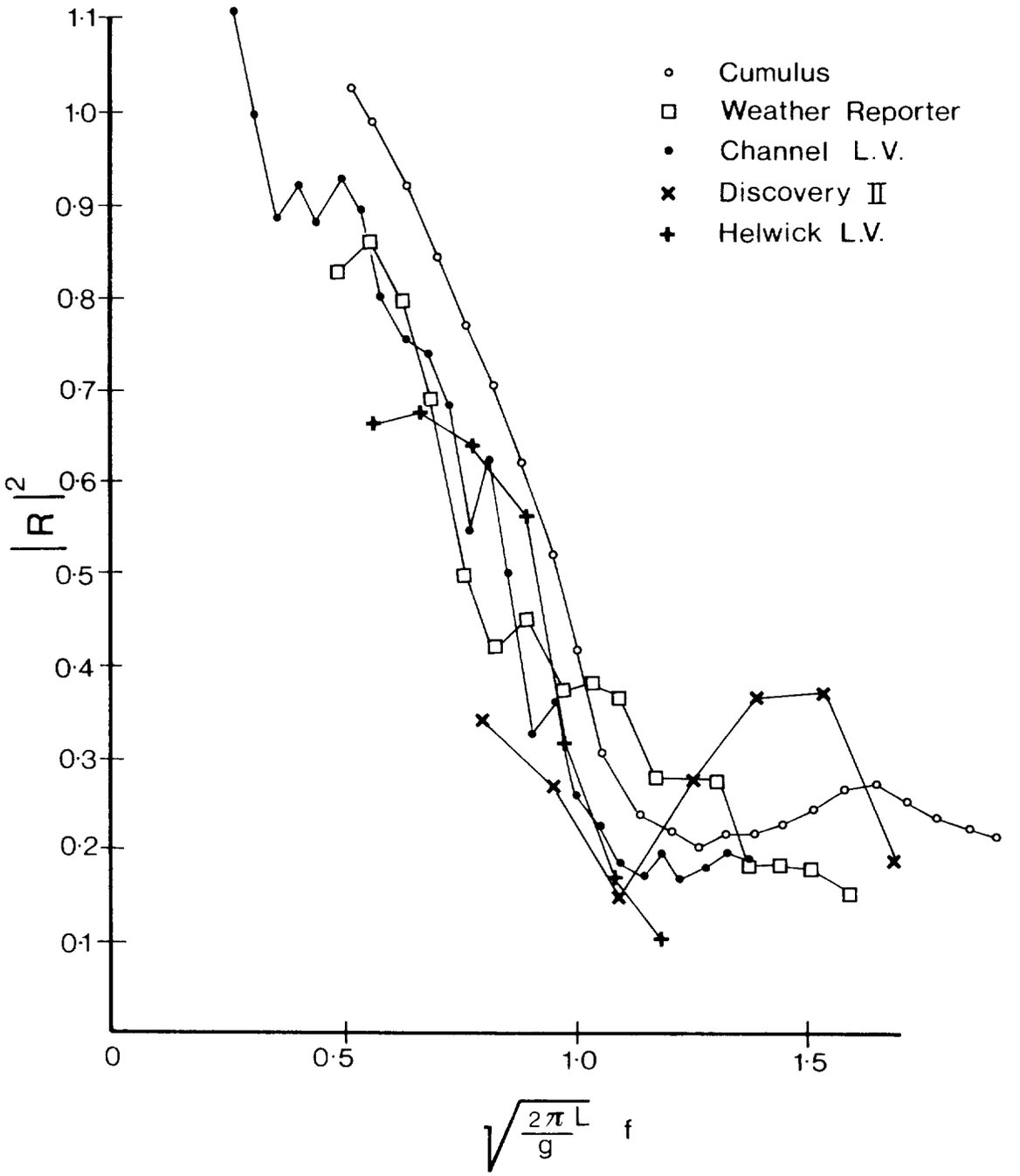

Fig 4.4 $|R|^2$ v_S frequency, nondimensionalised with respect to ship length.

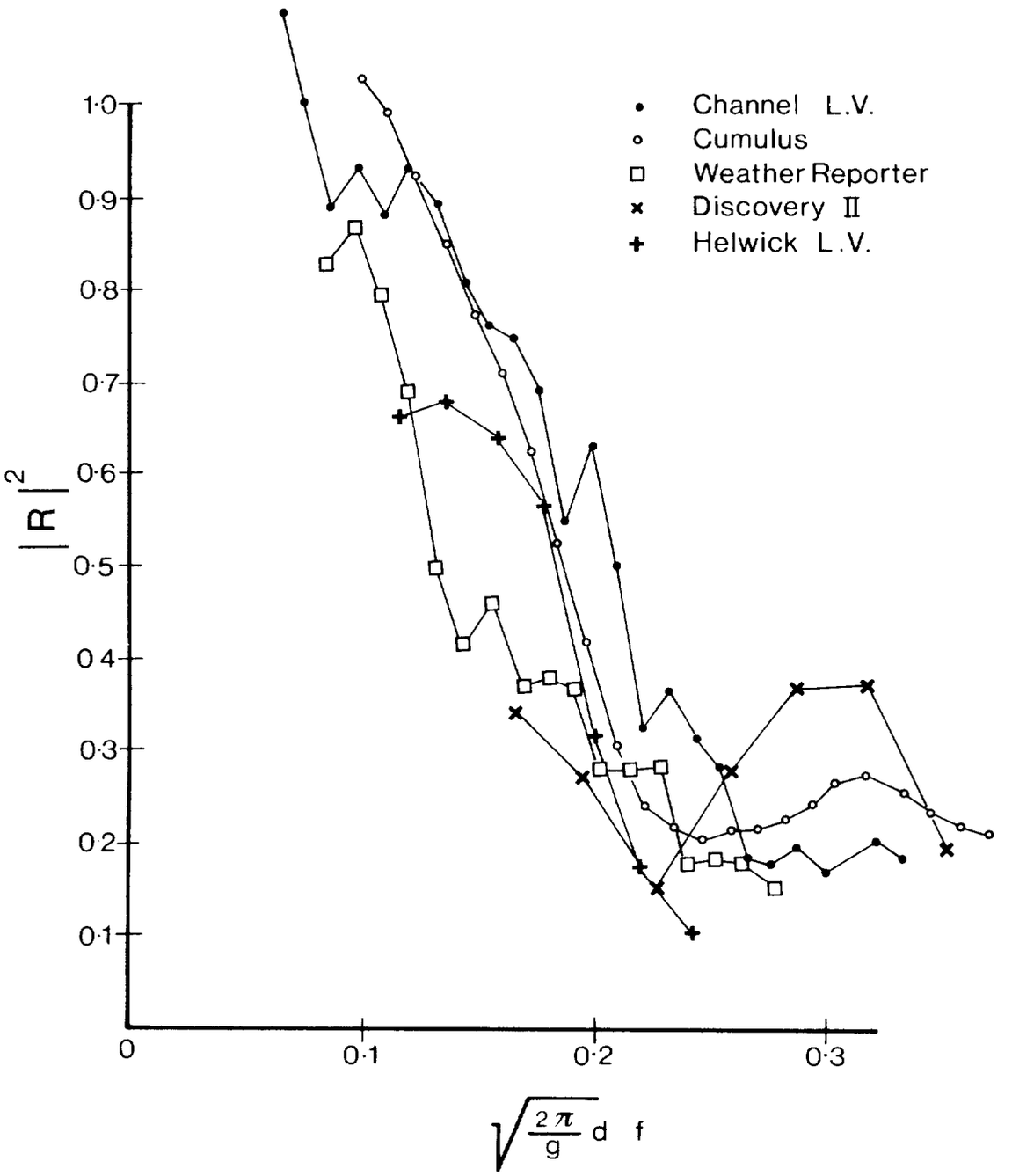

Fig 4.5 $|R|^2$ v_S frequency, nondimensionalised with respect to sensor depth.

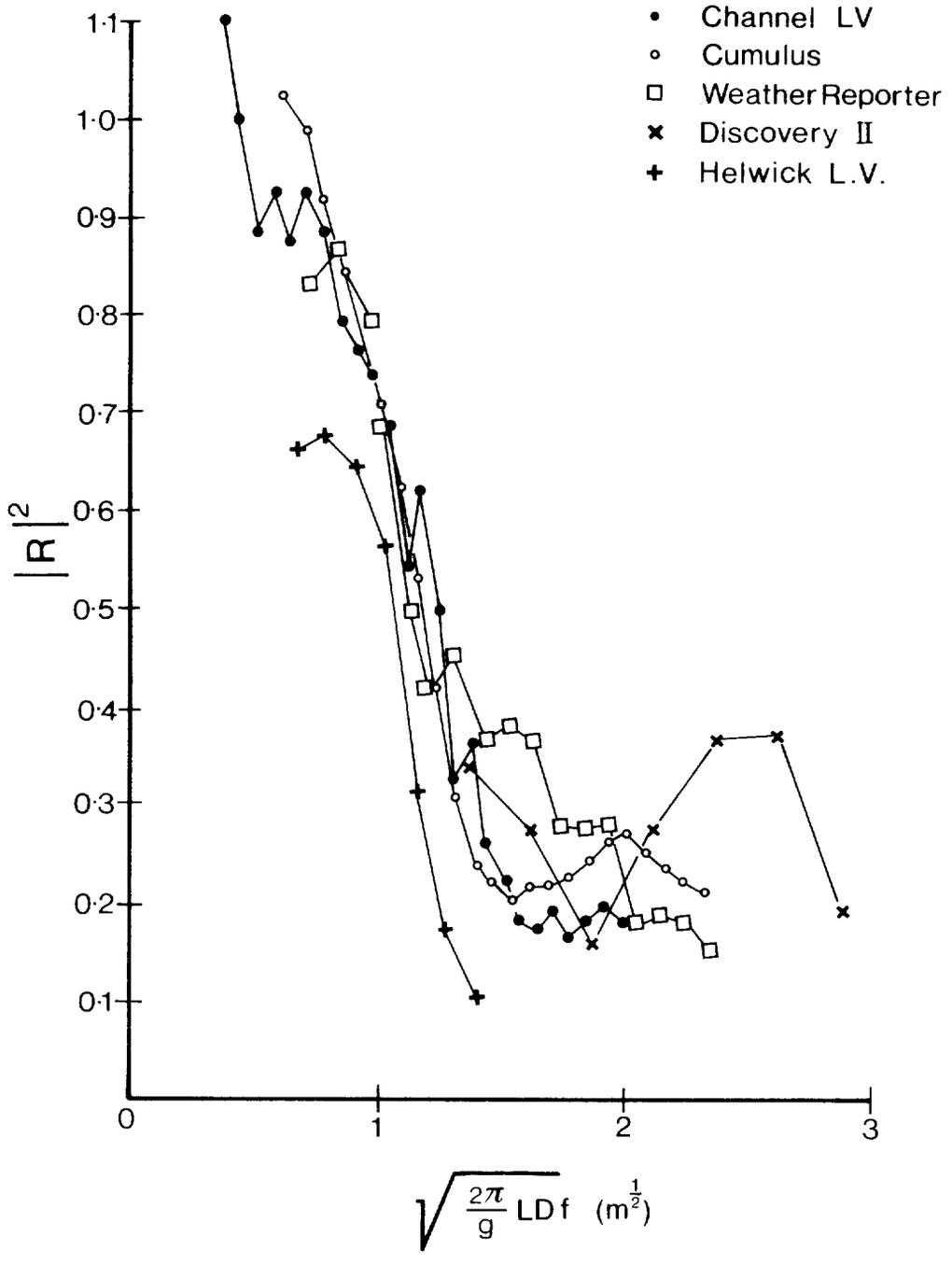

Fig 4.6 $|R|^2$ v_s the dimensional quantity $\sqrt{\frac{2\pi}{g} LD}$ f.

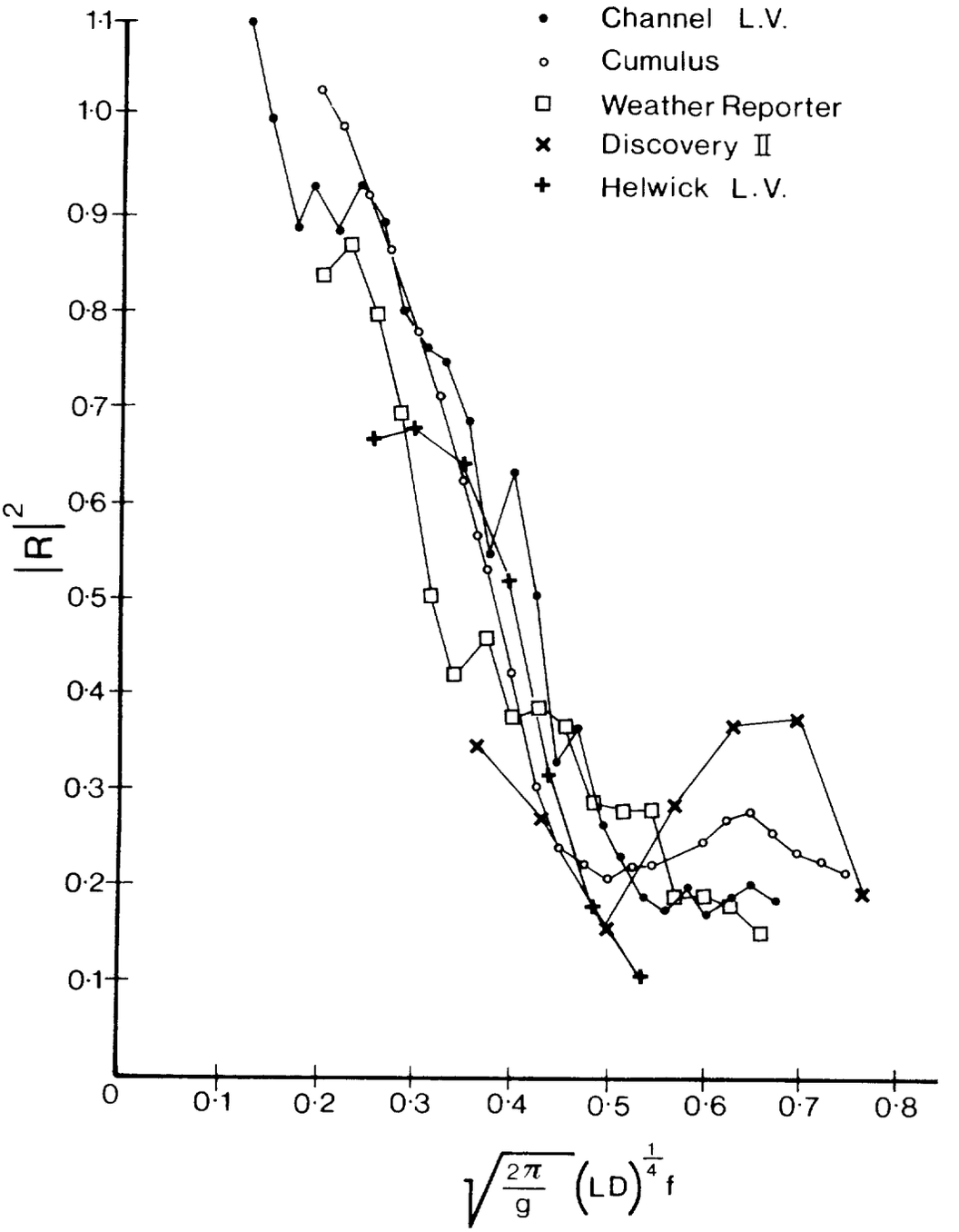

Fig 4.7 $|R|^2$ v_s frequency nondimensionalised with respect to the harmonic mean of sensor depth and shiplength.

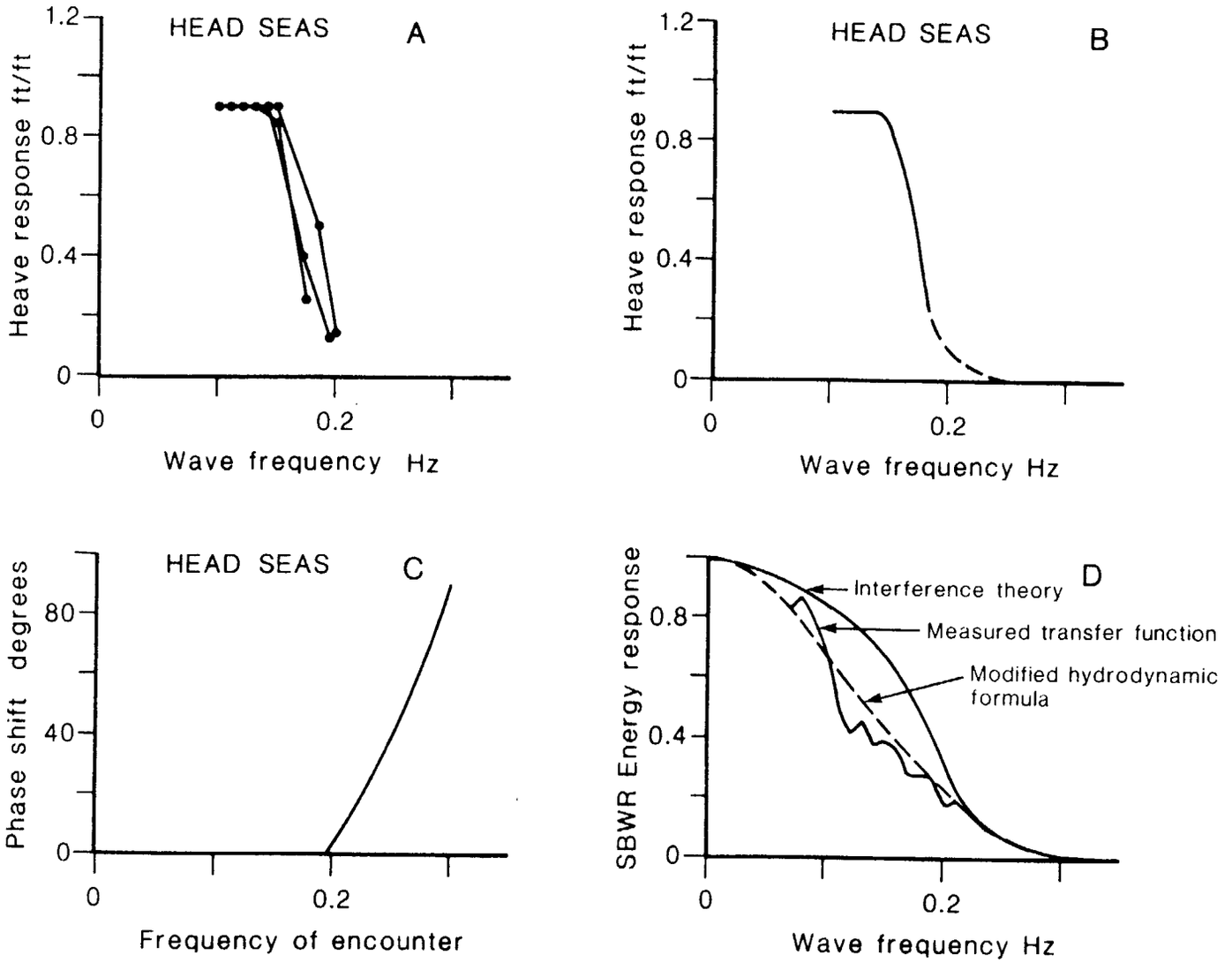

Fig 4.8 The calculation of SBWR Energy Transfer function for OWS Weather Reporter A) shows the measured heave responses which were approximated by the simple curve shown in B). The heave phase shifts shown in C) were included in the calculation. D) shows the interference SBWR theory, the modified hydrodynamic formula, and the measured transfer function.

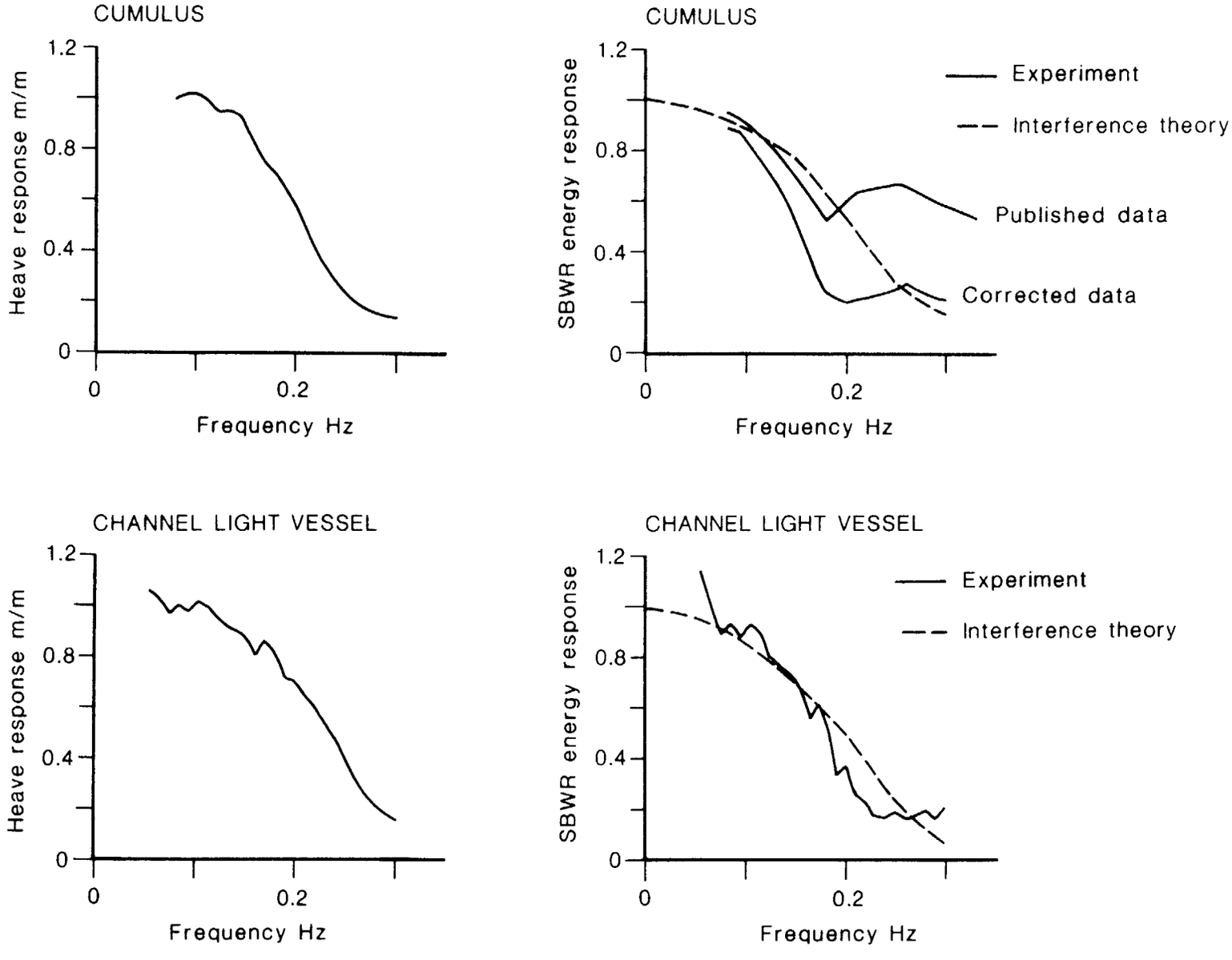

Fig 4.9 Comparison of SBWR Energy Transfer functions calculated using Equation 4.8.8 and measurements. The correction of the Cumulus data is described in appendix 5.

5 CONCLUSIONS

5.1 The accuracy of the Tucker Draper analysis method

Using the same method of analysis as Graham et al, we have found comparable errors in the estimation of H_s from SBWR data. Analysis of the data from the experiment described here indicates that these errors arise as the result of two factors. First the assumed SBWR response provides a poor description of the instrument's behaviour and second the values of T_z extracted from chart records are rather longer than can be accounted for by the instrument's transfer function up to the chart recorder input terminals. The combined influence of these two effects almost cancels so that the use of the empirical constant of 2.5 gives errors of the observed magnitude.

5.2 Frequency response and its dependence on ship's size

The frequency response is not in general of an exponential form so that neither the classical nor the modified hydrodynamic formulae apply universally. It appears that the response of the SBWR depends both upon the size of the ship on which the recorder is mounted and upon the mean depth at which the instrument's transducers are located. In general the low frequency response follows the classical hydrodynamic formula, but as the frequency is raised the response suddenly dips and then flattens out again. Previous experiments mainly involved longer ships for which the sudden dip in response occurs at lower frequencies and this gave rise to the necessity to invoke the modified hydrodynamic formula.

It has been shown in Section 4.3 that scaling laws can be constructed with a certain degree of success, but the choice of which particular formulation is best involves a fine judgement between the level of residual scatter in the scaled data and one's physical prejudice that the appropriate scaling law should involve a nondimensional frequency. The author is of the opinion that in the absence of a sound physical theory capable of explaining the observations, the scaling law shown in Figure 4.6 provides the best way of transferring the available data to other ships. Of course individual field calibrations would be preferable but these are expensive. Nevertheless it might be worth considering such an exercise in the case of those ships where very long data series have been recorded.

5.3 Theory

The existing theory for the instrument does not fit the data with sufficient accuracy to allow the response of a given recorder to be predicted. Nevertheless

some qualitative features of the data are reproduced by a theory which includes the modification of the wavefield in the vicinity of an idealised ship. It may be possible to improve such a theory by using numerical rather than analytical techniques thus allowing a more realistic ship shape to be modelled.

The effects of the direction of approach of the waves with respect to the ship have not been addressed in this report, although there is good theoretical and some empirical evidence to suggest that this is important. Since, in general, the directions of the waves have not been recorded, this may represent an important source of uncertainty in the determination of the response functions, and the application of the response corrections.

6. ACKNOWLEDGEMENTS

The author wishes to thank Trinity House for their permission to carry out the experiment at the Channel lightvessel, and for their help with the logistics of the project.

The analysis of the data and the preparation of this report were funded by the Department of Energy.

REFERENCES

AKEN, H M van and BOUWS, E, 1974. Frequency response of a shipborne wave recorder. Pp 281-300 in, Proceedings of the International Symposium on Wave Measurement and Analysis, New Orleans, 1974, Volume 1.
New York: American Society of Civil Engineers.

CANHAM, H J S, CARTWRIGHT, D E, GOODRICH, G J and HOGBEN, N, 1962. Seakeeping trials on ocean weathership Weather Reporter.
Transactions of the Royal Institute of Naval Architects, 104 447-492.

CARTWRIGHT, D E, 1963. The use of directional spectra in studying the output of a wave recorder on a moving ship.
Pp 203-218 in, Ocean Wave Spectra.
New Jersey: Prentice Hall Inc.

DARBYSHIRE, M, 1961. A method of calibration of shipborne wave recorders.
Deutsche Hydrographische Zeitschrift, 14 57-63.

DRAPER, L, 1967. The analysis and presentation of wave date - a plea for uniformity.
Pp 1-11 in, Proceedings of the 10th Conference on Coastal Engineering, Tokyo, September 1966. Volume 1.
New York: American Society of Civil Engineers.

DRAPER, L, HUMPHREY, J D, and PITT, E G, 1974. The large height response of two wave recorders.
Pp 184-193 in, Proceedings of the 14th Coastal Engineering Conference, Copenhagen, June 1974. Volume 1.
New York: American Society of Civil Engineers.

GRAHAM, C G, VERBOOM, G and SHAW, C J, 1978. Comparison of shipborne wave recorder and Waverider buoy data used to generate design and operational planning criteria.
Pp 97-113 in, Proceedings of the 16th Coastal Engineering Conference, 1978. Volume 1.
New York: American Society of Civil Engineers.

HAINE, R A, 1980. Second generation shipborne wave recorder.
Transducer Technology, 2 (2) 25-28.

HUMPHERY, J D, 1982. Operational experiences with Waverider buoys and their moorings.
Institute of Oceanographic Sciences Report. No. 145, 33pp.

KORVIN-KROUKOVSKY, B V and JACOBS, W K, 1957. Pitching and heaving motions of a ship in regular waves.
Pp 590-632 in, Proceedings of the Annual Meeting of the Society of Naval Engineers, New York, November, 1957.

STOKER, J J, 1957. Water waves: Vol 4 of Pure and Applied Mathematics.
New York: Interscience.

TANN, H M, 1976. The estimation of wave parameters for the design of offshore structures.
Institute of Oceanographic Sciences Report, No 23, 29pp.

TUCKER, M J, 1952. A wave recorder for use in ships.
Nature, 170 657-659.

TUCKER, M J, 1956. A shipborne wave recorder.
Transactions of the Royal Institution of Naval Architects, 98, 236-250.

TUCKER, M J, 1959. The accuracy of wave measurements made with vertical accelerometers.
Deep Sea Research, 5, 185-192.

TUCKER, M J, 1961. Simple measurement of wave records.
Pp 22-23 in, Proceedings of the Conference on Wave Recording for Civil Engineers.
Wormley UK: National Institute of Oceanography.

URSELL, F, 1954. Water waves generated by oscillating bodies.
Quarterly Journal of Mechanics and Applied Mathematics, 7, 427-437.

APPENDIX 1 CALIBRATION OF SENSORS AND ASSOCIATED ELECTRONICS

A1.1 Waverider calibration : summary

The Waverider signal was conditioned by double integrating circuits in the buoy; by modulation and demodulation circuits in the radio transmitter and receiver, and by interface electronics placed between the receiver and the data logger (see Figure A1.1). Each of these stages of signal processing was calibrated in the following way. Firstly the buoy and receiver were calibrated in isolation from the interface and data logger. Then a radio signal of known characteristics was injected into the receiver and the resulting signals at the inputs of the interface and data logger were measured allowing the sensitivities of both the receiver and the interface to be determined. Lastly the sensitivity of the data logger was measured, both using a monitor facility incorporated into the logger, and also by checking that the data written onto tape corresponded to the voltage presented at the data logger input.

A1.1.1 Buoy and receiver calibration

The Waverider buoy and Warep receiver used during the experiment were calibrated using a 3 m rotating arm rig. The buoy was clamped in a cradle suspended between two parallel bars which were supported at their midpoints on bearings. A variable speed motor was connected by belt drives to the parallel bars in such a way that the buoy could be driven, as a preselected speed, through a vertical circle of 3 m diameter. An arrangement of chain drives and sprockets maintained the vertical orientation of the buoy. Thus, with the apparatus maintained at a fixed speed of rotation, the buoy transmissions, received at a nearby receiver, corresponded to the sinusoidal variation of the buoy's vertical position.

Prior to making measurements, the buoy electronics were energised, and the receiver and a precision chart recorder connected to its analogue output were switched on. The rotating arm was set in motion at 3.33 rpm and the system left for 20 minutes to settle down. The calibration of the precision chart recorder was then checked using a standard DC voltage source. Then 20-30 cycles of the signal at the receiver's analogue output were recorded. This procedure was repeated at a number of rotational speeds; in each case sufficient time was allowed between recordings for any transients arising from the change in speed to die away. The rotational speeds used corresponded to frequencies in the range 0.28-0.025 Hz. The rotational speed of the calibration rig was measured by timing a number of revolutions using a stop watch.

It should be noted that the frequency response of the Warep receiver is governed by the characteristics of the phase locked loop used to detect the frequency modulated Waverider subcarrier. The analogue output of the receiver is such that the detector's sensitivity is enhanced at high frequency while the internal chart recorder's effective response remains constant. We have found that the frequency response of the phase locked loop, as measured at the analogue output of the Warep, is affected by the motion of the pen arm in the internal Warep chart recorder. So long as the pen arm is allowed to move freely, the response at the analogue output is in reasonable agreement with the specification supplied in the manufacturer's hand book. However, with the pen arm clamped a different response is obtained. For this reason the calibrations and the experiment at sea were both conducted with the Warep's pen arm free to move.

The average Waverider and receiver sensitivity was obtained from the calibration measurements as follows. The amplitude of the recorded sinusoidal trace corresponding to each rotational speed was obtained by averaging measurements of ten consecutive crest to trough heights. (This procedure reduces errors due to any variation of the mean value of the output during the measurement.) The average value thus obtained was corrected for the double integrator and phase locked loop amplitude responses using the response data specified in the manufacturer's handbooks. The corrected values at each frequency were then averaged to produce the average output voltage corresponding to 3 m of vertical displacement of the buoy.

A1.1.2 Receiver, interface and logger calibration

The calibration of the receiver, the Waverider interface and the data logger was carried out using a test signal whose frequency could be swept from 241.34 Hz to 276.22 Hz with great accuracy. The sweep rate was controlled in such a way that a linear sweep from 241.34 Hz to 276.22 Hz was executed in 6 seconds, the frequency was then held constant for 2 seconds and then linearly swept from 276.22 Hz back to 241.34 Hz in 6 seconds. After maintaining the lower frequency for a further 2 seconds the process was repeated automatically. Thus by amplitude modulating a 27 MHz carrier with this test signal and receiving the transmissions using a Warep, an output signal as illustrated in Figure A1.3 was obtained. With the receiver, interface and logger connected together as shown in Figure A1.2, a previously calibrated precision chart recorder was used to measure the signals at the Warep analogue output and the interface output. In addition the data logger's integral monitor display was used to measure the maximum excursion of the logger

input signal both with and without the precision chart recorder connected. Finally, a short section of tape was recorded to confirm that the use of the data logger's monitor facility had no effect upon the recorded data.

A1.2 SBWR Calibration

The SBWR used in this experiment was arranged as shown in Figure A1.4. The normal SBWR output was synthesised from the raw transducer signals using analogue circuits within the SBWR itself. In addition signals derived from each of the SBWR sensors were processed using additional electronics contained within a purpose built interface unit. Thus, for each sensor two separate signal paths had to be calibrated giving the response both at the normal output as well as the response at the appropriate individual sensor output.

A1.2.1 Accelerometer calibration

The SBWR accelerometers, together with their associated electronics, were calibrated using a 1 m diameter rotating arm apparatus. The apparatus similar in principal to the rotating rig used to calibrate Waverider buoys, was used to drive each accelerometer in turn through a vertical circle of 1 m diameter. All calibrations were carried out using a rotational speed of 5 RPM (.0833 Hz) and the resulting signals at the data logger input were measured using a previously calibrated precision chart recorder. The voltage swing at each output was estimated by averaging 10 consecutive peak to trough measurements from each chart record. The resulting values for the voltage swing at each output were then corrected by a factor of 1.018 in order to allow for the reduced equivalent response of the double integrating electronics at 0.0833 Hz.

A1.2.2 Pressure channel calibration

Signals derived from the SBWR pressure transducers are high pass filtered in the SBWR and interface electronics. As a result, static calibration of the system as a whole is not feasible. In view of the practical difficulties associated with generating standard low frequency pressure variations, the usual calibration method was adopted. This procedure is carried out in two stages; first each sensor is calibrated in isolation by making static measurements against a calibrated strain gauge manometer. The AC electrical gain of each highpass filter is then determined using a sinusoidal signal generator and precision pen chart recorder to measure input and output AC voltages. The calibration results are summarised in Tables A1.3-A1.5.

Table A1.1 Waverider calibrations

	Receiver Sensitivity V/Hz	Buoy Sensitivity Hz/m	Buoy and Receiver V/m	Interface Gain	System Sensitivity V/m
Before	0.5394	1.845	0.9952	0.09943	0.09895
After	0.5322	1.862	0.9910	0.10160	0.10068
Mean					0.09982

The logger sensitivity was 1 digit/mV

Table A1.2 SBWR Accelerometer Calibration

Transducer	Time	Norm O/P Voltage Swing mV	Interface O/P voltage mV	Norm O/P calibration factor	Interface O/P factor	Ref Oscillator voltage
Port Accelero-meter	Before	34.24	67.16	34.86	68.37	7.07
	After	32.75	63.15	33.34	64.29	7.01
Starboard Accelero-meter	Before	33.68	64.66	34.29	65.82	7.07
	After	31.89	62.32	32.46	63.44	7.01

Note

The calibration carried out after the experiment was conducted with the reference oscillator voltage 1% below nominal. The drift in voltage is probably due to a change in form factor arising from the experimental arrangement used in the laboratory. No attempt has been made to correct the calibration results for this drift.

Table A1.3 Pressure Transducer Calibrations

Transducer	Time	Sensitivity mV/m seawater	Ref osc volts
Port pressure	Before	333	7.07
Transducer	After	321	7.01
Starboard pressure	Before	333	7.07
Transducer	After	329	7.01

Table A1.4 High Pass Filter Gains

Filter	Time	Gain	Frequency Hz	Corrected Gain
Port Interface	Before	0.200	0.159	0.201
	After	0.203	0.159	0.204
Starboard Interface	Before	0.200	0.159	0.201
	After	0.205	0.159	0.206
SBWR High Pass Filter	Before	1.00	0.159	1.005
	After	1.03	0.159	1.008

Logger sensitivity was 1 mV/digit on all channels

Table A1.5 Overall Calibration Factors

Channel	Calibration factors
Port Accelerometer Channel	66.33 mV/m
Starboard Accelerometer Channel	64.63 mV/m
Port Pressure Channel	66.28 mV/m
Starboard Pressure Channel	67.34 mV/m
Normal SBWR output	33.74 mV/m

Overall system calibration factors for the individual sensors and their associated electronics were obtained by forming the average of the factors derived from the precalibration and from the postcalibration. In the case of the normal SBWR output it is assumed that the synthesised signal at the output is dominated by contributions derived from double integrated accelerometer signals. Thus the normal output calibration factor was obtained by averaging the calibration factors appropriate for the port and starboard accelerometer units as measured at the normal output. Precalibration and postcalibration values of this quantity were averaged to give the overall calibration factor.

A1.3 Ship Motion Sensor Calibration

A1.3.1 Heave channel calibration

The heave sensor used in the experiment was detached from its rather bulky gyro stabilised platform and mounted in the rotating arm apparatus used to calibrate the SBWR heave sensors. The calibration was conducted in the same manner as were the SBWR heave sensor calibrations. However, the gyro stabilised heave sensor, together with it's associated double integrator, displayed considerable low frequency instability which was apparent in the recorded output as a low frequency variation in the mean output. The magnitude of the low frequency noise varied according to the rotational speed of the calibration apparatus, and at 5 RPM corresponded approximately to 20 cm RMS variation in the accelerometer's position. For this reason, less confidence can be placed in the calibration factor for this sensor than can be placed in the factors derived from the SBWR calibrations.

Table A1.6

Calibration	Factor at 5 RPM	Frequency Response at 5 RPM	Corrected Factor
Heave sensor precalibration	69.38 mV/m	1.018	70.63
Heave sensor postcalibration	68.33 mV/m	1.018	69.56
Mean			70.09

A1.3.2 Pitch and roll sensor calibration

The pitch and roll sensor used in this experiment measured angular displacements with respect to a tied gyro. The gyro control was affected by mercury switches together with a pair of orthogonal torque motors which were interconnected in such a way that the gyro's axis of symmetry was maintained in the vertical direction. Thus on long time scales the pitch and roll measurements are referred to the direction of the local gravity vector rather than to an inertial reference frame, while for short time scales the platform is designed to behave as an inertial reference frame.

A. Gyro stability

Prior to calibrating the sensor, tests were carried out to assess the stability of the reference gyro. The instrument was placed on a level table and the gyro run up. The instrument was allowed to settle for some minutes and was then placed upon an inclined plane in such an orientation that the net rotation was about one sensor axis. The time evolution of the signal derived from the orthogonal sensor was recorded. Such measurements were conducted with angular displacements from 10° to 25° with rotations being performed about each sensor axis in turn. The results are summarised in Figures A1.5 and A1.6. As the signal which was measured corresponded to a sensor which had experienced no rotation, any signal detected must indicate a drift in the reference gyro. As can be seen from both diagrams, displacements in excess of 15° give rise to an approximately constant rate of rotation of the reference about the relevant sensor axis, moreover the rate of drift increases rapidly with the angular displacement of the sensor. Thus measurements made with static displacements in excess of 15° are subject to significant systematic errors.

B. Calibration method

The gyro stability measurements suggest that at inclinations in excess of 15° the reference gyro is set into motion when the instrument is inclined. In order to obtain a greater range of calibration displacements than ± 15° the following calibration procedure was adopted.

The roll sensor was connected to a digital data logger in the same configuration as was used during the experiment. The sensor was placed on a level table and allowed to settle for some minutes. It was then placed on an inclined surface set at a preset angle and the roll signal was measured after allowing 2-3 seconds. This

delay is sufficient to allow any electronic transients to decay. It is believed that for inclinations up to 20° the gyro reference remains reasonably stable over this time period and that this method provides the best static calibration available for the type of sensor used. The pitch sensor was calibrated in the same way and both sensors were calibrated both prior to the experiment and after its conclusion. The calibration curves are shown in Figures A1.7-A1.10. It should be noted that the measurements plotted in Figures A1.9 and A1.10 were carried out in two stages. The table was levelled approximately and a series of measurements made with positive angular displacements. Then the sensor unit was rotated through 180° about the gyro axis and a series of measurements made at the same table positions but with negative angular displacements. Thus the discontinuity at the origin in Figures A1.9 and A1.10 indicates that when the table was nominally level, it was in fact inclined at a small angle to the horizontal. Allowance has been made for this when deriving calibration factors from these curves. In the case of the calibrations conducted before the experiment, no such discontinuity can be seen, indicating that the table used was accurately level.

C. Calculation of calibration factors

Calibration factors were calculated from the above data by regressing angle upon signal. The slope of the regression being taken as the appropriate calibration factor. In the case of the data shown in Figures 3.6 and 3.7, the data for $\theta > 0$ and $\theta < 0$ were treated separately and the average value of each pair of regression slopes was taken as the calibration factor. The average of precalibration and postcalibration factors was used to correct the measured data.

Table A1.7 Regression coefficients for pitch/roll sensor calibrations

Sensor	N	Calibration	Regression of signal on θ		Regression of θ on signal		Correlation Coefficient
			Slope mV/deg	Intercept mV	Slope deg/mV	Intercept deg	
Pitch	9	Pre cal, all θ	34.6	-7.7	0.0288	+0.22	0.99988
Pitch	5	Post cal, θ > 0	32.9	-6.7	0.0304	+0.21	0.99982
Pitch	8	Post cal, θ < 0	33.4	-43.6	0.0300	+1.30	0.99972
Roll	9	Pre cal, all θ	33.9	+4.9	0.0295	-0.14	0.99953
Roll	4	Post cal, θ > 0	34.5	-27.1	0.0290	+0.79	0.99999
Roll	5	Post cal, θ < 0	32.6	-46.2	0.0306	+1.41	0.99982

Table A1.8 Calibration factors for pitch and roll sensors

Sensor	Pre Calibration Factor	Post Calibration Factor	Mean	Drift %
Pitch	0.0288 deg/mV	0.0302 deg/mV	0.0295 deg/mV	+4.8
Roll	0.0295 deg/mV	0.0298 deg/mV	0.0297 deg/mV	1.1

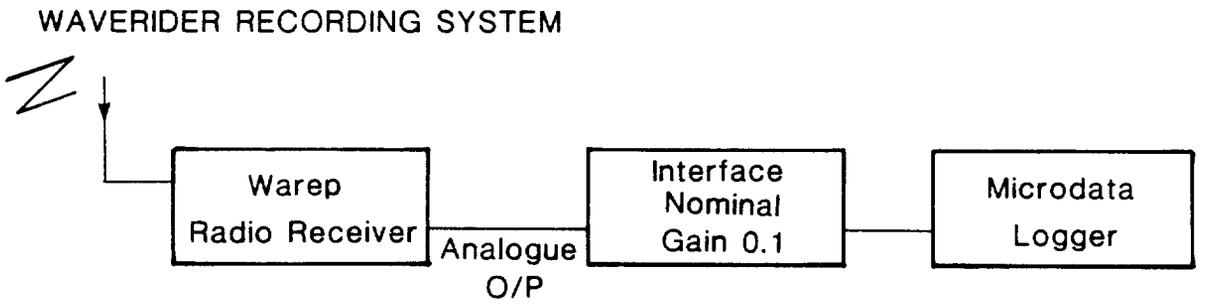

Fig A1.1 Waverider recording system

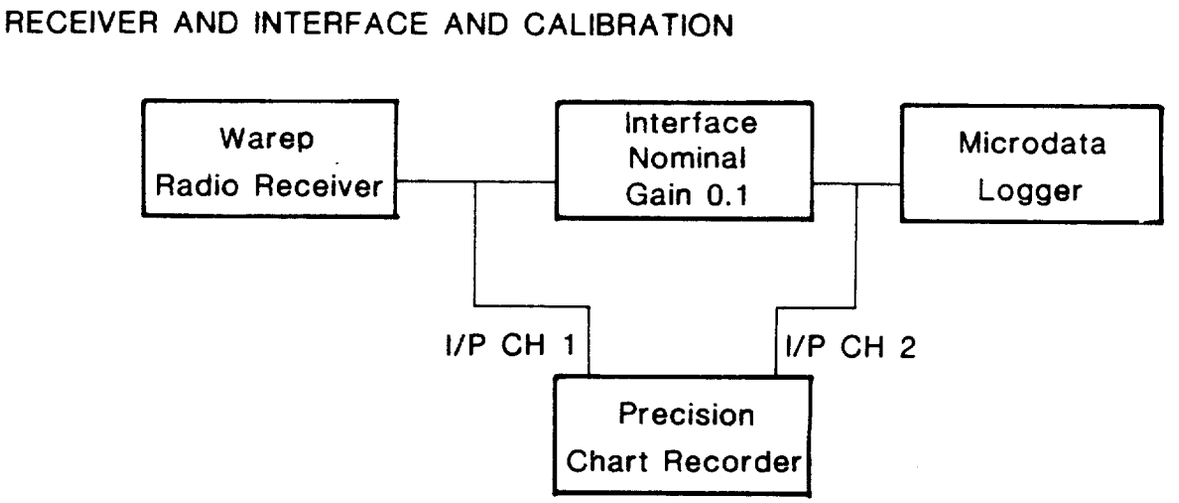

Fig A1.2 Receiver and Interface calibration

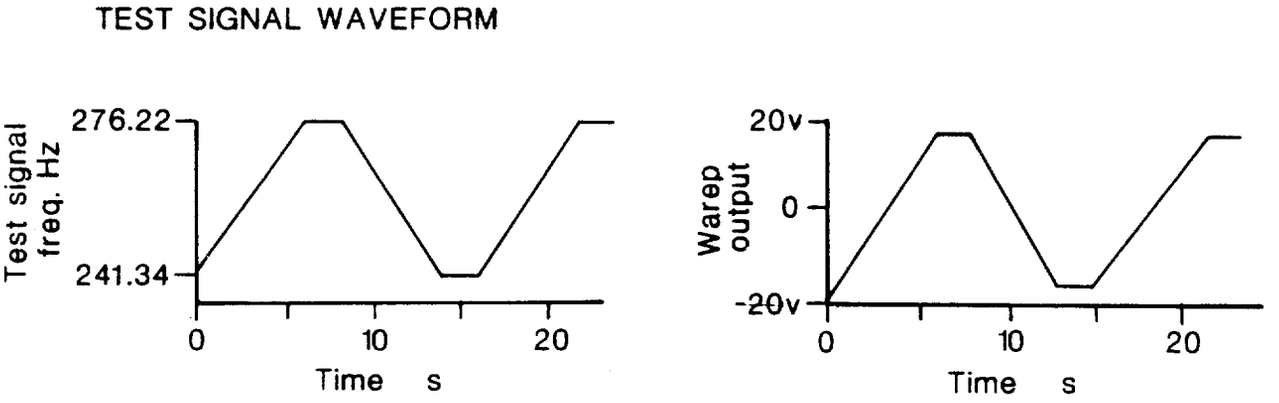

Fig A1.3 Test signal wave forms

4 CHANNEL SHIPBORNE WAVE RECORDER ELECTRONICS

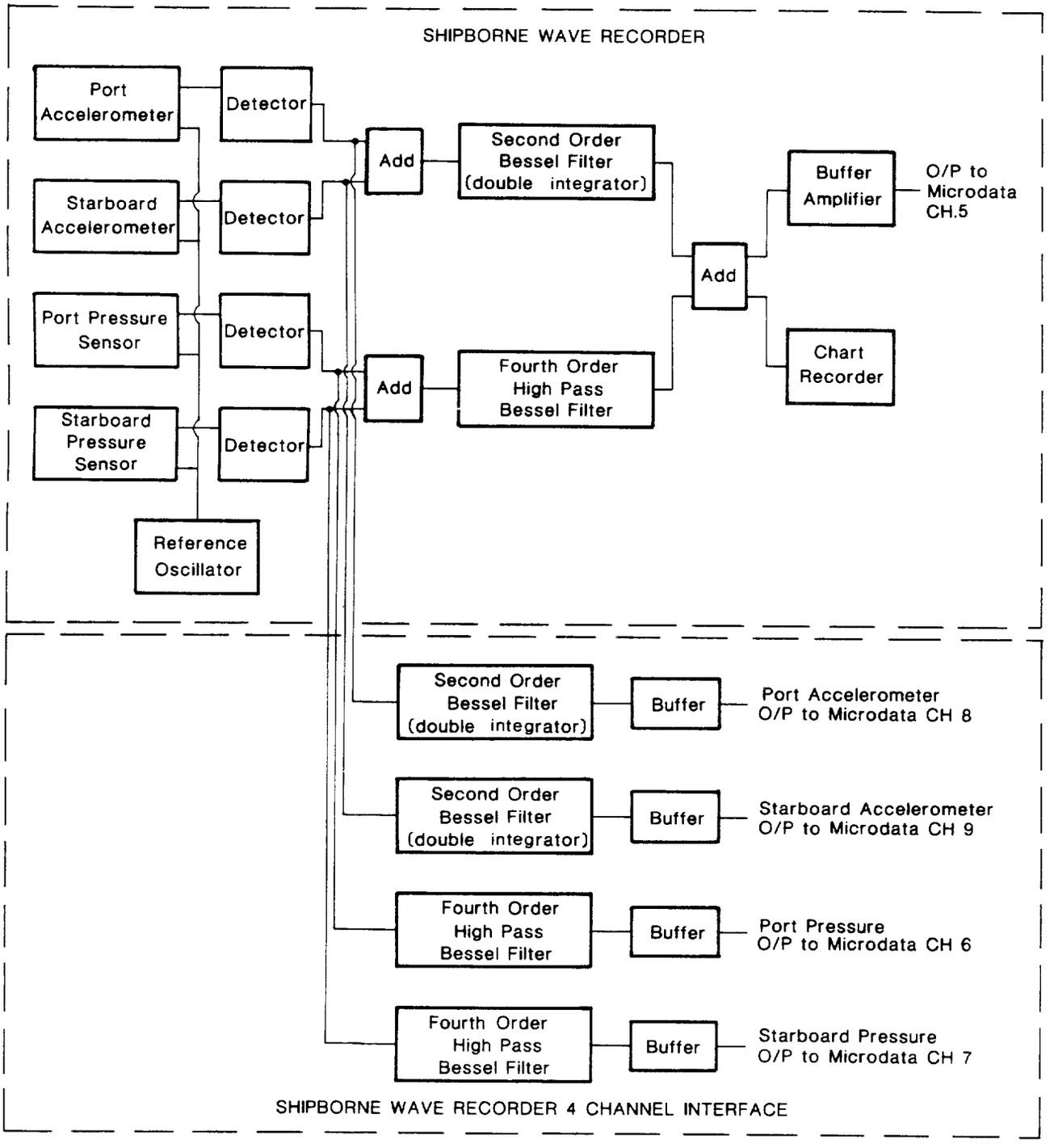

Fig A1.4 4 Channel SBWR

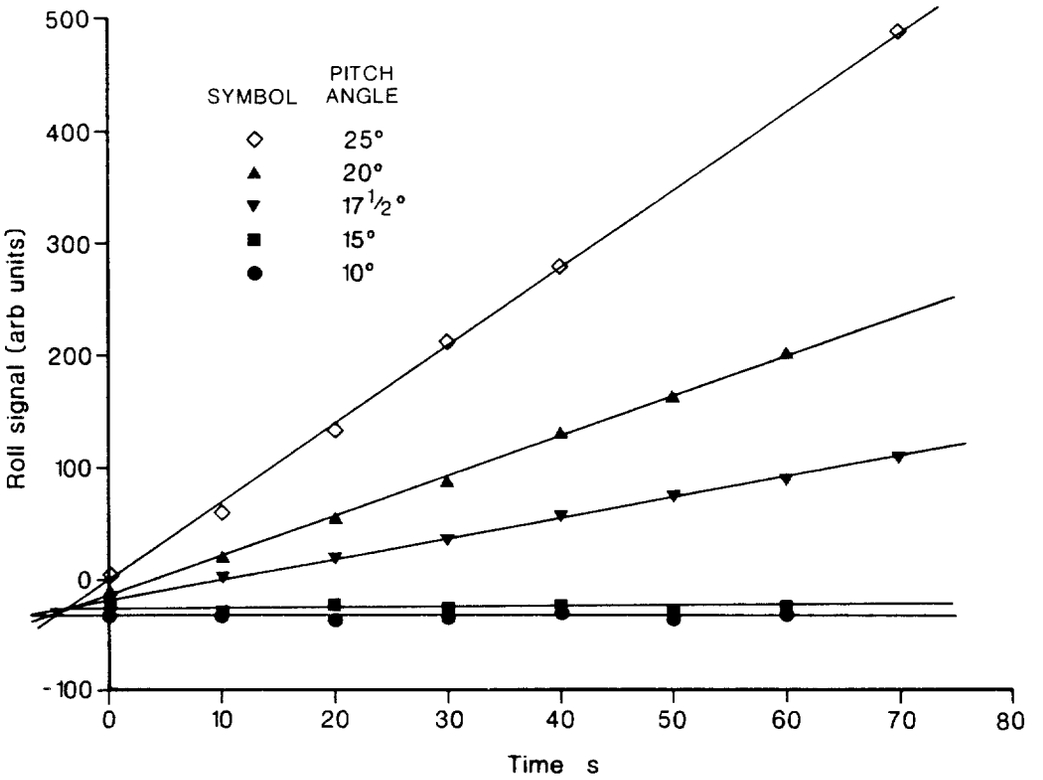

Fig A1.5 Time variation of roll sensor output following a sudden change in pitch

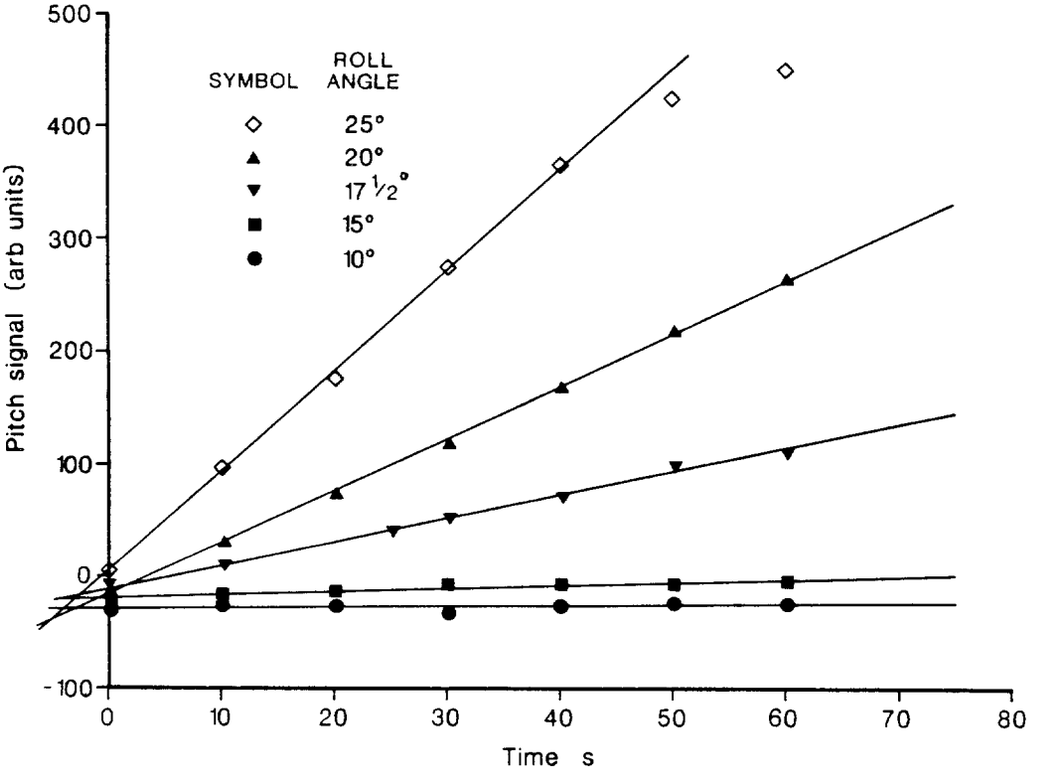

Fig A1.6 Time variation of pitch sensor output following a sudden change in roll

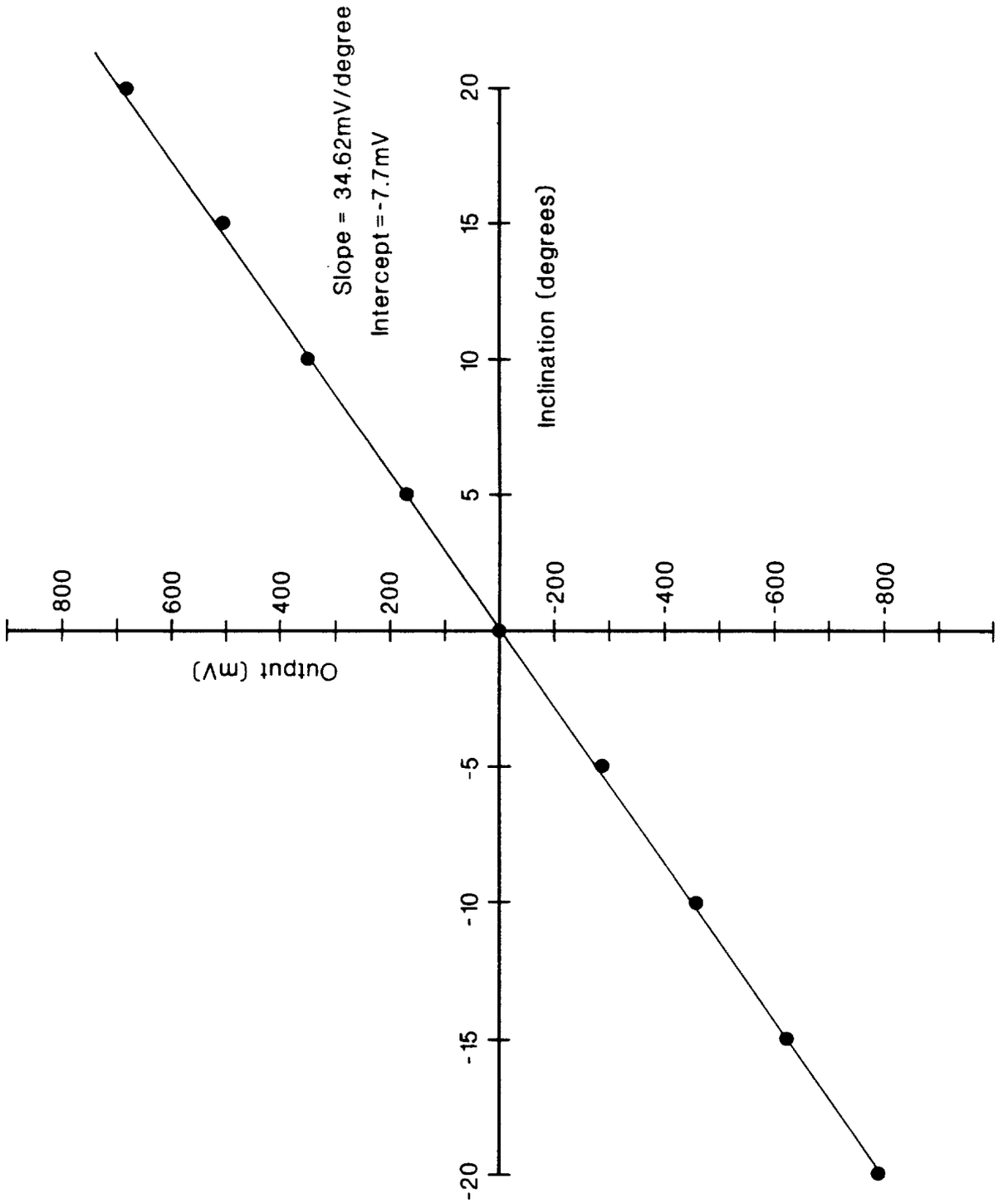

Fig A1.7 Pitch sensor calibration prior to experiment

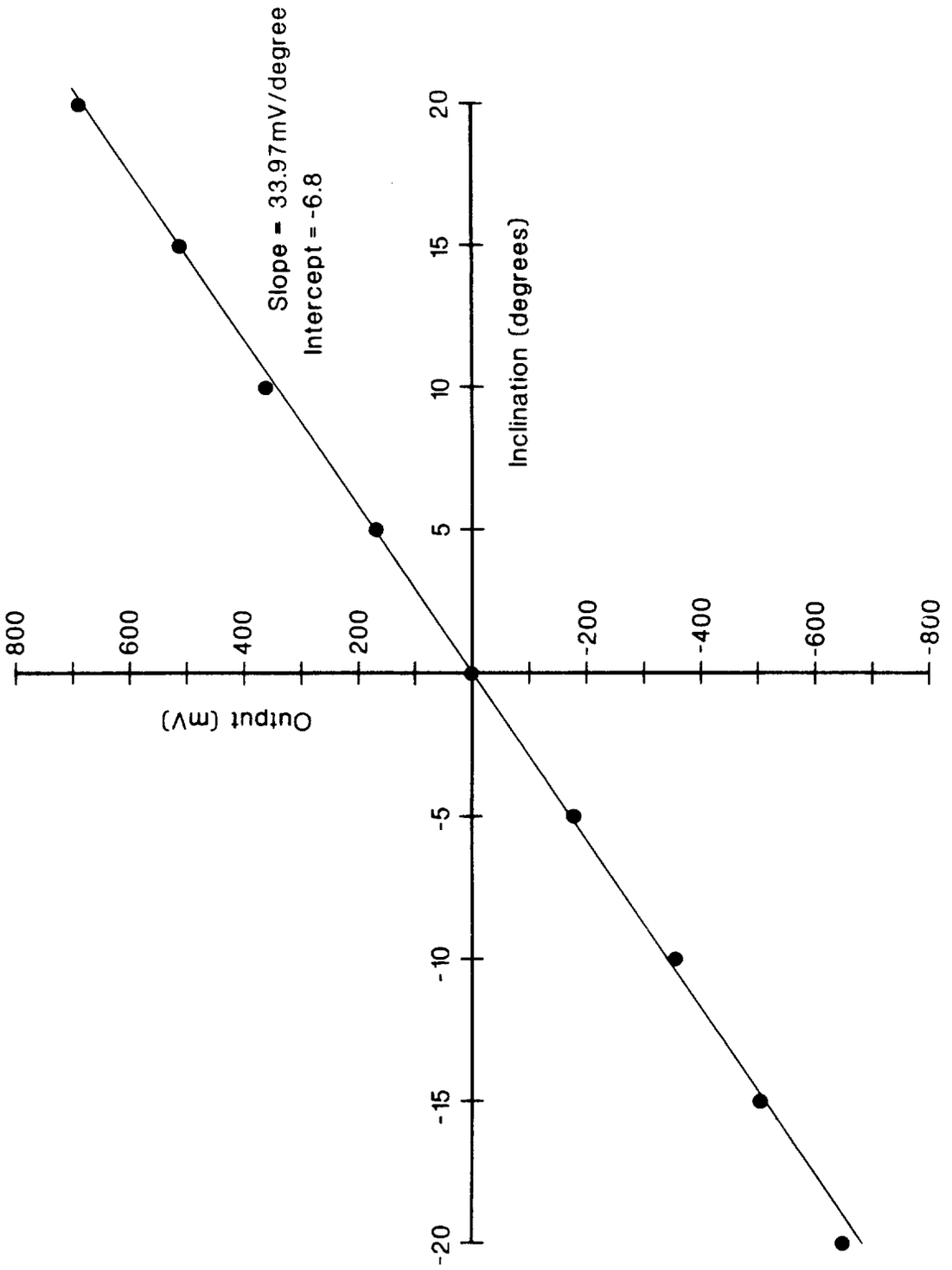

Fig A1.8 Roll sensor calibration prior to experiment

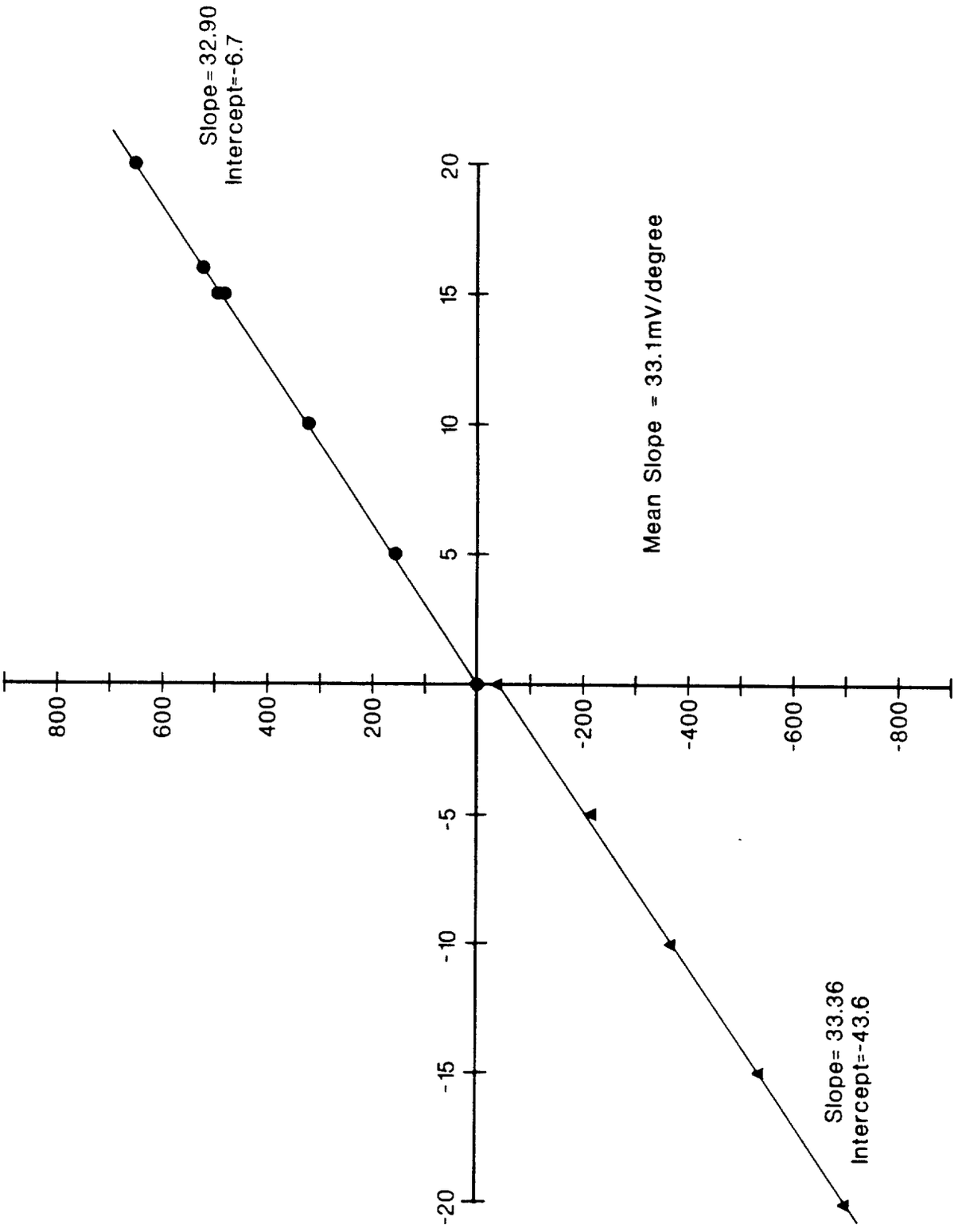

Fig A1.9 Pitch sensor calibration after the experiment

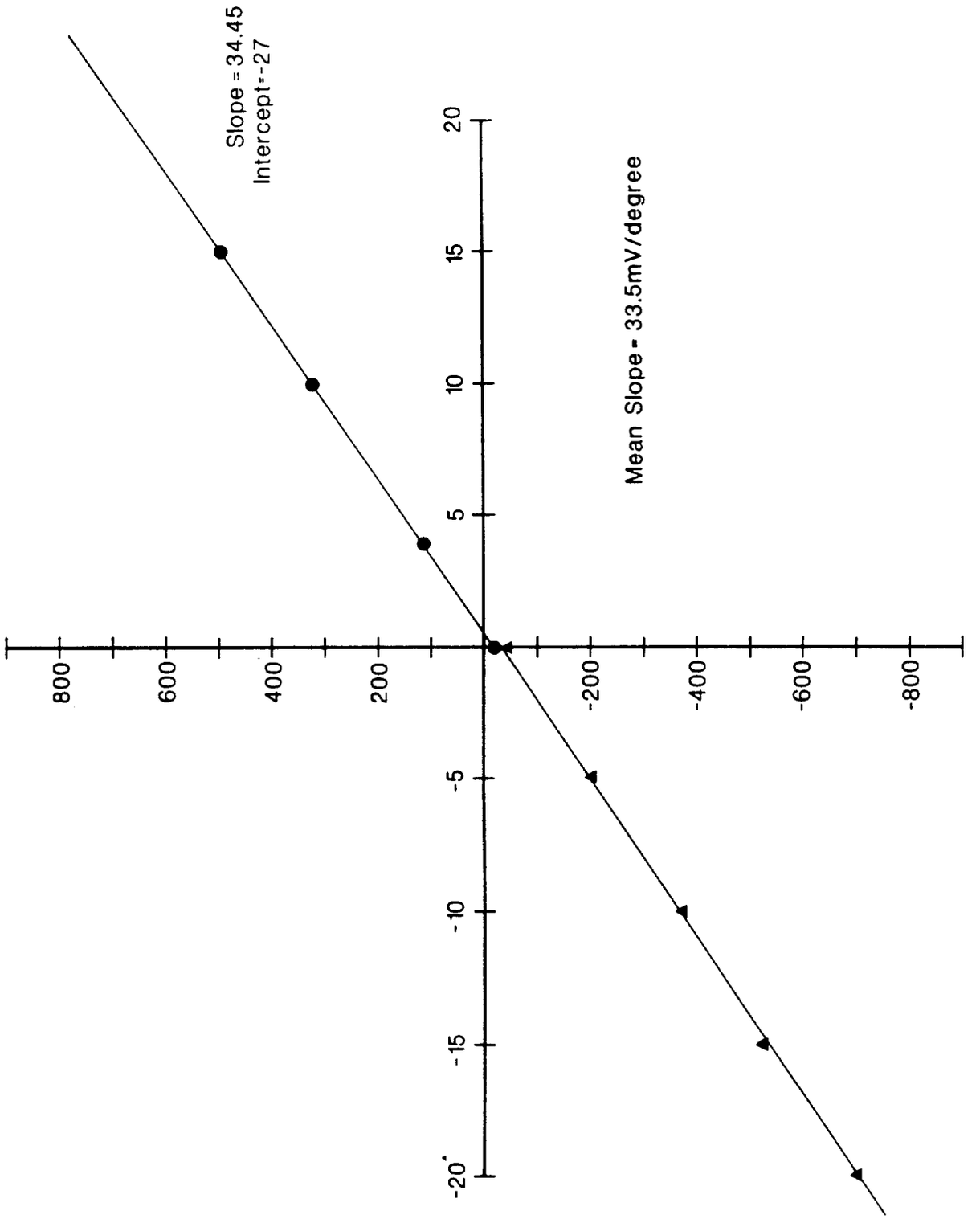

Fig A1.10 Roll sensor calibration after the experiment

APPENDIX 2 EXPERIMENTAL ARRANGEMENTS

A2.1 Data acquisition and recording

The data described in this report were measured using a modified Mk 2 SBWR, a Waverider buoy and a set of commercially available ship motion sensors. The general electronic arrangement is shown in block diagram form in Figure A2.1. The signals derived from each sensor were conditioned by analogue circuits and then digitised and recorded using a standard data logger. In this appendix details are given of the signal conditioning electronics, and in particular the frequency response characteristics of the electronics associated with each signal are described.

A2.2 The SBWR system

The SBWR used in the experiment was a solid-state version of the instrument which is described by Haine (1980). It was modified so that signals derived from each of the instrument's transducers were available separately as well as the usual SBWR output. The transducers, which are described by Tucker (1956), were mounted approximately amidships on the recording vessel, at a depth of 2.2 m below the water line. The overall beam at this point was about 8 m and the accelerometers, which are somewhat inboard of the ship's side, were separated by 7.2 m athwartships.

The SBWR accelerometers consist of a seismic mass which is mounted on a spiral spring and connected mechanically to a linear differential transformer type of displacement sensor. The mass-spring system is designed to be resonant at 4 Hz and is surrounded by oil of such a viscosity that it is critically damped. Thus the transducer is expected to have a flat frequency response over the frequency range in which it is operated. The accelerometers are mounted in gimbals so that each is able to maintain its axis parallel to the local vertical. This arrangement is equivalent to a short pendulum mounting.

The pressure transducers which are mounted on the inside of ship's hull are connected to the surrounding water by a hole drilled through the side of the ship. The pressure in the water adjacent to the sensor's face is transmitted via a flexible membrane backed with oil to a flexible capsule. The face of the capsule moves in response to pressure variations and is connected by a rod to a displacement sensor similar to that used in the accelerometers. The author has found no information concerning the mechanical frequency response of the pressure sensors,

but there is no reason to believe that it should be inferior to the accelerometer's response.

In Figure A2.2 the SBWR electronics are shown in block diagram form.

Each of the second order Bessel filters, which are included in the accelerometer channels, is equivalent to a perfect double integrator in series with a fourth order high pass filter with a theoretical response given by:

$$H_1(S) = \frac{S^4}{(S^2 + \alpha_1\omega_1 S + \omega_1{}^2)(S^2 + \alpha_2\omega_2 S + \omega_2{}^2)}$$

where

$\alpha_1 = 1.916$ $\alpha_2 = 1.241$

$\omega_1 = 0.09498$ rad/s $\omega_2 = 0.1065$ rad/s

The pressure channels include fourth order high pass Bessel filters designed to match the equivalent response of the double integrators. The theoretical response of these filters is given by:

$$H_2(S) = \frac{S^4}{(S^2 + \alpha_1\omega_1 S + \omega_1{}^2)(S^2 + \alpha_2\omega_2 S + \omega_2{}^2)}$$

where

$\alpha_1 = 1.926$ $\alpha_2 = 1.244$

$\omega_1 = 0.09441$ $\omega_2 = 0.1026$

The response of each filter was measured in the laboratory by injecting a signal of known amplitude and phase into the filter and measuring the resulting output on a precision hot wire chart recorder. The normalised measured responses,

together with the theoretical response curves are shown in Figures A2.3-A2.10. It should be noted that the double integrator responses have been normalised with respect to a perfect double integrator rather than unity.

A2.3 Ship motion measurements

Ship motion measurements were made using a Colnbrook pitch/roll/heave sensor package, mounted 2.5 m forward of the SBWR transducers on the ship's centre line. The sensor consists of a gimballed platform which is stabilised by a gravity-tied gyro. In this type of platform, mercury switches, mounted upon the platform, are used to actuate electromagnetic erection motors, whose action ensures that the platform is maintained in a horizontal position. The ship's vertical acceleration was measured using an accelerometer mounted upon the stabilised platform. Pitch and roll signals were derived from potentiometers mounted in the gimbals' bearings.

A2.3.1 Heave measurements

The accelerometer used to make heave measurements was a Schaevitz type A410 inductive accelerometer. This transducer detects the motion of a seismic mass mounted on spider diaphragm springs. The mass is resonant at 32 Hz and is damped with a silicon fluid in such a way that the damping ratio is approximately 0.5. Thus the mechanical response of the transducer is expected to be flat over the whole spectrum of wave frequencies.

The accelerometer was connected in an A.C. bridge circuit, energised by a 2 KHz sinewave oscillator as shown in Figure A2.11. The inductors L_1 and L_2 vary differentially according to the position of the slug mounted on the accelerometer springs, while R_1 and R_2 are the equivalent series losses in L_1 and L_2 and, at the working frequency, vary only slightly with acceleration. Assuming that the accelerometer itself is linear, L_1 and L_2 are given by

$$L_1 = L(1 + \alpha)$$

$$L_2 = L(1 - \alpha) \qquad \text{A2.1}$$

where α is proportional to the absolute acceleration.

In this case, assuming $R_1 = R_2 = R$ for simplicity, the bridge output is given by

$$V_{out} = -V_{osc} \left\{ \frac{R_4(R_4R_6+R_4R_5+R_5R_6)(R+j\omega L(1+\alpha))-R_3(R_4R_6+R_4R_5)(R+j\omega L(1-\alpha)}{2R_3R_4R_6(R+j\omega L)} \right\}$$

The bridge is balanced for zero (in practice for minimum) output with $\alpha=0$ by adjusting the ratio R_3/R_4 with the accelerometer axis horizontal.

The output is then given by

$$V_{out} = -V_{osc} \left\{ \frac{j\omega L\alpha(R_4R_6+R_4R_5+R_5R_6)}{(R+j\omega L)R_3R_6} \right\} \qquad \text{A2.2}$$

In practice Vout is measured by rectifying and low pass filtering the bridge signal. The resulting dc offset voltage generated by the acceleration due to gravity is inconvenient, so in the practical circuit an additional rectifier and filter, connected directly to the bridge supply, is used to balance out this offset. This method automatically reduces the circuit's sensitivity to changes in the bridge supply voltage.

The low pass filters used to smooth the rectifier outputs were two pole Butterworth types with a cut-off frequency of 0.7 Hz. Thus the accelerometer signal low pass filter's response is given by

$$H_3(S) = \frac{1}{S^2 + \sqrt{2}\ \omega_0 S + \omega_0^2}$$

where $\omega_0 = 4.4$ rad/s

This is compared with the measured filter characteristics in Figures A2.12 and A2.13.

The filtered heave acceleration signal was analogue double integrated to give a measure of the heave displacement. The double integration was performed with a two pole high pass Bessel filter which was identical to those used in conjunction

with the SBWR accelerometers. These have an equivalent high pass response given by $H_1(S)$ defined previously. Thus the heave signal was subject to a total response given by

$$H_4(S) = H_1(S)\, H_3(S)$$

Where $H_4(S)$ is the response of the instrument, normalised with respect to the ship's vertical motion. Figures A2.14 and A2.15 show the measured responses of the relevant double integrator.

A2.3.2 Pitch and roll measurements

The pitch and roll sensing potentiometers were connected into a dc Wheatstone bridge supplied from a solid state dc reference voltage source of 2.5 v (AD 580). This device maintains its specified output voltage within 0.5% over a wide range of operating conditions and has a long term stability of 100 ppm.

The bridge output was sensed at the differential input of an active low pass two pole Butterworth filter with a cut-off frequency of 0.7 Hz. The arrangement is shown in Figure 2.16, and the measured filter characteristics are shown in Figures A2.17-A2.20.

A2.4 Waverider measurements

Waverider measurements were made using a standard buoy and "Warep" radio receiver. The buoy was moored approximately ½ nm NNE of the lightvessel, using a rope and chain mooring illustrated in Figure A2.21. It should be noted that great care must be exercised in deploying a mooring of this type and the interested reader is referred to a report by Humphery (1982), where this is discussed in detail.

The analogue output from the receiver was low pass filtered using a two pole Butterworth filter of the same design as those described above. The response characteristics of this filter are shown in Figures A2.22 and A2.23. Thus the overall frequency response of the measurement system, ignoring the buoy's hydrodynamic response, is given by

$$H(S) = H_{int}(S)\, H_{rec}(S)\, H_3(S)$$

Where $H_{int}(S)$ is the equivalent response of the buoy's double integrating electronics,

$H_{rec}(S)$ is the response of the Warep radio receiver and $H_3(S)$ is defined above.

$H_{int}(S)$ is specified in the manufacturer's handbook and is given by:

$$H_{int} = \frac{S^2}{(S^2 + \sqrt{2}\,\omega_1 S + \omega_1{}^2)} \cdot \frac{S^3}{(S + \omega_2)^3}$$

where

$$\omega_1 = \frac{2\pi}{30.8} \text{ rad/s} \qquad \omega_2 = \frac{2\pi}{460} \text{ rad/s}$$

$H_{rec}(S)$ is dominated by the characteristics of the second order phase locked loop detector, used in the receiver in order to demodulate the wave information which is frequency modulated onto a low frequency subcarrier. The phase locked loop is so arranged that $H_{rec}(S)$ is dependent upon the characteristics of the integral chart recorder's movement. This is in turn influenced by the degree to which the recorder's pen arm is free to move. We have found that significant changes in the receiver's high frequency response result from clamping the pen arm. Consequently the receiver was operated throughout the experiment with its pen arm free to move, and we have measured the receiver's response in this condition. Figure A2.24 shows the measured amplitude response of the phase locked loop together with the values obtained by fitting the measured values to the general expression for the response of a second order phase locked loop, using the damping ratio ξ and the characteristic frequency ω_n as fitting parameters. The resulting expression for $H_{rec}(S)$ is:

$$H_{rec}(S) = \frac{2\xi\omega_n S + \omega_n^2}{S^2 + 2\xi\omega_n S + \omega_n^2}$$

where

$$\omega_n = 10.47 \text{ rad/s} \qquad \xi = 0.602$$

The phase locked loop introduces negligible phase shifts. These are less than 5° for all frequencies below 0.6 Hz.

A2.5 Data recording

The data derived from each of the 9 instrument channels described above were recorded using a digital data logger. An additional 10th channel was used to record the output of a constant voltage reference source, so that in the event of a recorder failure, this channel could be used to identify the start of each recording sequence. The data logger was equipped with sample and hold circuits on each of its inputs so that simultaneous samples could be made of each channel. Following each sampling operation, the sampled voltages were digitised in sequence and recorded on standard magnetic tape cartridges.

The logger was configured so that records consisted of 6144 data values per channel sampled at a rate of 2 Hz. The digitisation was performed with a resolution of 1 mV.

The recording of a single record took a period of 0.853 hours and records were taken every 2 hours during the experiment. As each tape cartridge could accommodate 4 of these 10 channel records, tapes needed to be changed at 8-hour intervals. This was done by IOS personnel who supervised the equipment during the experiment.

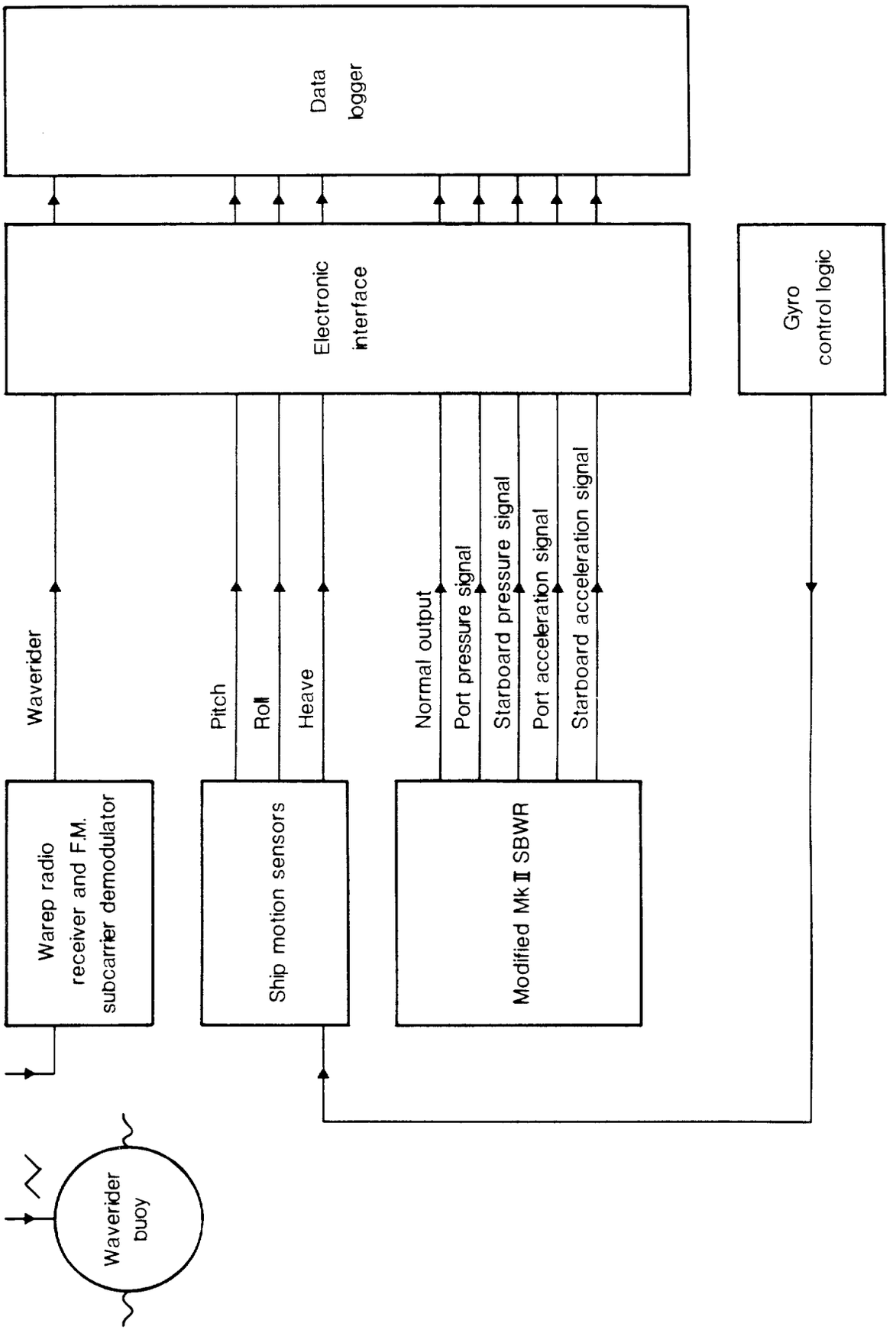

Fig A2.1 Block Diagram of Experimental Arrangement

4 CHANNEL SHIPBORNE WAVE RECORDER ELECTRONICS

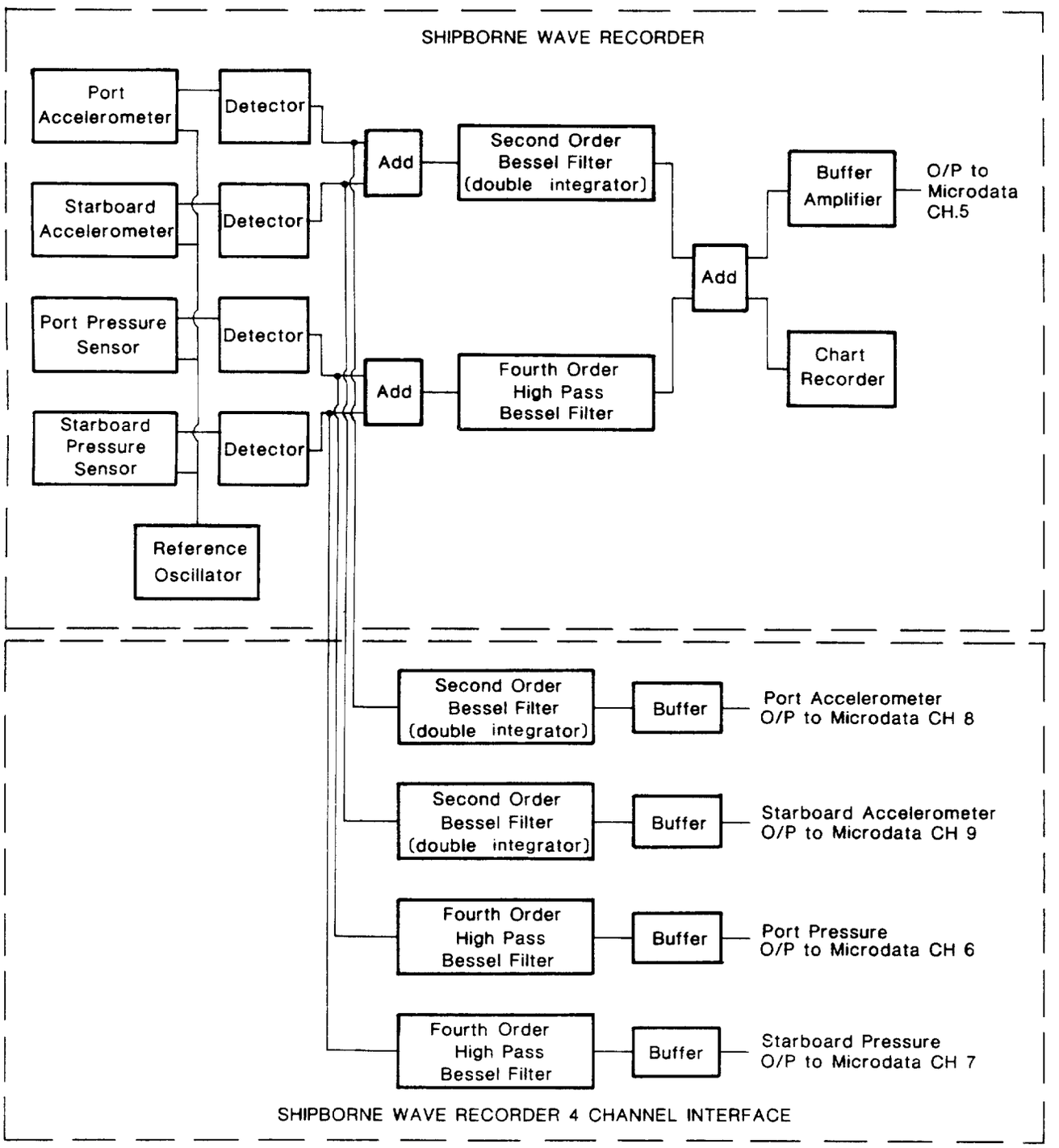

Fig A2.2 4 channel shipborne wave recorder electronics

For clarity the reference oscillator supply to each detector has been omitted.

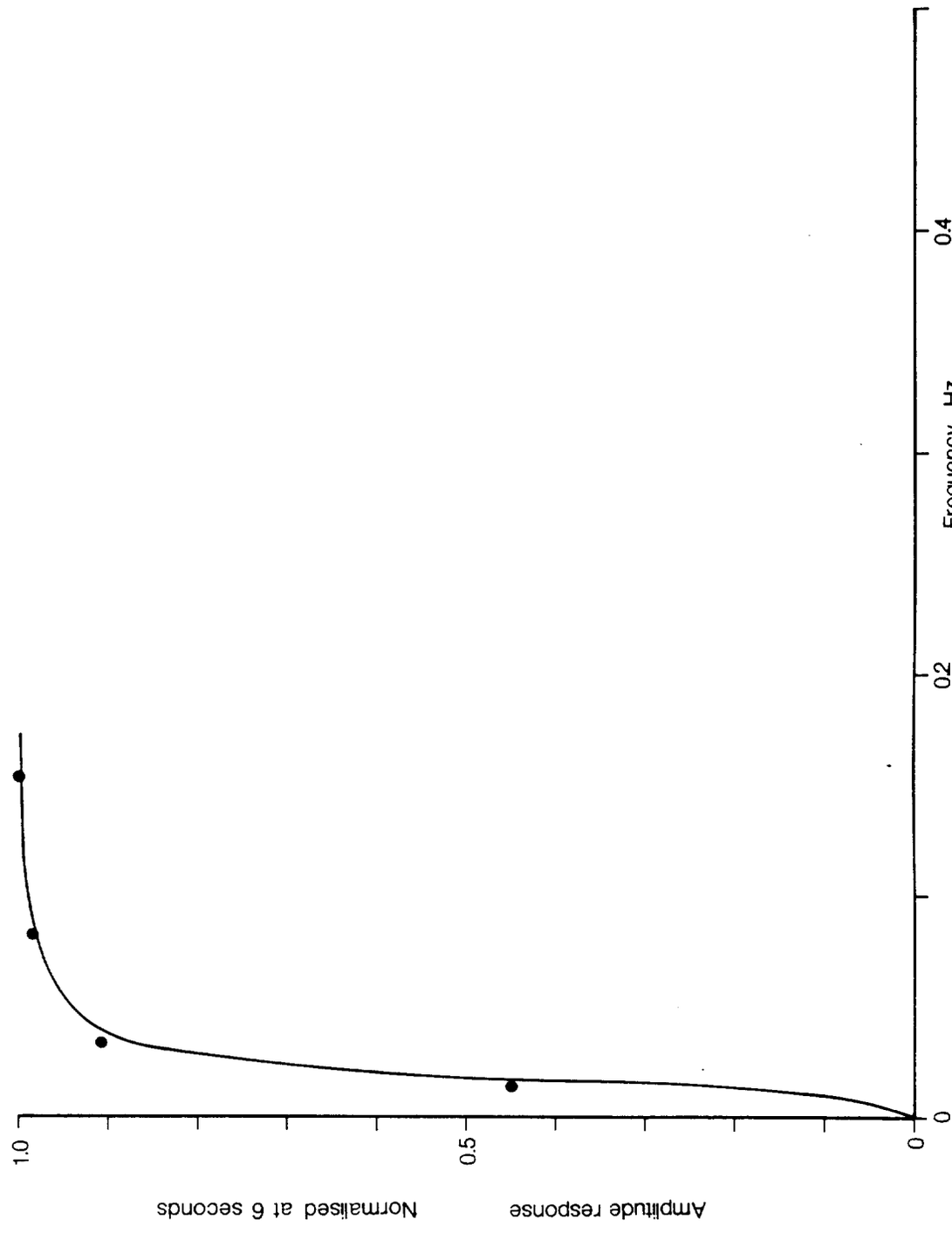

Fig A2.3 Amplitude response of SBWR High Pass Filter

This filter is used to condition those signals derived from the SBWR pressure sensors which are used to synthesise the SBWR's normal output

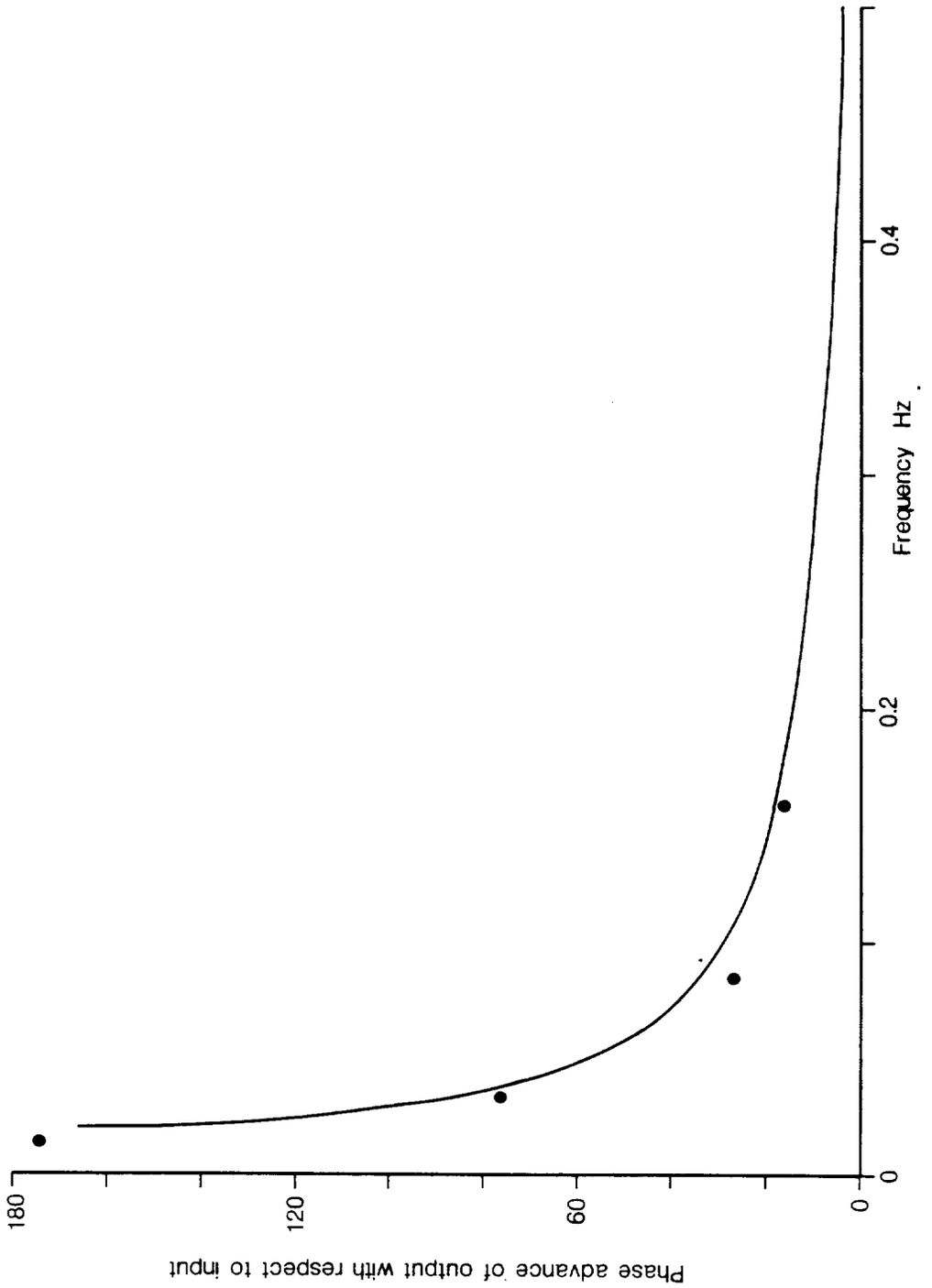

Fig A2.4 Phase response of SBWR High Pass Filter

This filter is used to condition those signals derived from the SBWR pressure sensors which are used to synthesise the SBWR's normal output

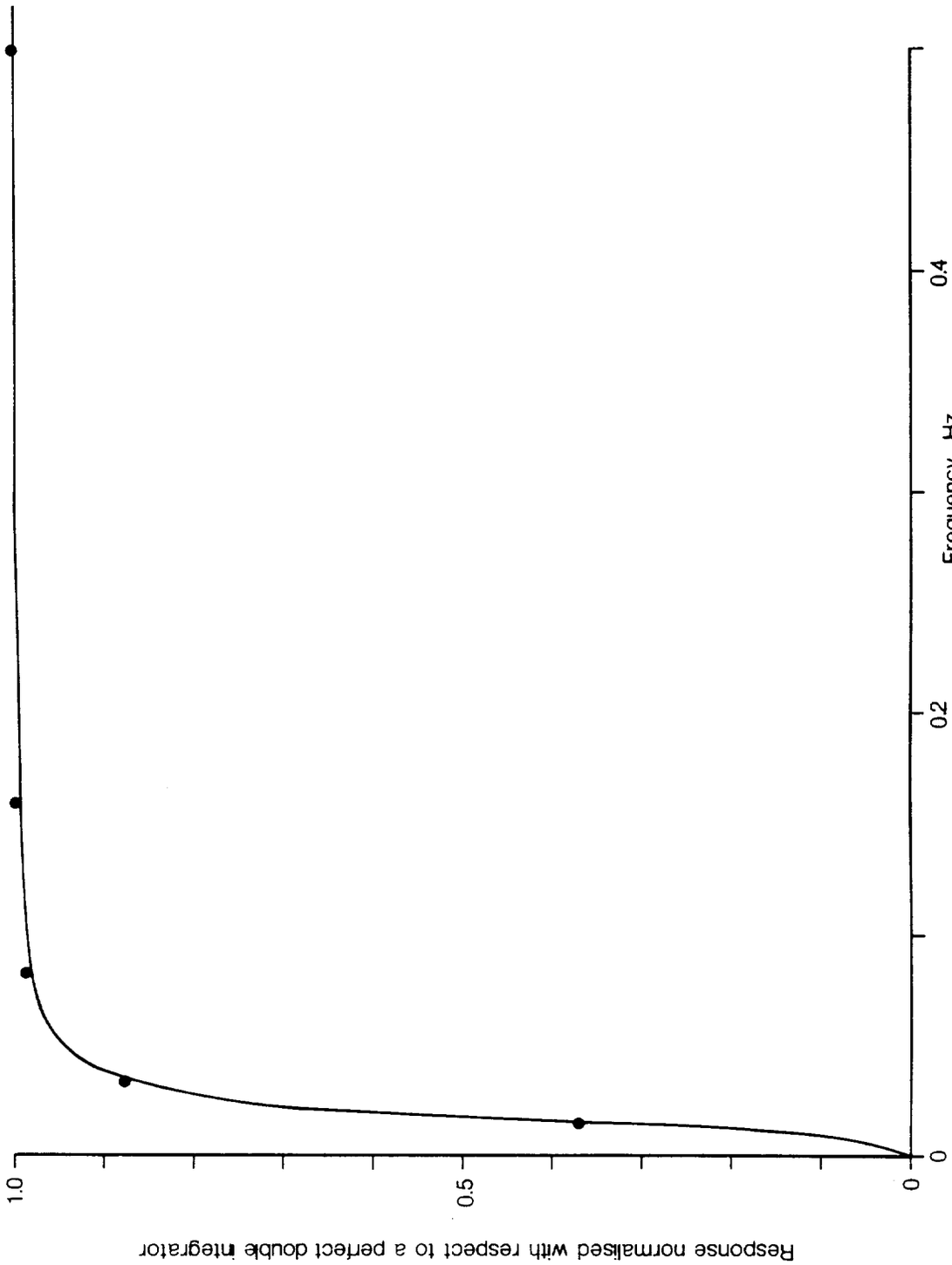

Fig A2.5 Equivalent amplitude response of SBWR double integrator

This double integrator is used to condition those signals derived from the SBWR accelerometers which are used to synthesise the SBWR's normal output

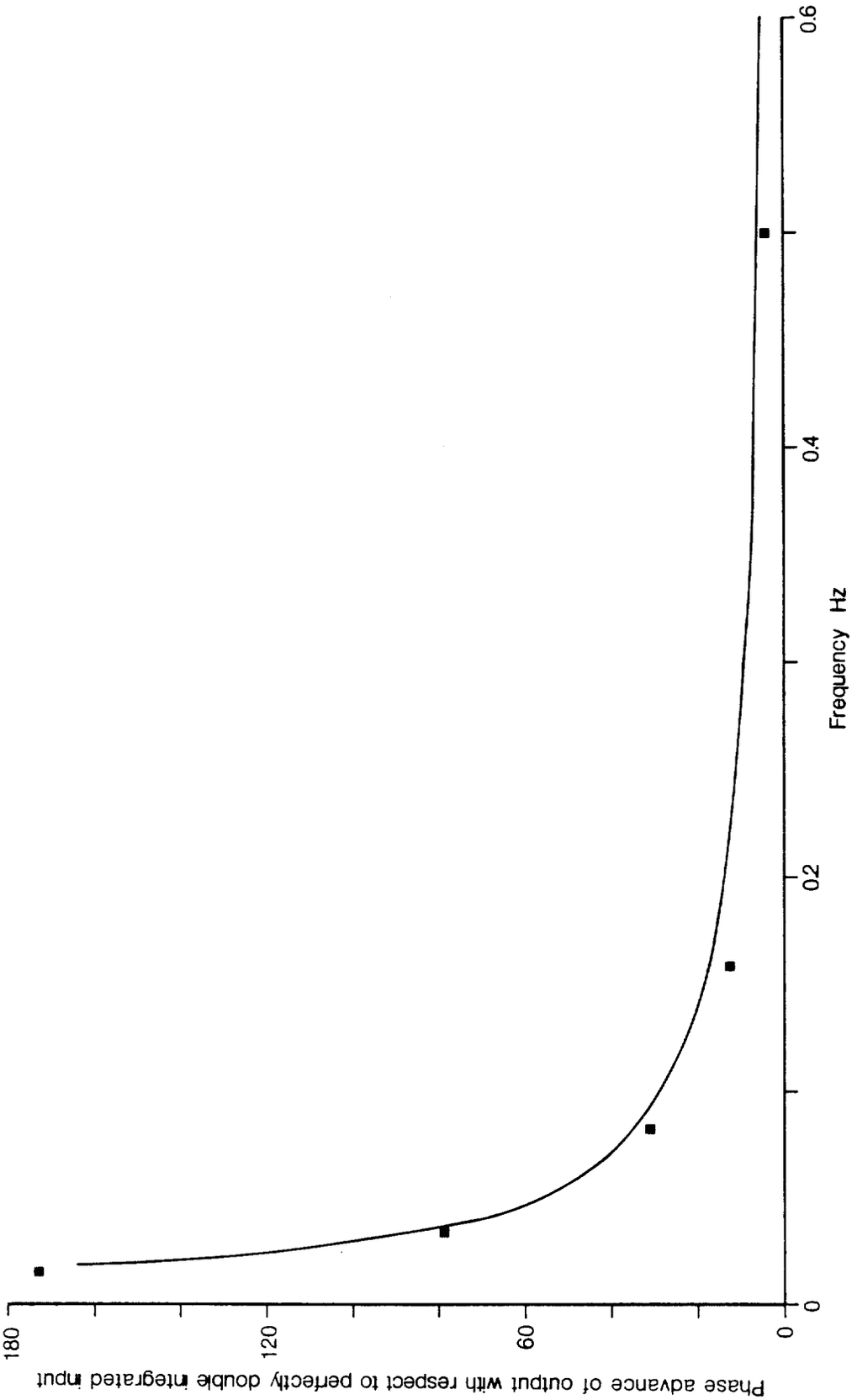

Fig A2.6 Equivalent phase response of SBWR double integrator

This filter is used to condition those signals derived from the SBWR accelerometers which are used to sythesise the SBWR's normal output

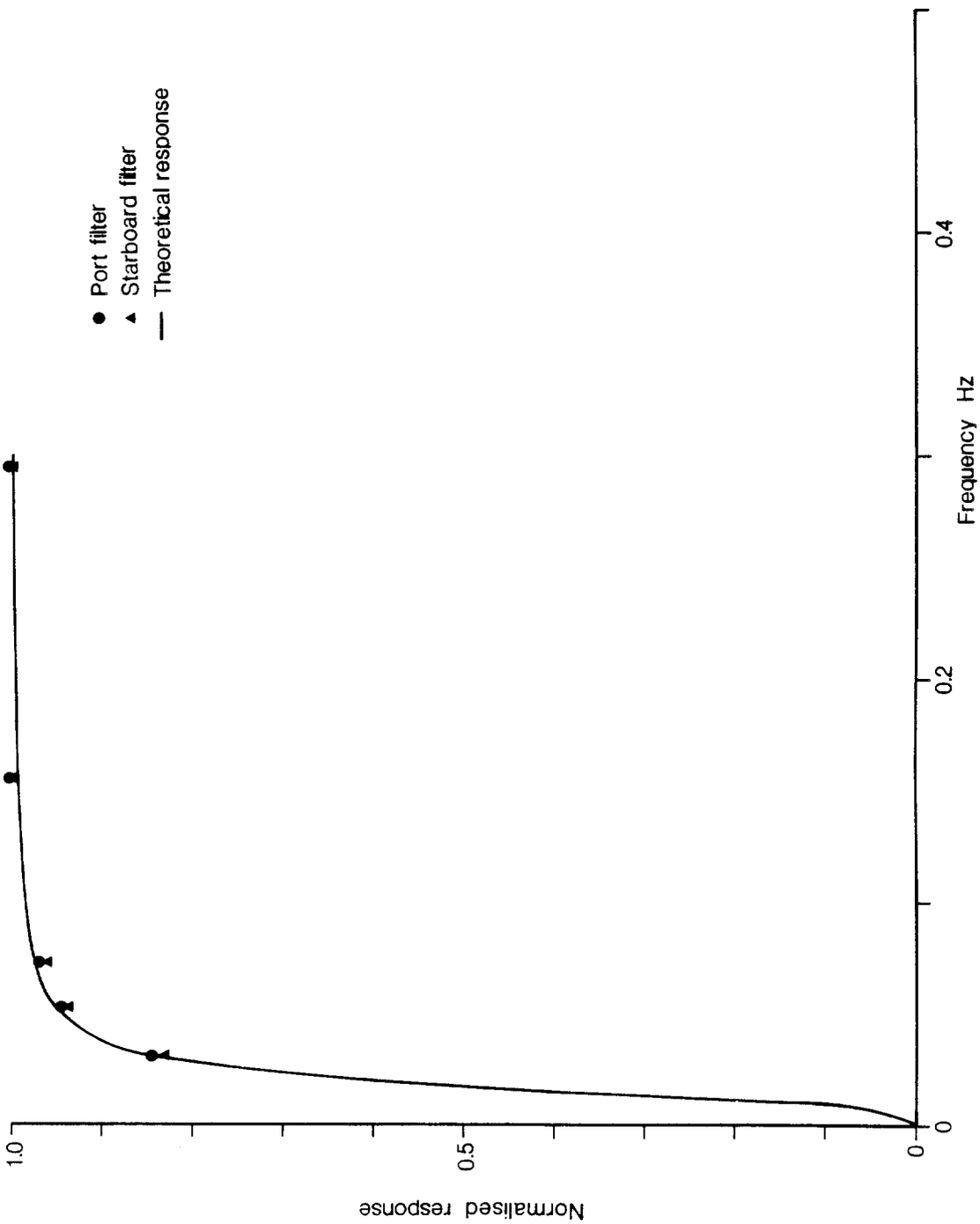

Fig A2.7 Amplitude response of SBWR Interface High Pass Filters

These filters were uses to condition those signals derived from the SBWR pressure sensors which were recorded separately

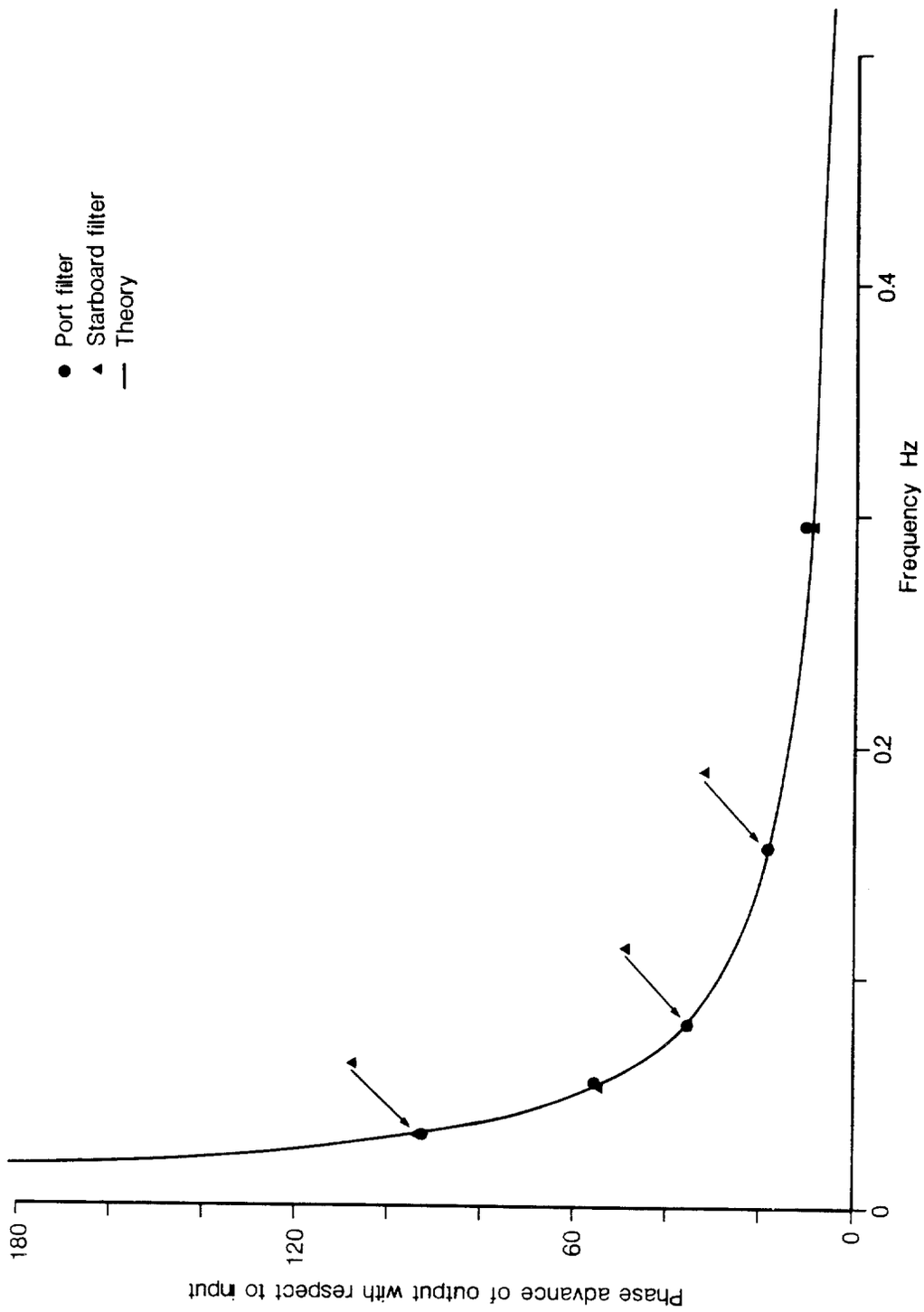

Fig A2.8 Phase response of SBWR Interface High Pass Filters

These filters were used to condition those signals derived from the SBWR pressure sensors which were recorded separately

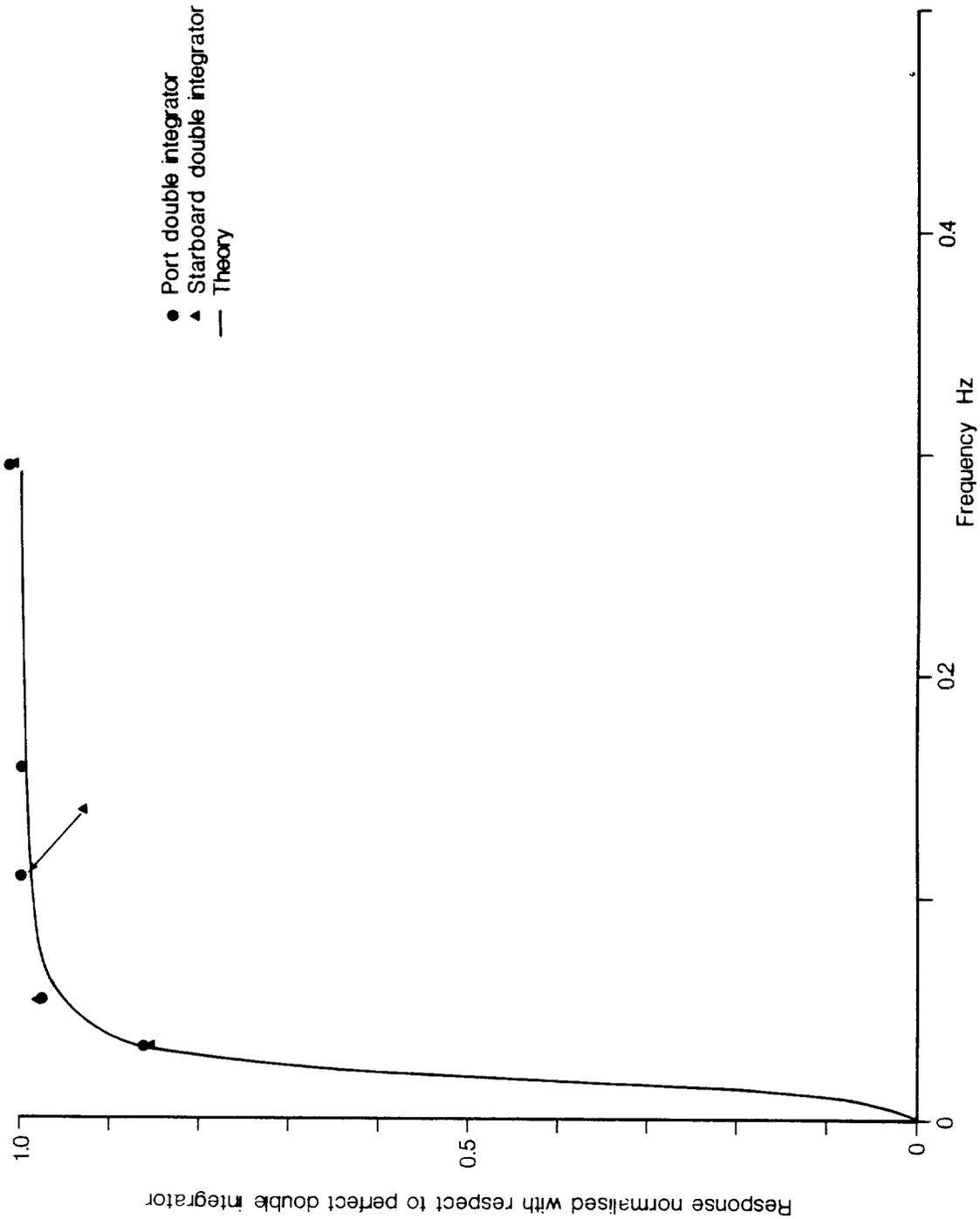

Fig A 2.9 Equivalent amplitude response of SBWR interface double integrators

These double integrators were used to condition those signals derived from the SBWR accelerometers which were recorded separately and which corresponded to the heave displacement at each side of the ship

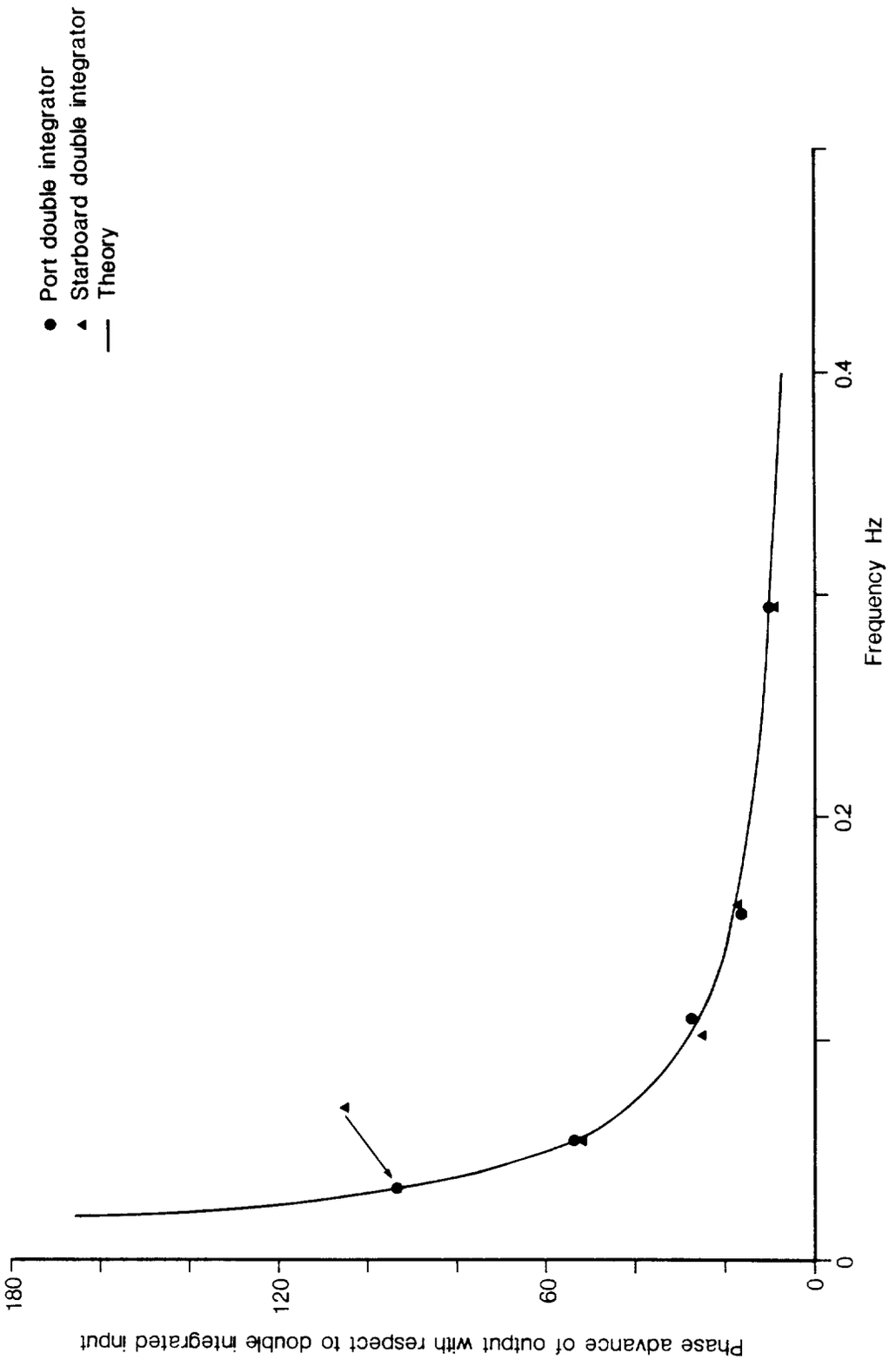

Fig A2.10 Equivalent phase response of SBWR interface double integrators

These double integrators were used to condition those signals derived from the SBWR accelerometers which were recorded separately and which corresponded to the heave displacement at each side of the ship

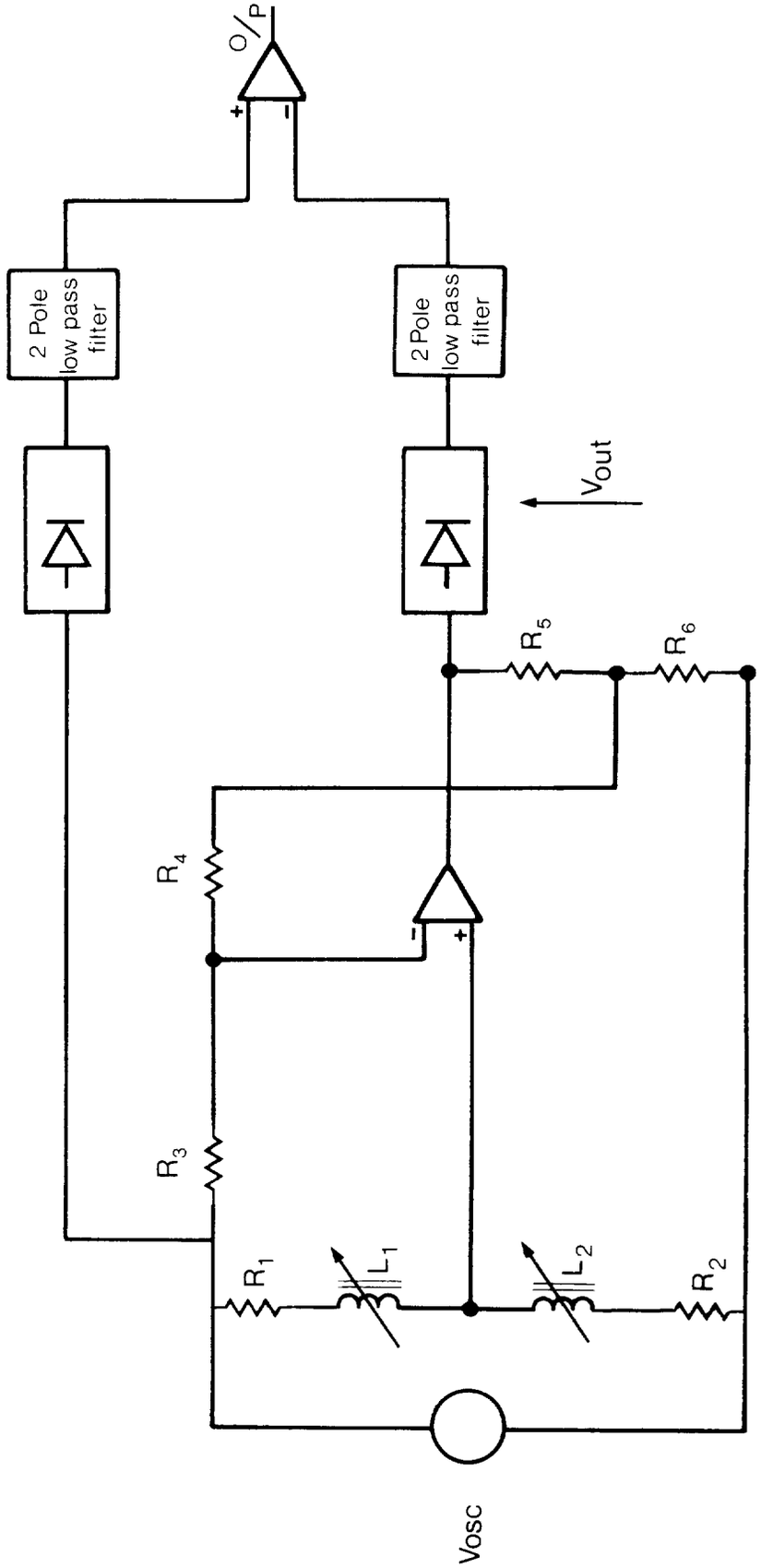

Fig A2.11 Schematic circuit of Gyro stabilised heave accelerometer and its associated detector

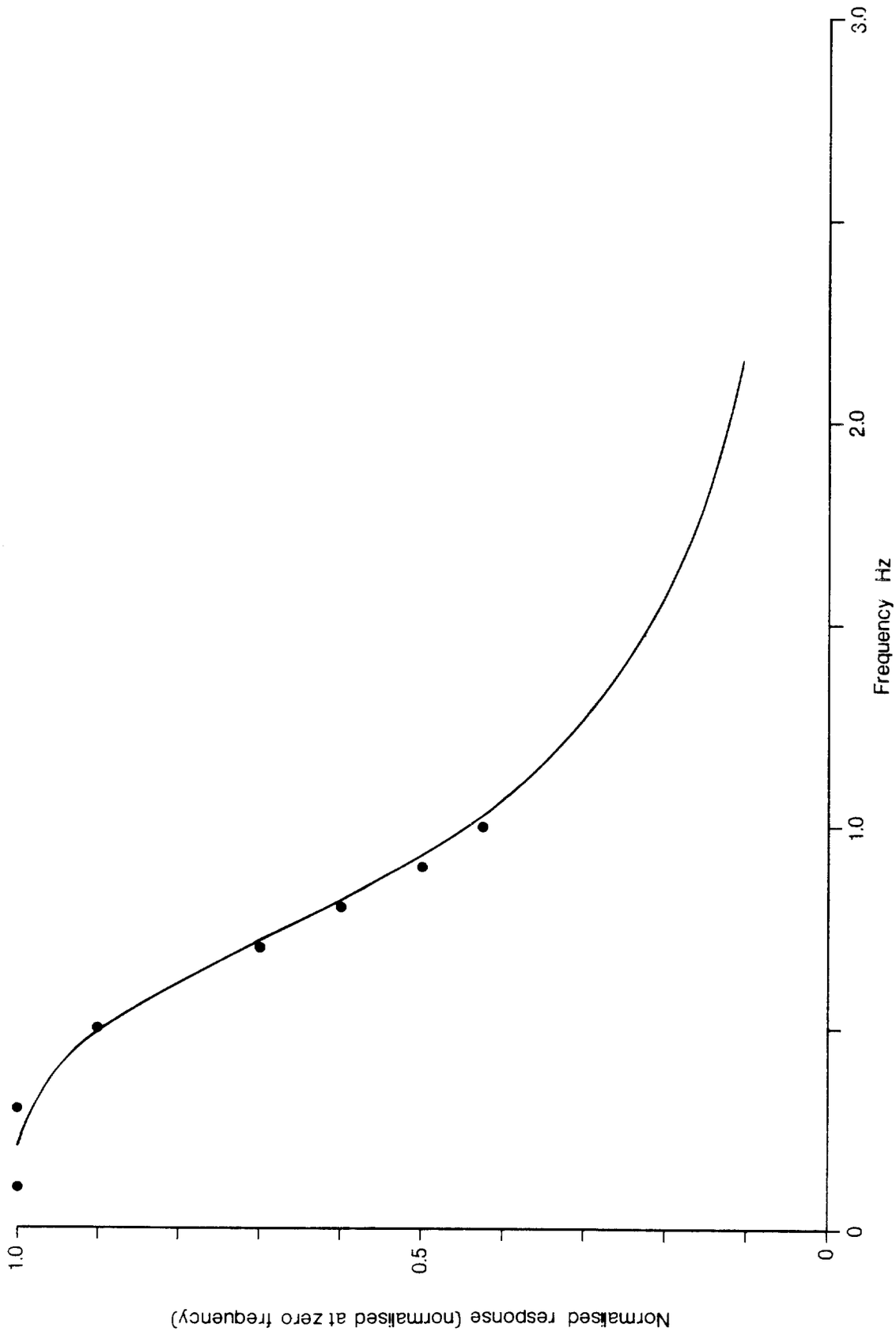

Fig A2.12 Normalised amplitude response of Gyro stabilised heave accelerometer's low pass filter

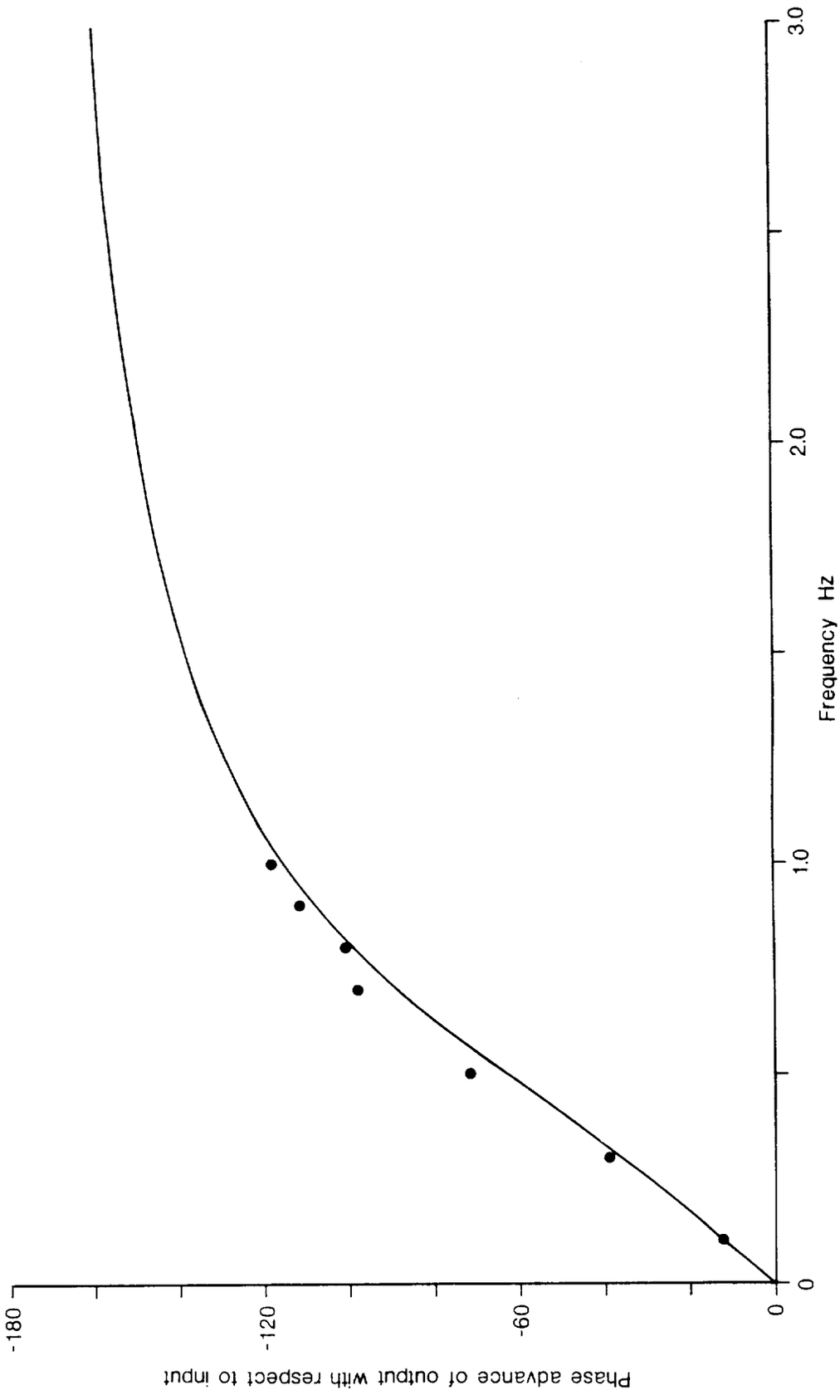

Fig A2.13 Phase response of Gyro stabilised heave accelerometer's low pass filter

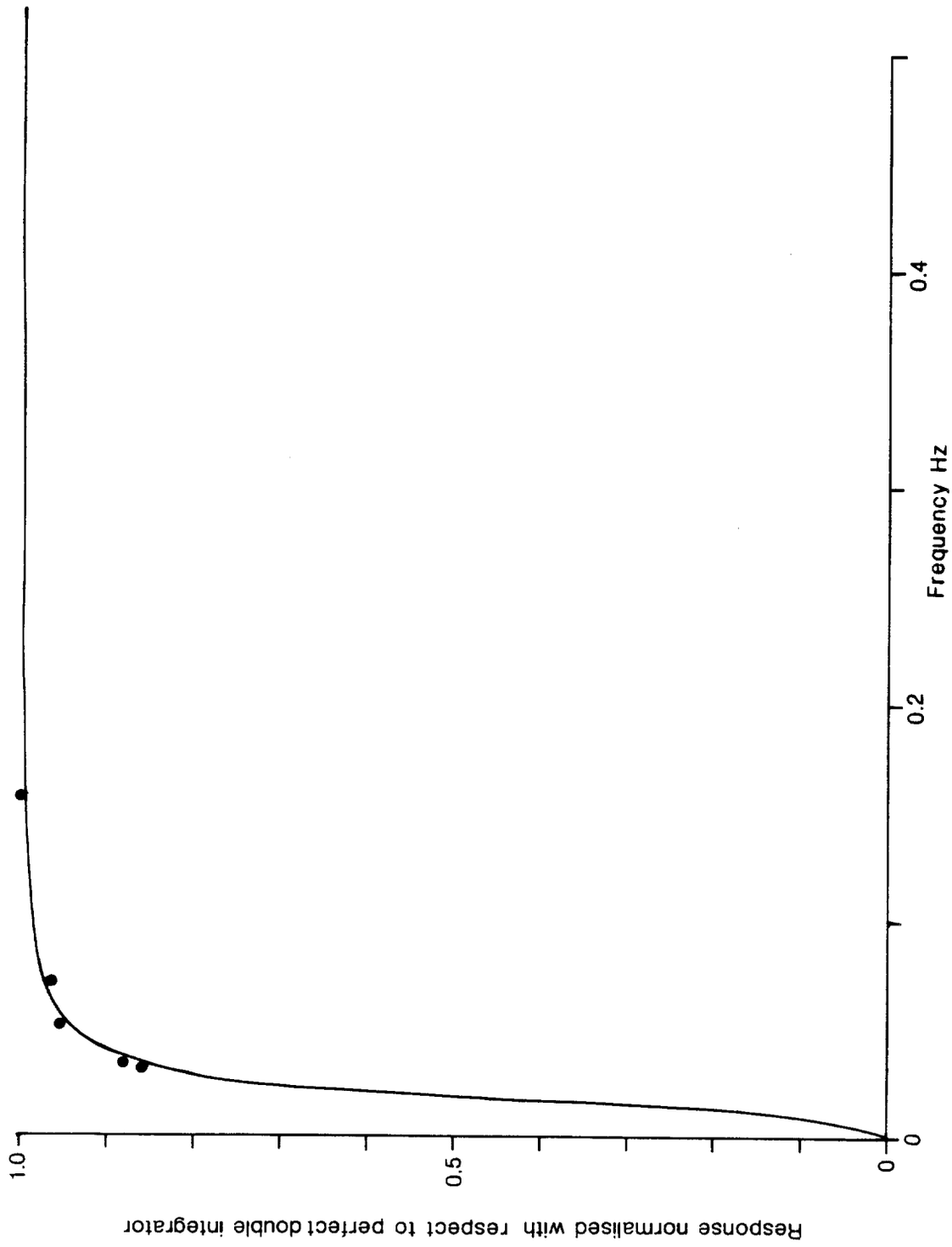

Fig A2.14 Equivalent amplitude response of Gyro stabilised accelerometer's double integrator

This double integrator was used to condition the heave acceleration signal obtained from the ship motion sensor

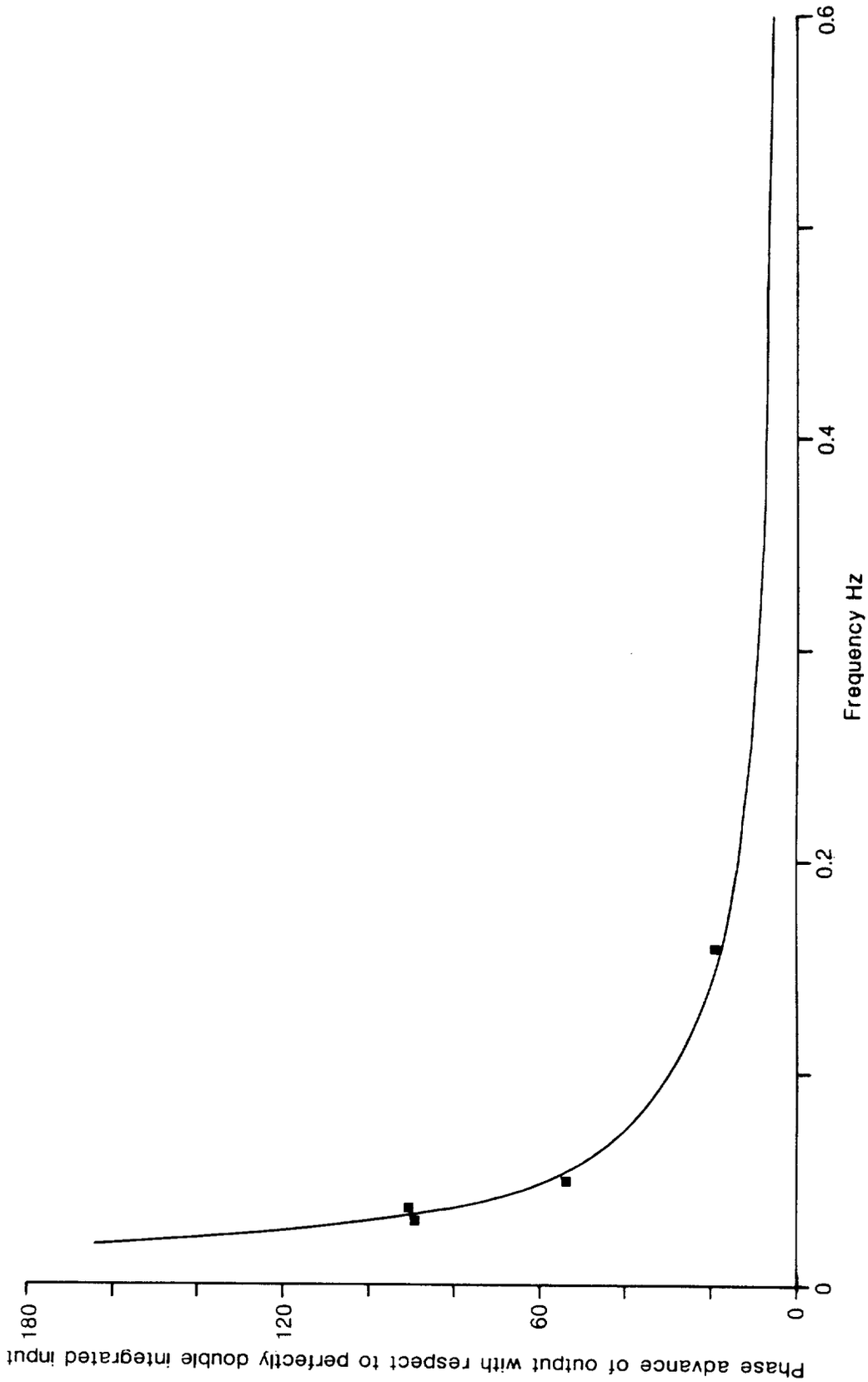

Fig A2.15 Phase response of Gyro stabilised accelerometer's double integrator

This double integrator was used to condition the heave acceleration signal obtained from the ship motion sensor

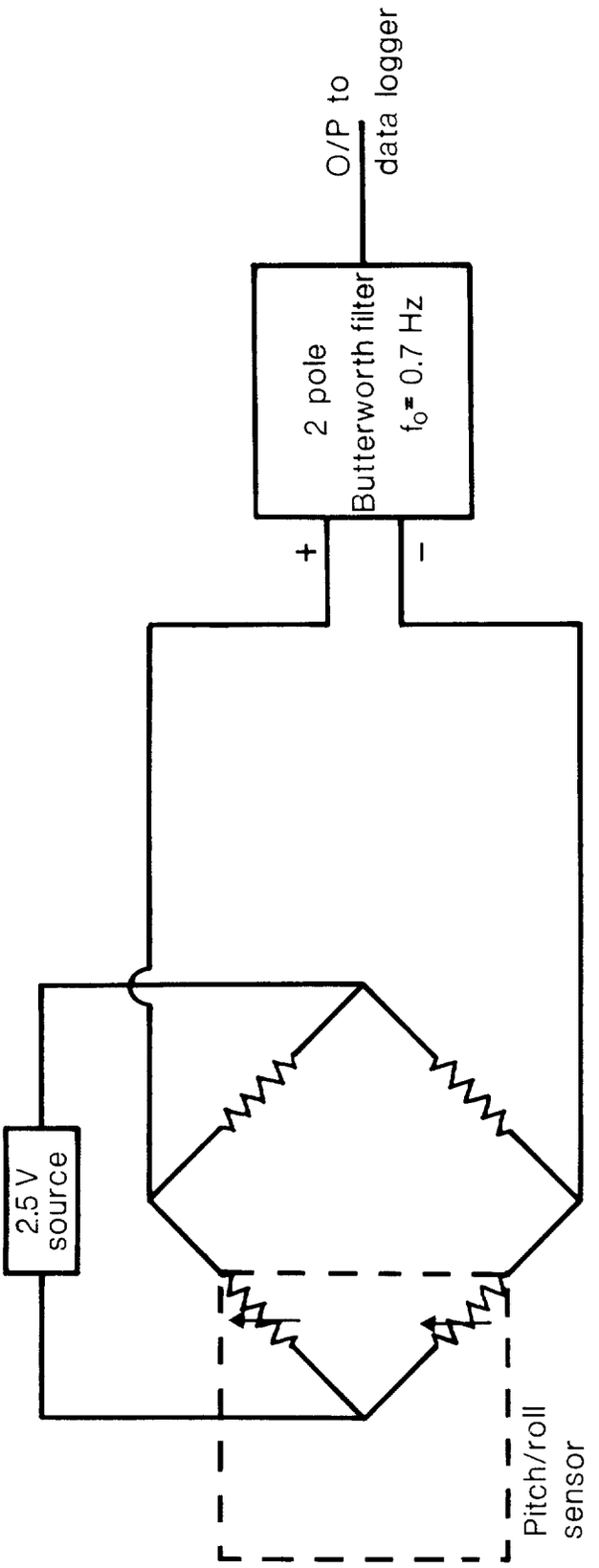

Fig A2.16 Pitch and roll sensor electronics

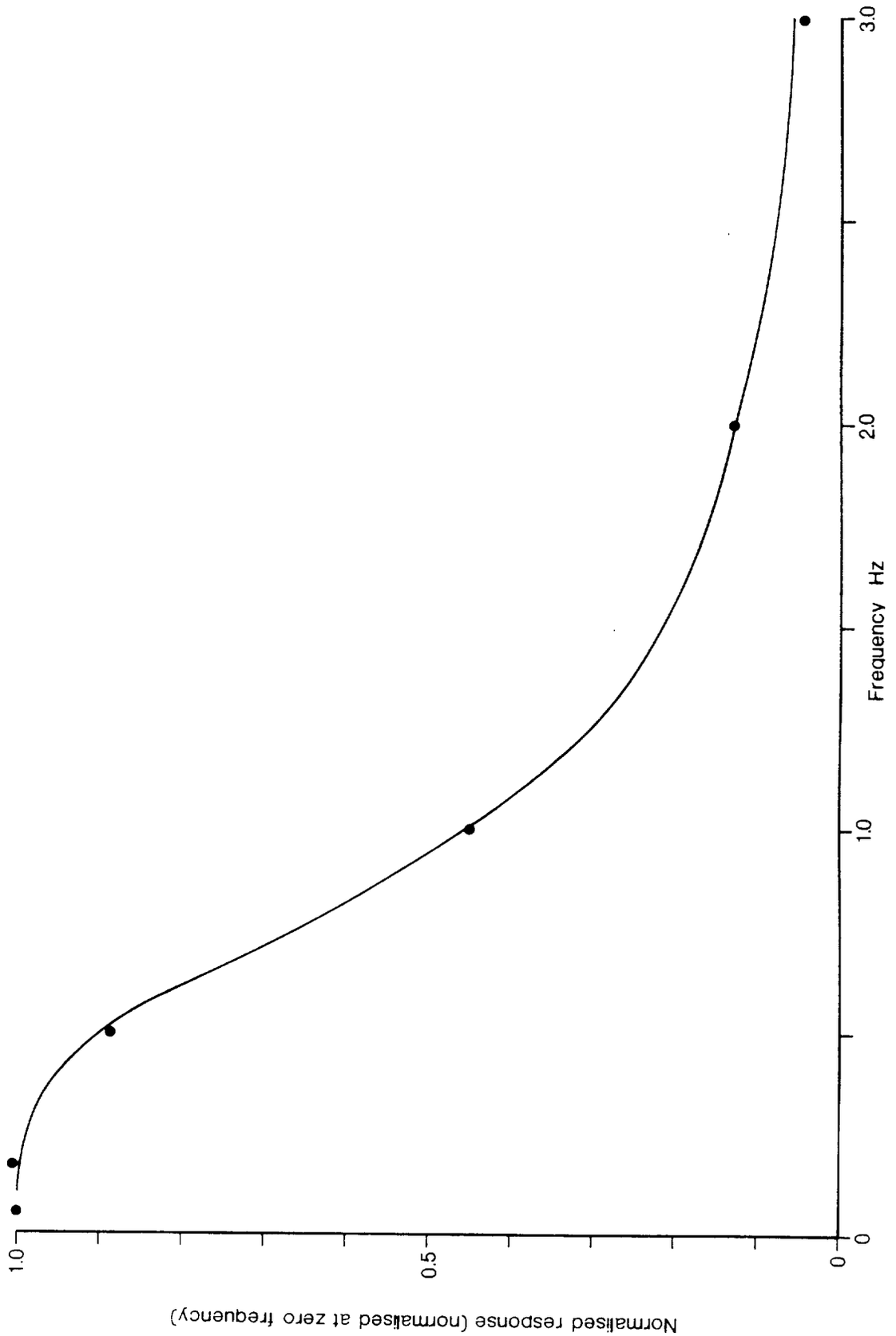

Fig A2.17 Amplitude response of pitch low pass filter

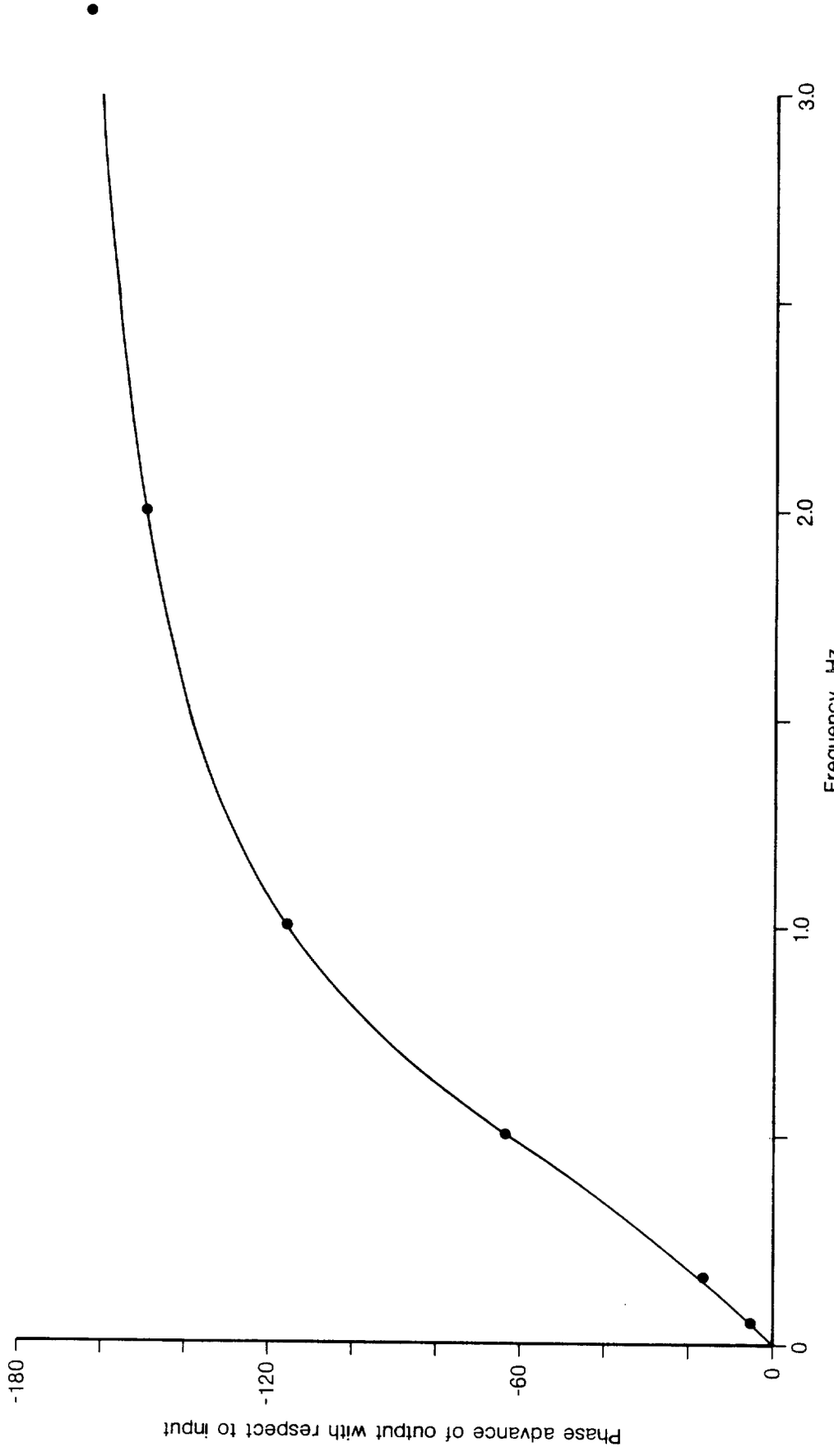

Fig A2.18 Phase response of pitch low pass filter

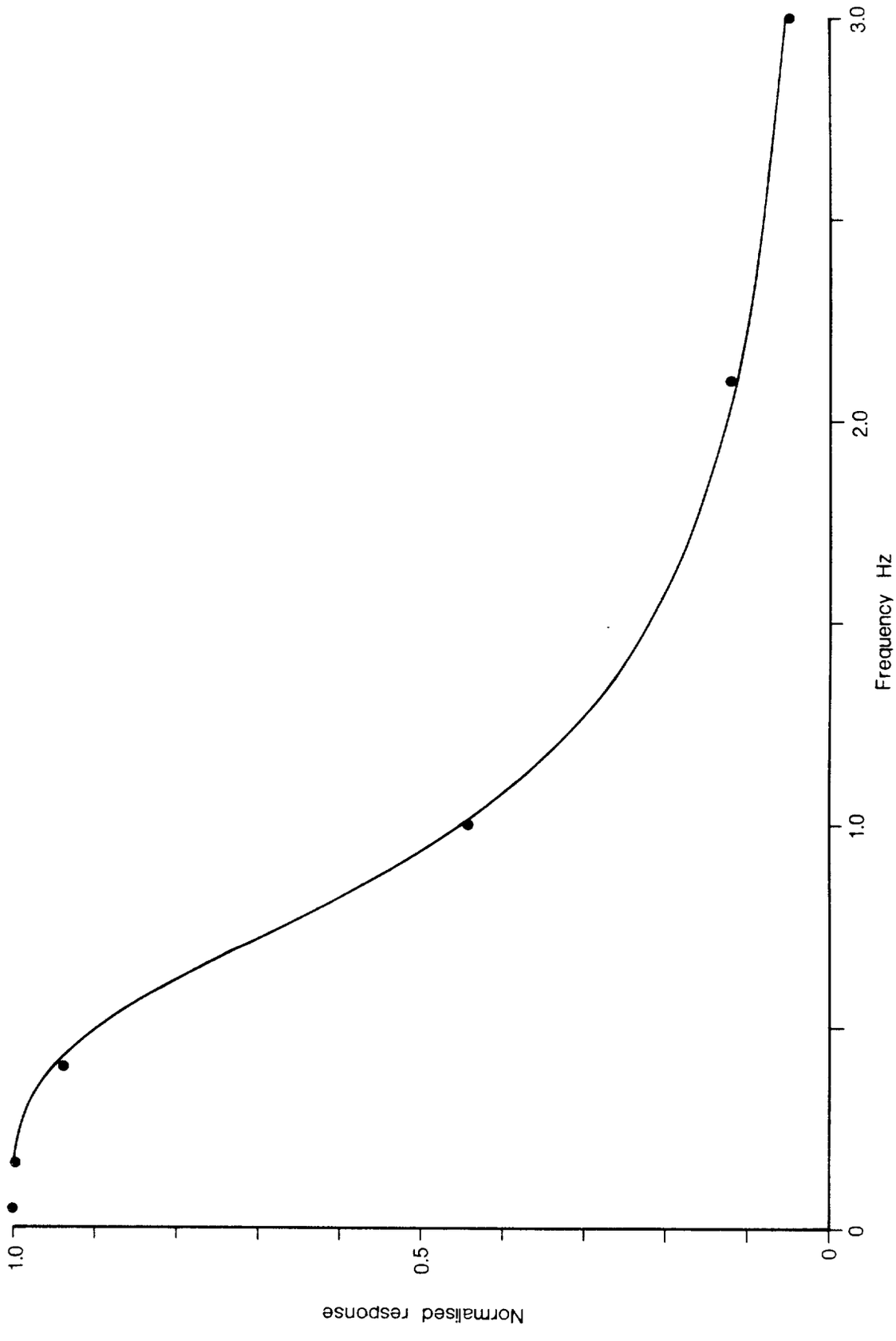

Fig A2.19 Amplitude response of roll low pass filter

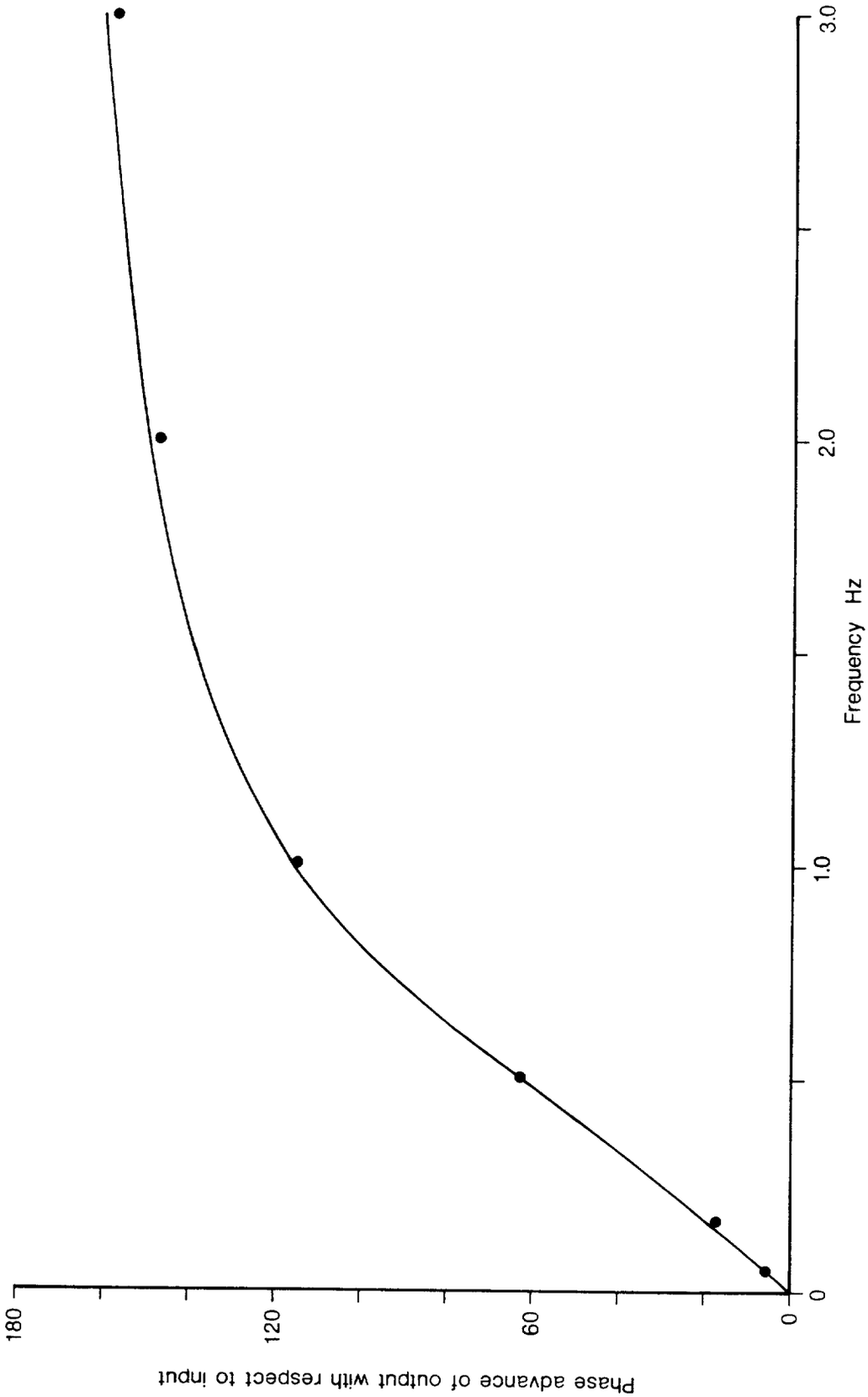

Fig A2.20 Phase response of roll low pass filter

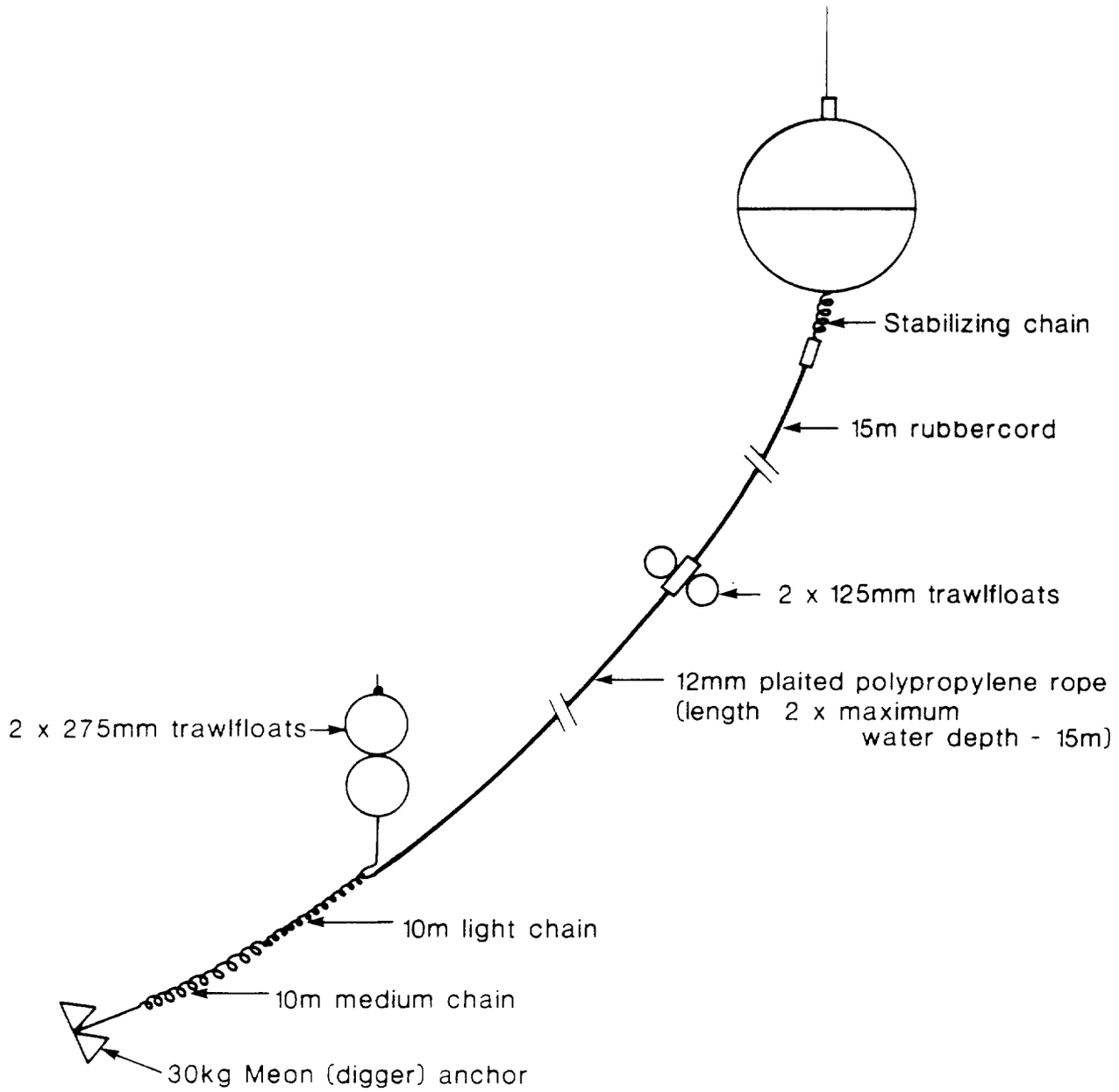

Fig A2.21 Waverider mooring arrangement

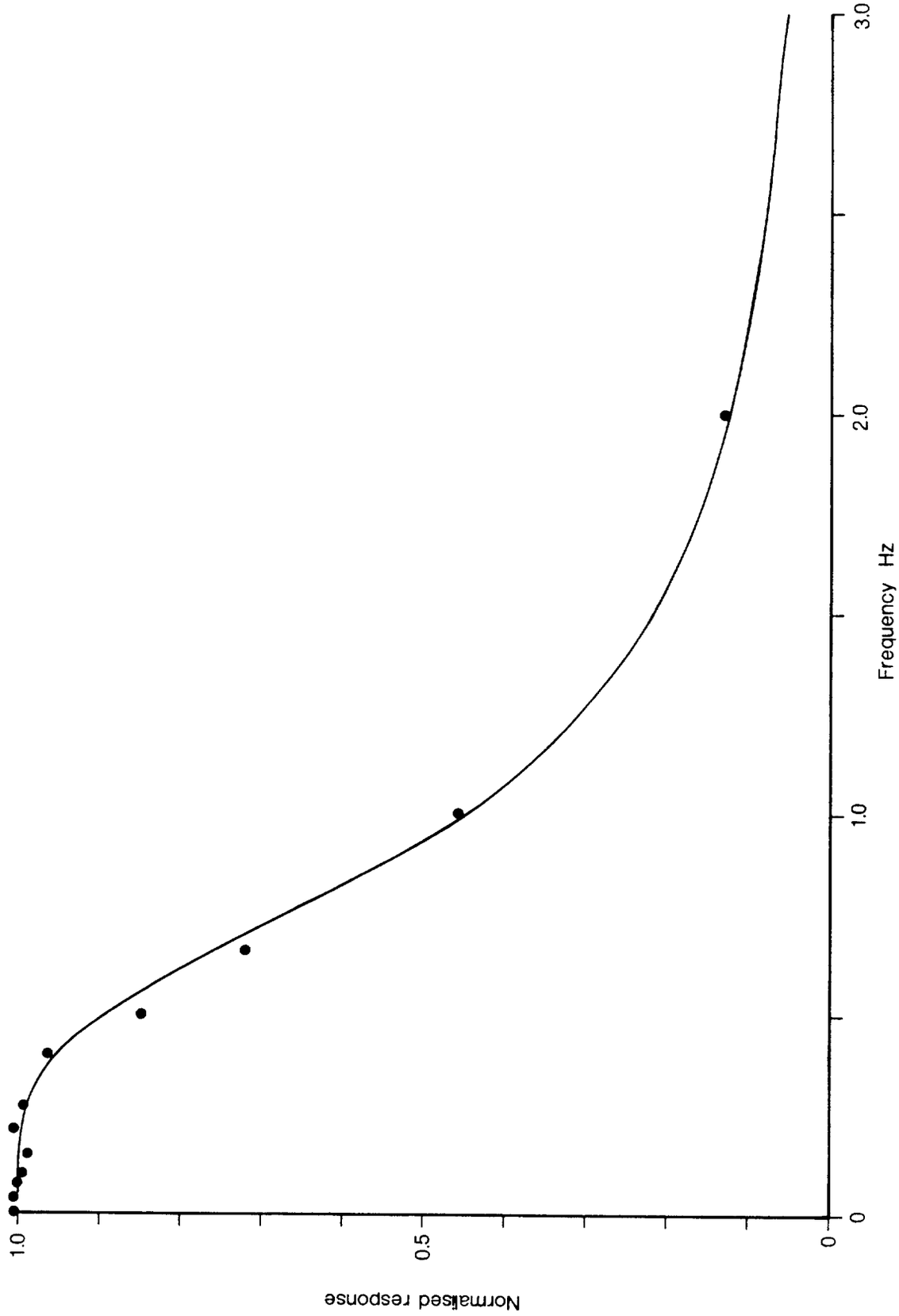

Fig A2.22 Amplitude response of Waverider low pass filter

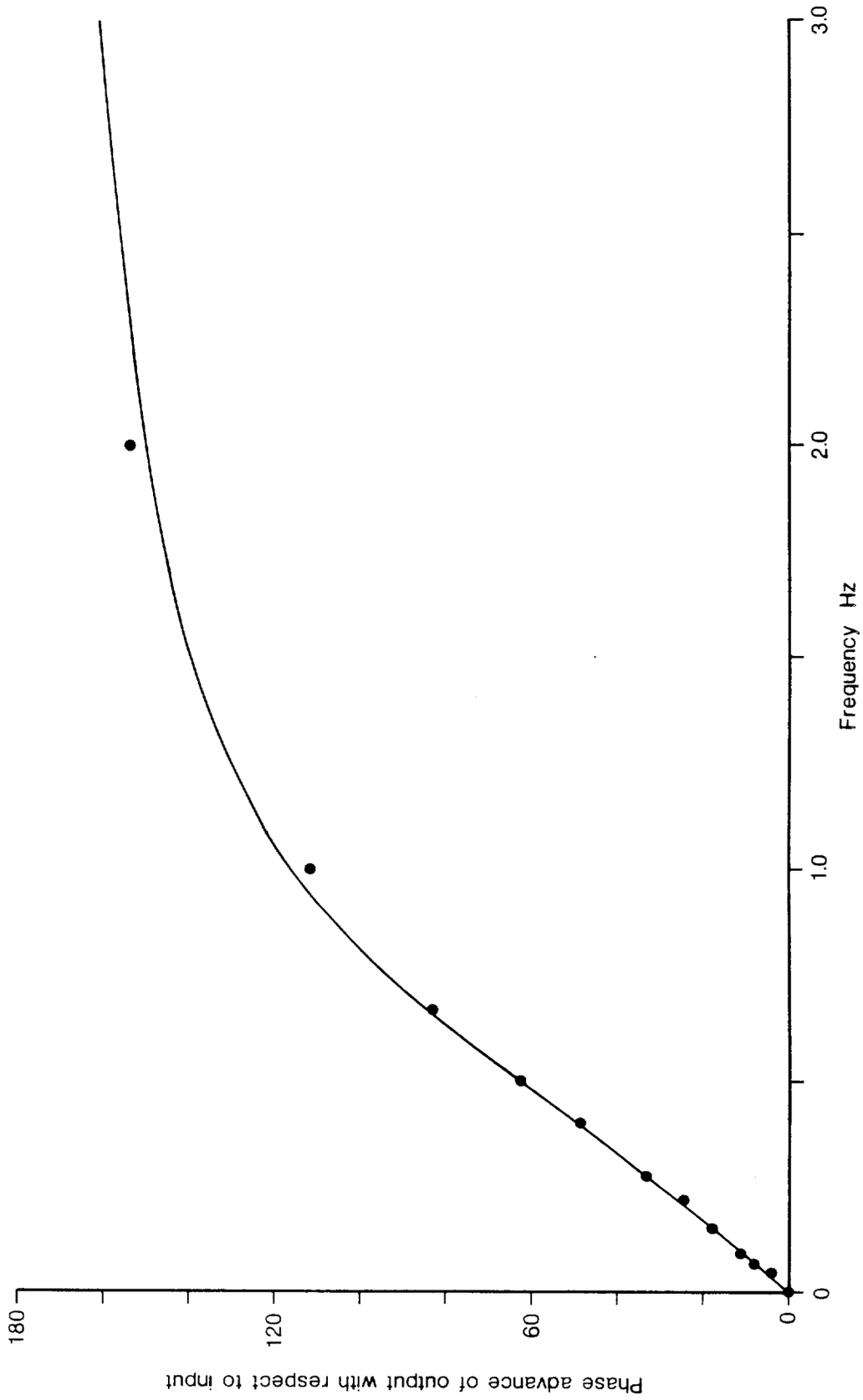

Fig A2.23 Phase response of Waverider low pass filter

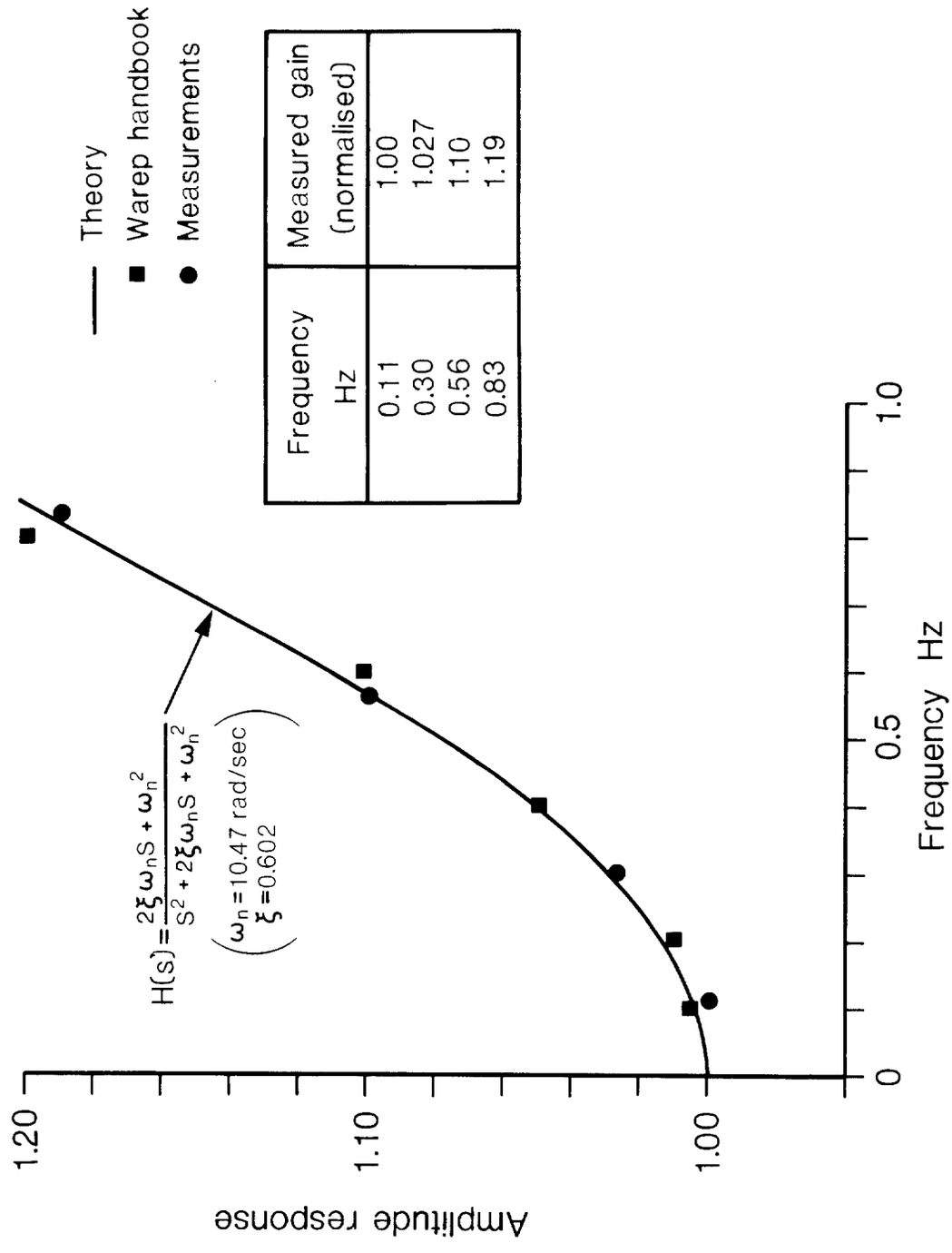

Frequency Hz	Measured gain (normalised)
0.11	1.00
0.30	1.027
0.56	1.10
0.83	1.19

Fig A2.24 Response of Warep phase-locked loop detector

APPENDIX 3 DATA PROCESSING

A3.1 Introduction

The raw data were analysed using the scheme shown diagrammatically in Figure A3.1. In this appendix the transcription, validation and spectral analysis of the data are described, while the subsequent analysis of the spectra is described in the main text of this report.

A3.2 Format of primary data

The data which were recorded aboard the lightvessel consisted of time series data from 9 sources. These were:

1. Pitch sensor
2. Roll sensor
3. Gyro stabilised heave accelerometer double integrated output
4. Waverider
5. SBWR normal output
6. Port SBWR pressure sensor
7. Starboard SBWR pressure sensor
8. Port SBWR double integrated accelerometer output
9. Starboard SBWR double integrated accelerometer output.

An additional tenth data channel was used to monitor a constant voltage reference so that any recorder failures resulting in an altered sequence of the recorded data could be easily identified. The 10 channels were sampled simultaneously at a rate of 2 Hz and the resulting data values were recorded in a fixed sequence. Each data value was recorded digitally with a resolution of 1 mV and a maximum range of ± 1999 mV. Records of 3072 seconds duration were recorded continuously.

A3.3 Transcription and validation

The raw data were recorded on certified data cartridges. These were replayed at IOS and transcribed onto computer compatible tape for transfer to a main-frame computer.

The transcribed field tape images were validated using a standard IOS computer program which was modified to handle multichannel data. This program has been in routine use in IOS for some years, and it has proved successful in identifying instrumental faults at those of our wave measuring sites which are equipped with Waverider buoys.

The purpose of the validation program is twofold; firstly the program identifies unreasonable data values and behaviour; secondly, where possible, the program replaces individual erroneous values so that the modified time series may be used in subsequent analyses. In order to do this the program makes several passes through the data which must therefore be held in the computer memory. However, because of their large size (61440 data values per 10 channel record), the records recorded at Channel lightvessel had to be subdivided to allow this to be done economically. The most straightforward way of doing this would be to extract from each record all of the data which originated from a given data channel, and then validate each channel's data in turn. However, this would be an inefficient way to proceed as it would involve 10 passes through the transcribed data tape. Instead, blocks of 5120 data values were read and divided into 10 series of 512 values corresponding to the 10 channels. These were validated and read to 10 output disk files, so that twelve such sub-blocks constituted a complete record.

The validation tests were originally designed to identify the characteristic errors found in data derived from Waverider buoys. Fortunately most of these tests can be applied to any stationary, random, Gaussian time series as those tests which are Waverider specific do not result in any modified data values. Thus all of the data could be validated using the existing program in the following way. The tests described below were applied to each time series and where possible erroneous data values were corrected. In addition a record was made of all test failures for each channel and data block. In the subsequent data analysis this record was inspected and the relevant data was accepted or rejected using criteria which reflected the properties of the relevant data channel.

If a large number of correctable errors occurred in a given data block the data were still rejected as such behaviour might indicate a general degradation of the data.

The tests applied to each time series were as follows:

a. Format test

The format of each data value was compared with the recording specification. Any incorrectly formatted points were replaced by interpolation with neighbouring points.

b. Consecutive format test

A check was conducted to establish if any format errors occurred on neighbouring points. Failures of this test were recorded separately from failures of test (a).

c. Mean values tests

The mean value of each data block was compared with the mean expected for the relevant channel. This test will detect a change in the recording sequence resulting from lost data values. These might otherwise result in data being ascribed to the wrong channel. The constant voltage reference channel, incorporated into the recording sequence, was included to ensure that this test would operate successfully.

d. Equal value test

Occurrences of ten consecutive equal data values were recorded as failures of this test.

e. Long zero up cross period test

Each individual zero up cross wave period was measured. Occurrences of periods in excess of 25 seconds were recorded as failures of this test. This test is Waverider specific and indicates low frequency noise in the record. The test was used on other data channels using the modified rejection criteria described below.

f. Rate of change test

Neighbouring data values were compared to obtain an estimate of the instantaneous rate of change. A data value was rejected if this rate of change exceeded a critical value given by:

$$R_{crit} = \frac{2\pi\sigma}{T_z} \left(2\log_e(T/T_z)\right)^{\frac{1}{2}} \Delta t$$

This rather complicated expression is obtained on a statistical basis and represents the maximum rate of change associated with a wave of period Tz and whose zero up cross height is the largest expected in a given wave record.

Where Δt = sample interval

σ = block standard deviation

T_z = block mean zero up cross period

T = block length

Isolated failures of this test were corrected by interpolation.

g. Consecutive rate of change test
Neighbouring points were inspected to establish if both failed test (f). In this case a separate record was made of the failure.

h. Large data value test
Data values whose deviation from the mean exceeded 4σ were regarded as suspicious. Each occurrence was recorded but no correction was applied to the data.

i. Consecutive large data value test
If two neighbouring data values failed test (h) a separate record of the failure was made.

For the purpose of generating spectra, each of the records consisting of 6144 samples per channel was divided into three sections of 2048 points, each section being analysed separately. Consequently the validation results corresponding to those blocks which comprised a given section of data were amalgamated into a table, which catagorised the number of failures of each test associated with a given data channel. This table was compared with a table of critical values shown below in order to decide if a given section of data would be included in the analysis (see Table A3.1).

The data set which was used in the analysis described in the main text of this report was made up of records for which all of the data met the validation criteria, apart from data derived from the roll channel. The roll data set was treated as a special case as much of it was contaminated with high frequency noise. When analyses were conducted which used roll data, a subset was extracted for which the data from all channels were valid.

It should be noted that in the absence of serious instrument or recorder failures, the most common errors which were encountered were due to interference spikes in the data. The validation procedures described above can successfully distinguish these from the data only when they occur sufficiently infrequently that σ and Tz for a given record have not been unduly influenced by the erroneous data points. Records which contain gross interference may be accepted by the above procedures as valid data. However, such conditions may frequently be identified from their

unusual spectral characteristics and appropriate action can then be taken.

A3.4 Spectral Analysis

The spectral analysis procedure described in this section was used to calculate spectra for two purposes. These were:

1. To allow internal consistency checks to be applied to the data
2. To allow frequency domain comparison of the SBWR and Waverider.

The internal consistency checks were possible because some of the data which were recorded were redundant. Thus spectra derived from different measures of the same physical quantity could be calculated and compared. In order to do this, the data from certain pairs of sensors had to be combined linearly so that the spectra of appropriate quantities would be available. Specifically, the two SBWR heave channels and the two SBWR pressure channels were combined to provide measures of the ships roll which was measured independently by the roll sensor.

In addition the ship motion sensor's heave data were combined with the output of the pitch sensor so that the resulting heave spectrum would be referred to that position along the ship's length where the SBWR heave sensors were located.

The data from the SBWR sensors had also to be combined so that they could be compared with the Waverider data. This process was complicated by uncertainties associated with the form of the appropriate corrections which should be applied to the SBWR data in order to take account of the hydrodynamic attenuation with depth of pressure fluctuations. The procedure which was used allowed a number of formulations, and corresponding corrected spectra were calculated for each.

In practice the spectral analysis procedure which was adopted had to be designed so that the large volume of data could be processed economically. The constraints on computer storage made it both desirable to perform as many calculations as possible in place, and to retain the processed data in a reduced form only. It was therefore decided, in the interests of efficiency, to perform the analysis in the following manner:

1) Each data channel in turn was used to calculate a corresponding Fourier transform.
2) The Fourier transforms from different channels were combined linearly as required.

3) The resulting Fourier transforms were used to calculate unsmoothed power spectra.
4) The power spectra were used to calculate the moments of each spectrum; the spectra were then smoothed, thus effecting a reduction in the data volume as well as an increase in the statistical stability of the stored data.
5) The smoothed spectra and spectral moments were stored for further analysis.

Each of these stages in the analysis is described in more detail below. The procedure is illustrated in diagramatic form in Figures A3.2 and A3.3.

A3.5 Calculation of Fourier transform

Each of the recorded time series consisted of 6144 data values per channel. In order to Fourier transform the data, each record was divided into three sections of 2048 data values, each section being transformed separately. The results of the validation procedure corresponding to each section of data were inspected and the corresponding time series were accepted for analysis or rejected according to the procedure described previously. The data which were of acceptable quality were first scaled using the appropriate calibration information to convert the logged values into scientific units, and were then Fourier transformed using a standard Fast Fourier Transform algorithm. It is common practice in analysis of this kind, to multiply the time series with a window function. This reduces the amplitude of the side lobes associated with each harmonic in the spectrum but does so at the expense of the statistical stability of the spectral estimates. A pilot study was conducted to evaluate the benefit obtained by using a cosine window function and it was concluded that no windowing of the data was necessary.

At this stage corrections were applied to compensate for the filtering to which each signal was subjected in the measuring electronics. In the case of the accelerometers, the equivalent responses of the double integrators were used so that the resulting corrected transforms corresponded to perfectly double integrated accelerations. In the case of the ship motion sensor's heave signal, the correction for a two pole Butterworth filter was omitted in error. Thus these data retain a certain amount of low pass filtering, but, frequency components below 0.45 Hz will not be significantly influenced by this omission (this filter had the characteristics shown in Figure A2.12). The data corresponding to the remaining channels were corrected for all of the filters described in Appendix 2.

A3.6 Combination of data from different channels

The corrected Fourier transforms were combined linearly in order to calculate the following spectra:

1) Roll spectrum derived from difference of SBWR heave signals.
2) Roll spectrum derived from difference of SBWR pressure signals
3) Heave spectrum referred to the position of the SBWR accelerometers, derived from the ship motion sensor's heave signal and pitch signal.
4) Total SBWR heave spectrum derived from sum of port and starboard heave signals.
5) Total SBWR pressure spectrum derived from sum of port and starboard pressure signals.

The combined total SBWR heave and total SBWR pressure Fourier transforms were then themselves combined in various ways to provide a set of wave spectra. In order to allow for the hydrodynamic attenuation of pressure fluctuations with depth, a correction factor of the form $e^{\alpha(2\pi f)^2 d/g}$ was used, where

d = mean depth of pressure sensor
g = acceleration due to gravity
f = frequency
α = adjustable dimensionless constant

Two formulations for this correction were used; in the first the pressure Fourier transform was corrected and then combined with the heave transform, in the second, the two transforms were summed and the combined transform was corrected using the frequency dependent factor given above. During the subsequent analysis of the SBWR spectra it was found that only those spectra which were obtained using the second formulation described above were useful and only these spectra are described in Section 3 of this report. Each of these formulations was applied using three values for the dimensionless constant, namely 0, 1 and 2.5.

$\alpha = 0$ corresponds to no correction, $\alpha = 1$ corresponds to the classical hydrodynamic formula for the attenuation of gravity waves with depth and $\alpha = 2.5$ corresponds to the modified hydrodynamic formula conventionally used in the analysis of SBWR data.

A3.7 Calculation of power spectra and spectral moments

Each of the Fourier transforms was used to calculate the corresponding periodogram using the formula:

$$S_i(f) = \frac{T}{2} \left(a_i^2 (f) + b_i^2 (f)\right)$$

where $S_i(f)$ is the ith periodogram estimate and a_i and b_i the corresponding real and immaginary parts of the Fourier transform.

The periodogram was smoothed to render smoothed spectral estimates with improved statistical stability. This was done by forming the simple average over sets of 10 adjacent non-overlapping components in the periodogram.

Table A3.1 Maximum allowed test failures for each channel

Test	Channel Reference voltage	Pitch	Roll	Heave	Waverider	SBWR Norm O/P	SBWR Port Heave Channel	SBWR Stbd Heave Channel	SBWR Port Pressure Channel	SBWR Stbd Pressure Channel
a)	10	10	10	10	10	10	10	10	10	10
b)	512	0	0	0	0	0	0	0	0	0
c)	0	0	0	0	0	0	0	0	0	0
d)	512	0	0	0	0	0	0	0	0	0
e)	512	5	5	5	0	0	5	5	0	0
f)	512	10	10	10	10	10	10	10	10	10
g)	512	0	0	0	0	0	0	0	0	0
h)	512	3	3	3	3	3	3	3	3	3
i)	512	3	3	3	3	3	3	3	3	3

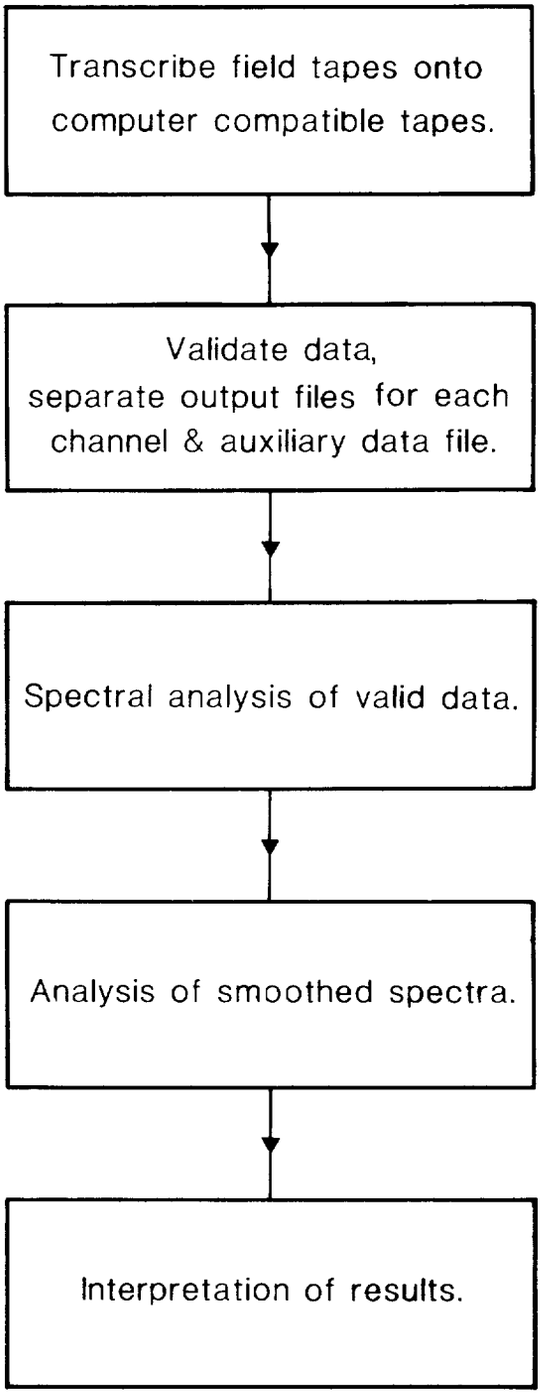

Fig A3.1 Flow diagram for data processing

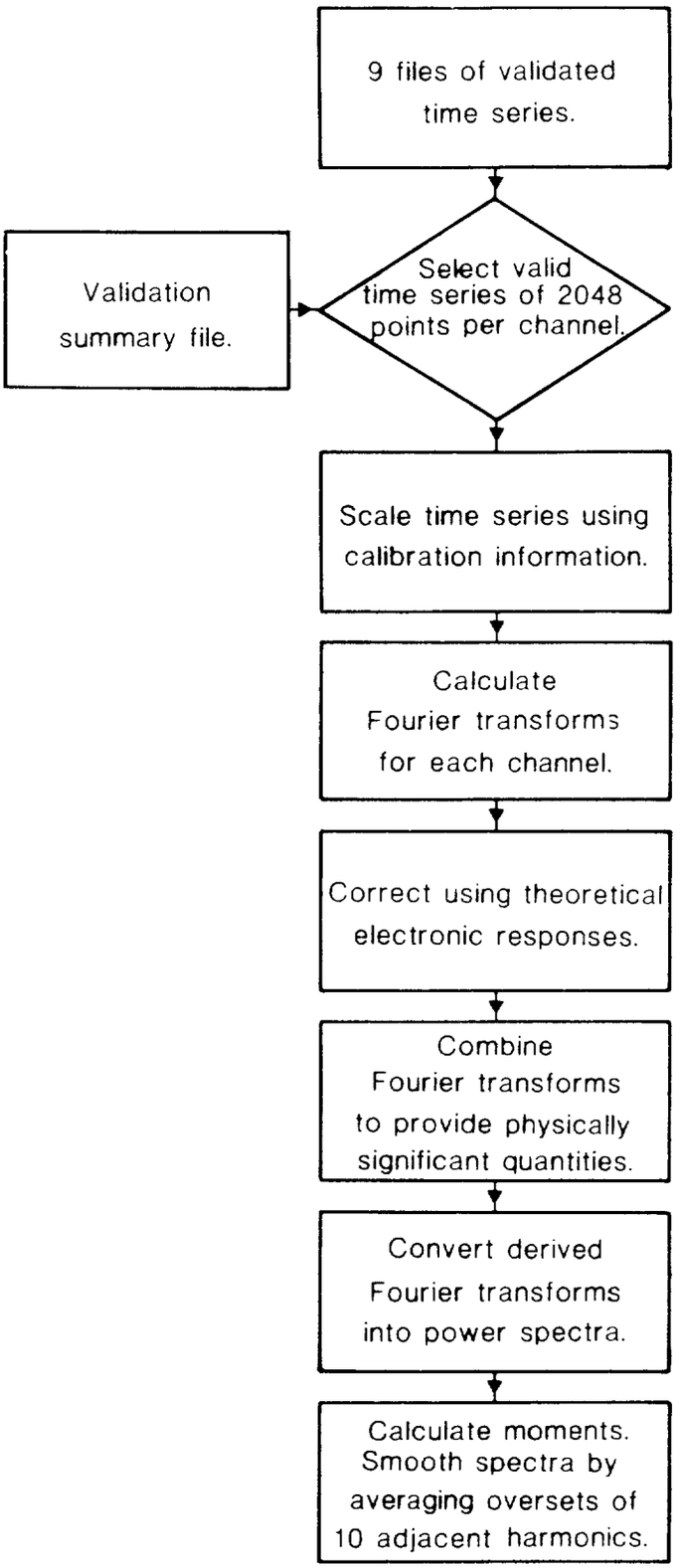

Fig A3.2 Flow diagram for the spectral analysis of each quantity of interest

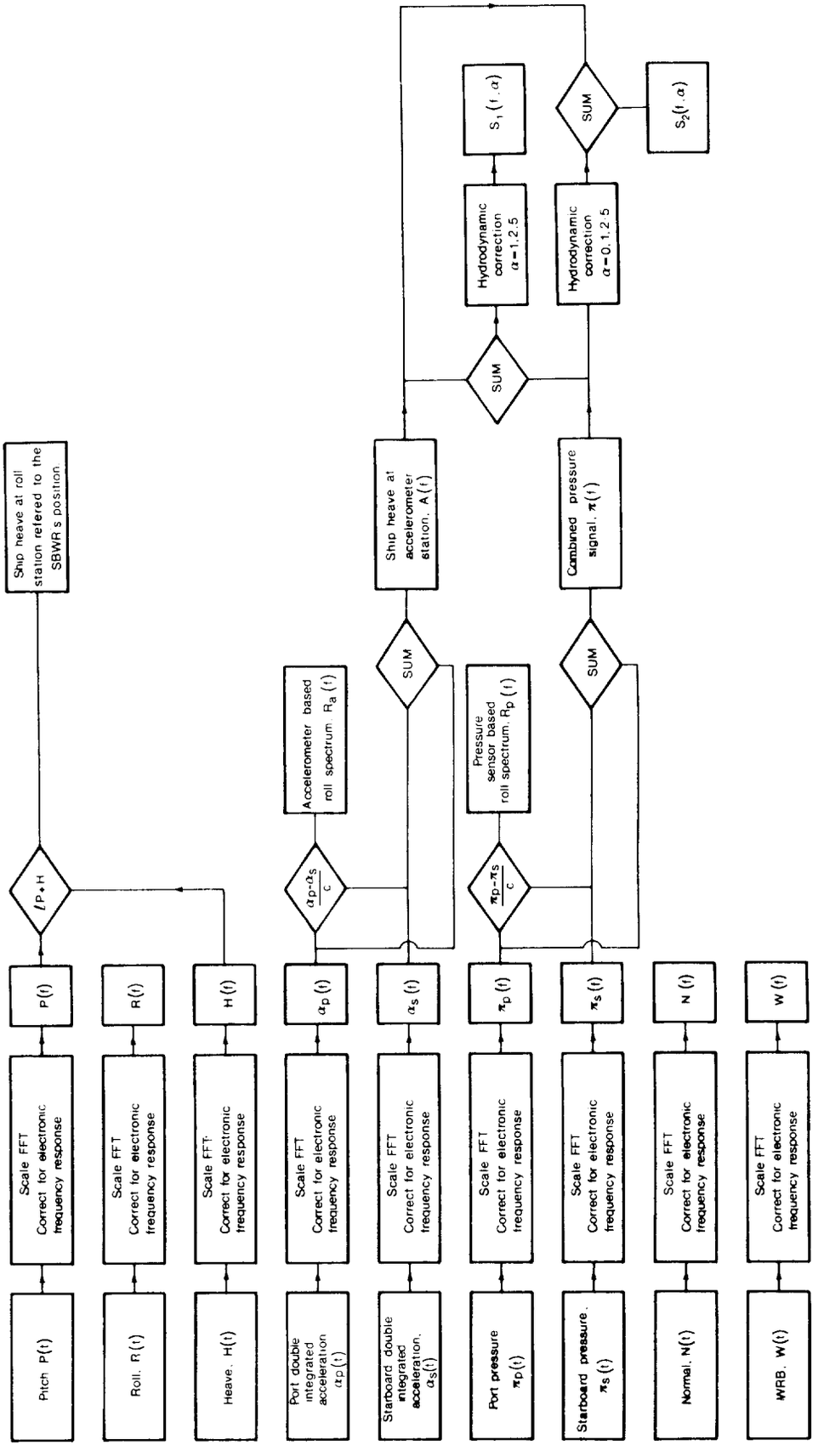

Fig A3.3 Flow diagram showing the various ways in which Fourier Transforms were combined prior to forming spectra

APPENDIX 4 LINEAR THEORY OF THE NEAR SURFACE PRESSURE DISTURBANCE UNDER A WAVE FIELD

In order to construct a simplified theory for the SBWR, it is necessary to evaluate the pressure field caused by a specified system of surface waves. This calculation is not as straightforward as it might seem because the pressure variations close to the surface must be calculated. The usual linear formulations for the waves' hydrodynamics approximate the free surface by infinitely small departures from the still water level. In this case it is immaterial whether measurements are referred to the still water level or the free surface. In the case of a simple sinusodal wave this procedure is justified, and for most applications such a theory is adequate. However, as the ship must ride over the longer wavelength components in the sea-way, the depth relative to the mean water level at which the SBWR pressure sensors operate varies and can be small or even negative. Superimposed upon the long wave components any shorter components must generate distrubances which are detected by the pressure sensors. It is clear that a proper calculation must distinguish between the position of the free surface and the still water level. In the analysis which is presented below such a theory is developed and an expression for the subsurface pressure in terms of the surface displacement is obtained.

In order to simplify the analysis the pressure in the fluid is calculated in the absence of the ship. Also the problem is treated as two-dimensional for clarity, although generalisation to three dimensions is not difficult. The method, which is outlined below, uses a perturbation expansion which is treated by STOKER (1957). It is assumed that the velocity potential in the fluid, Φ, and the surface displacement, η, may be expanded in terms of a small parameter ε in the following way:

$$\Phi = \varepsilon\Phi^{(1)} + \varepsilon^2\Phi^{(2)} \quad \varepsilon^3\Phi^{(3)} + \ldots \qquad \text{A4.1}$$

$$\eta + \eta^{(0)} + \varepsilon\eta^{(1)} + \varepsilon^2\eta^{(2)} + \ldots \qquad \text{A4.2}$$

Here $\Phi^{(1)}$, $\Phi^{(2)}$ etc are functions of x, y, z and t which are to be determined and $\eta^{(0)}$, $\eta^{(1)}$ etc are functions of x, z and t. (The y axis is defined to be in the vertical direction with y increasing upwards.)

Because (1) is linear in $\Phi^{(1)}$, $\Phi^{(2)}$ etc, the continuity equation, $\nabla^2 \Phi = 0$ gives the condition

$$\nabla^2 \Phi^{(n)} = 0 \qquad \text{A4.3}$$

Equation A4.3 must be solved with the boundary conditions for the free surface and the sea bed. These conditions are first, that the pressure at the free surface is constant; second, that a fluid particle in the free surface always remains in the surface through the fluid motion; and third, that the vertical component of velocity shall be zero at the sea bed. The first of these conditions may be written as

$$gy + \Phi_t + \frac{1}{2}\left[(\Phi_x)^2 + (\Phi_y)^2 + (\Phi_z)^2\right] = \text{constant}^* \qquad \text{A4.4}$$

where the left-hand side is evaluated on the free surface $y = \eta$.
The second condition gives

$$\eta_t + \Phi_x \eta_x + \Phi_z \eta_z = \Phi_y \qquad \text{A4.5}$$

again at the free surface.

Equation (A4.4) may be written as an expansion in ε by substituting Φ and η from (A4.1) and (A4.2) so that to second order in ε (A4.4) gives

$$g[\eta^{(0)} + \varepsilon\eta^{(1)} + \varepsilon^2\eta^{(2)}..] + [\varepsilon\Phi^{(1)} + \varepsilon^2\Phi^{(2)}..] + \frac{1}{2}[\varepsilon^2(\Phi_x^{(1)}\Phi_x^{(1)} + \Phi_y^{(1)}\Phi_y^{(1)} + \Phi_z^{(1)}\Phi_z^{(1)})]$$

$$= \text{constant} \qquad \text{A4.6}$$

---

* Through this appendix subscripts denote partial differentiation thus

$$\Phi_t = \frac{\partial \phi}{\partial t} \qquad \Phi_x = \frac{\partial \Phi}{\partial x}$$

etc.

By equating the coefficients of ε in A4.6:

$$g\eta^{(0)} = \text{constant} \qquad \text{(coefficient of } \varepsilon^0\text{)} \qquad \text{A4.7}$$

$$g\eta^{(1)} + \Phi_t^{(1)} = 0 \qquad \text{(coefficient of } \varepsilon^1\text{)} \qquad \text{A4.8}$$

$$g\eta^{(2)} + \Phi_t^{(2)} + \frac{1}{2}\left[(\Phi_x^{(1)})^2+(\Phi_y^{(1)})^2+(\Phi_z^{(1)})^2\right]=0 \qquad \text{(coefficient of } \varepsilon^2\text{)} \qquad \text{A4.9}$$

Similarly equation A4.5 becomes, upon noting that A4.7 gives $\eta_x^{(0)}=\eta_z^{(0)}=\eta_t^{(0)}=0$

$$\varepsilon^1\eta_t^{(1)} +\varepsilon^2\eta_t^{(2)} + \varepsilon^2\left[\Phi_x^{(1)}\eta_x^{(1)} + \Phi_z^{(1)}\eta_z^{(1)}\right] = \varepsilon\Phi_y^{(1)} + \varepsilon^2\Phi_y^{(2)} \qquad \text{A4.10}$$

so that

$$\eta_t^{(1)} = \Phi_y^{(1)} \qquad \text{(coefficient of } \varepsilon^1\text{)} \qquad \text{A4.11}$$

$$\eta_t^{(2)} + \Phi_x^{(1)}\eta_x^{(1)} + \Phi_z^{(1)}\eta_z^{(1)} = \Phi_y^{(2)} \qquad \text{(coefficient of } \varepsilon^2\text{)} \qquad \text{A4.12}$$

The lowest order non-trivial solution is therefore obtained by using the boundary condition equations whose coefficients in the expansions A4.6 and A4.10 are of order $\varepsilon^{(0)}$ and ε. These are:

$$g\eta^{(1)} = \text{constant} \qquad \text{A4.13} \quad \text{at the free surface}$$

$$g\eta^{(1)} + \Phi_t^{(1)} = 0 \qquad \text{A4.14} \quad \text{at the free surface}$$

$$\eta_t^{(1)} - \Phi_y^{(1)} = 0 \qquad \text{A4.15} \quad \text{at the free surface}$$

In addition the governing equation $\nabla^2\Phi^{(1)} = 0$ A4.16 and the bottom boundary condition $\Phi_y^{(1)} = 0$ A4.17 (at bottom boundary) must also be satisfied.

It is worth noting that these equations are identical to equivalent expressions derived by Stoker (1957), with the exception that A4.13-A4.15 are to be satisfied at the free surface rather than at the still water level. For clarity two dimensional solutions to the problem are considered, with all of the component waves travelling in the +ve x direction in deep water so that the solution to A4.16 is of the form

$$\Phi^{(1)} = \sum_n [a_n \sin(\omega_n t - k_n x) + b_n \cos(\omega_n t - k_n x)] e^{k_n y} \qquad \text{A4.18}$$

so that from A4.14

$$\eta^{(1)} = \sum_n -\frac{\omega_n}{g} [a_n \cos(\omega_n t - k_n x) - b_n \sin(\omega_n t - k_n x)] e^{k_n \eta} \qquad \text{A4.19}$$

The pressure in the fluid is given by Bernoulli's equation

$$\frac{p}{\rho} + gy + \Phi_t + \frac{1}{2}[(\Phi_x)^2 + (\Phi_y)^2 + (\Phi_z)^2] = \text{constant} \qquad \text{A4.20}$$

which to first order in ε gives upon substituting from A4.18 for Φ

$$\frac{p}{\rho} + gy + g\sum_n \frac{\omega_n}{g} [a_n \cos(\omega_n t - k_n x) - b_n \sin(\omega_n t - k_n x)] e^{k_n y} = \text{constant} \qquad \text{A4.21}$$

By selecting $p = 0$ on $y = \eta$ the right-hand side of A4.21 can be eliminated and writing:

$$\eta_n = \frac{-\omega_n}{g} [a_n \cos(\omega_n t - k_n x) - b_n \sin(\omega_n t - k_n x)] e^{k_n \eta} \qquad \text{A4.22}$$

so that

$$\eta = \sum_n \eta_n$$

Equation A4.21 becomes

$$p + \rho g y - \rho g \sum_n \eta_{(n)} e^{k_n y} e^{-k_n \eta} = 0 \qquad \text{A4.23}$$

and

$$p = -\rho g [y - \sum_n \eta_{(n)} e^{k_n (y-\eta)}] \qquad \text{A4.24}$$

Equation A4.24 is a generalisation of the usual result in linear theory which may be obtained by imposing the additional condition $|y| >> \eta$ so that A4.25 becomes

$$p = -\rho g y + \rho g \sum_n \eta_n e^{k_n y} \qquad \text{A4.25}$$

Nomenclature - Appendix 4

$\overline{\phi}$	velocity potential
ε	small parameter
η	surface elevation
y	vertical co-ordinate
t	time
x	horizontal co-ordinate
z	horizontal co-ordinate
ω	wave angular frequency
k	wave number (2π/wavelength)
p	pressure
ρ	density of sea water
g	acceleration due to gravity
a_n) b_n)	Fourier coefficients

APPENDIX 5 CORRECTION OF VAN AKEN AND BOUWS' DATA

The SBWR used by van Aken and Bouws (1971) was calibrated in an unconventional way. The pressure sensors were arranged to give nominal sensitivity per meter static head of water and the accelerometers were adjusted so that a displacement of 1 m, when corrected for the instrument's electronic frequency response, would give an output of 0.795 of the nominal sensitivity. This procedure was intended to give equivalent dynamic sensitivities to the two channels, assuming a modified hydrodynamic response for the pressure sensors of the form

$$P(f) = P(0)e^{-2.4(2\pi f)^2 d/g}$$

Normally the instrument is adjusted so that, when the response of the electronics has been allowed for, the two channels have the same sensitivity for frequencies approaching zero. Thus if A(f) and P(f) are the Fourier transforms of the accelerometer and pressure sensor signals, corrected for the electronics' response, the output of the instrument is given by

$$S(f) = A(f) + P(f) \qquad \text{A5.1}$$

so that the spectrum of the output is given by

$$|S(f)|^2 = SS^* = (A + P)(A + P)^* = AA^* + PP^* + AP^* + A^*P \qquad \text{A5.2}$$

The output of the unconventionally calibrated instrument may be expressed as

$$B(f) = \alpha A(f) + \beta P(f) \qquad \text{A5.3}$$

where $\alpha = 1.02$ $\beta = 1.28$

Thus the spectrum of the combined output becomes

$$|B|^2 = (\alpha A + \beta P)(\alpha A + \beta P)^* = \alpha^2 AA^* + \beta^2 PP^* + \alpha\beta(PA^* + AP^*) \qquad \text{A5.4}$$

So that

$$AP^* + A^*P = \frac{1}{\alpha\beta}\left(|B|^2 - \alpha^2|A|^2 - \beta^2|B|^2\right) \qquad \text{A5.5}$$

substituting A5.5 into A5.2 gives

$$|S|^2 = |A|^2(1 - \frac{\alpha}{\beta}) + |P|^2(1 - \frac{\beta}{\alpha}) + |B|^2(\frac{1}{\alpha\beta}) \qquad \text{A5.6}$$

If the corresponding spectrum obtained from an accelerometer buoy is divided into equation A5.6 we obtain with a little manipulation the following expressions for the relative response of the SBWR, compared with that of a Waverider buoy:

$$\frac{|s|^2}{|w|^2} = \frac{1}{\alpha\beta}\left[\alpha^2 \frac{|A|^2}{|w|^2}\frac{\beta}{\alpha} - 1 + \beta^2\frac{|P|^2}{|w|^2}\frac{\alpha}{\beta} - 1 + \frac{|B|^2}{|w|^2}\right] \qquad \text{A5.7}$$

Now $\frac{|s|^2}{|w|^2}$ is the relative energy response of the conventionally calibrated instrument and $\frac{|B|^2}{|w|^2}$ is the relative energy response of the unconventionally calibrated SBWR which corresponds to the square of the amplitude response, Rt given by van Aken et al. Similarly $\beta^2 \frac{|P|^2}{|w|^2}$ and $\alpha^2 \frac{|A|^2}{|w|^2}$ are the relative energy responses of the individual pressure and accelerometer channels as measured using the unconventionally calibrated instrument. The corresponding amplitude responses, Rp and Ra, are also given by van Aken et al, so that all of the quantities on the right hand side of A5.7 are known, and the equation may be solved at each frequency to give the response which would have been obtained had the instrument been calibrated in the conventional way.

Substituting numerical values for α and β the corrected response is given by

$$\frac{|S|^2}{|w|^2} = 0.766\ [R_t^2 + 0.255R_a^2 - 0.203R_p^2]$$

Nomenclature - Appendix 5

d	depth
f	frequency
g	acceleration due to gravity
S(f)	SBWR output signal
A(f)	SBWR double integrated accelerometer signal
P(f)	SBWR pressure signal

APPENDIX 6 THE INFLUENCE OF A TIME VARYING PRESSURE SENSOR DEPTH UPON THE SBWR OUTPUT SPECTRUM

The secondary maximum which is evident in some empirically determined SBWR response transfer functions suggest that some intermodulation may occur between the Fourier components in the SBWR signal. This would give rise to side bands which, for a continuous wave spectrum, might enhance the SBWR signal at high frequencies. This idea was proposed by van Aken and Bouws (1974) who give a simplified analysis of such effects.

The analysis which they conducted was based upon a formulation for the variation of subsurface pressure with depth which the author believes to be incorrect. In their formulation van Aken et al assume that the subsurface pressure decays as e^{ky} whereas the analysis presented in Appendix 4 gives a decay with depth which varies as $e^{k(y-\eta)}$ so that the pressure at depth y, measured with y increasing in the vertical direction is given by

$$p(t) = -\rho g y + \rho g \sum_n (a_n \cos\omega_n t + b_n \sin\omega_n t) e^{kn(y-\eta)} \qquad A6.1$$

where η is given by

$$\eta = \sum_m a_n \cos\omega_m t + b_m \sin\omega_m t \qquad A6.2$$

The hydrostatic term, $-\rho g y$, is cancelled out by the double integrated accelerometer signal so that, introducing the ship's heave response operator, R_m defined by

$$y = -d \sum_m R_m (a_m \sin\omega_m t + b_m \sin\omega_m t) \qquad A6.3$$

the SBWR output V(t) may be obtained as

$$V(t) = \sum_n (a_n \cos(\omega_n t) + b_n \sin(\omega_n t)) e^{-k_n d \sum_m k_n (1-R_m)(a_m \cos\omega_m t + b_m \sin\omega_m t)} \qquad A6.4$$

Equation A6.4 is similar to that given by van Aken et al, but in our formulation the second exponential term contains a factor $(1 - R_m)$ while their equivalent expression contains instead a factor of R_m only. The author believes that this difference may be interpreted physically in a simple way. When the ship follows the surface waves perfectly, $R_m = 1$. In the present formulation, the dynamic pressures decay exponentially with the distance of the sensor below the free

surface, which is constant. Thus under these conditions the output of the instrument is not distorted as a result of the ship's vertical motion. In van Aken's analysis the subsurface pressures are assumed to decay according to the distance of the sensor below the mean water level and consequently a perfectly heaving ship causes the maximum distortion in their model. There are no physical constraints in either model which prevent the instantaneous position of the pressure sensor being above the mean water level. In van Aken's formulation this corresponds to an attenuation in excess of unity, so that his model predicts that the dynamic pressures are magnified under these conditions. The author thinks that the attenuation of pressure with depth which occurs under all conditions in his own formulation is more reasonable.

In order to proceed further the spectrum of the signal given by Equation A6.4 must be calculated. This may be done approximately by expanding the second exponential to first order in k_n:

$$V(t) = \sum_n \sum_m (a_n \cos\omega_n t + b_n \sin\omega_n t)(k_n(1-R_m)(a_m \cos\omega_m t + b_m \sin\omega_m t)e^{-k_n d} + \sum_n (a_n \cos\omega_n t + b_n \sin\omega_n t)e^{-k_n d} \qquad \text{A6.5}$$

The double sum represents distortions of the wave record while the second, single sum, represents a wave record subjected to ideal attenuation with depth. The double sum may be expanded into products of trigonometric functions which may then be expressed in terms of $\underset{\sin}{\cos}(\omega_m \pm \omega_n)$. After some manipulation, the error terms may be written as

$$E(t) = \frac{1}{2} \sum_m \sum_n ([\alpha_n\alpha'_m + \beta_n\beta'_m] \cos(\omega_n - \omega_m)t + [\beta_n\alpha'_m - \alpha_n\beta'_m]\sin(\omega_n - \omega_m)t + [\alpha_n\alpha'_m - \beta_n\beta'_m] \cos(\omega_n + \omega_m)t + [\beta_n\alpha'_m - \alpha_n\beta'_m]\sin(\omega_n + \omega_m)t) \qquad \text{A6.6}$$

where

$$\alpha_n = a_n k_m \quad \alpha'_n = a_n(1-R_n) \quad \beta_n = b_n k_n \quad \beta'_n = b_n(1-R_n)$$

Note that the angular frequencies, ω_n, are harmonically related so that

Using the identities

$$\sum_{m=1}^{N}\sum_{N=1}^{N} A_{mn} \begin{matrix}\cos\\ \sin\end{matrix} (\omega_m - \omega_n)t = \sum_{r=1}^{N-1}\sum_{q=1}^{N-r} A_{r+q,q} \begin{matrix}\cos\\ \sin\end{matrix} (\omega_r t)$$

$$+ \sum_{r=1}^{N-1}\sum_{q=1}^{N-r} A_{q,r+q} \begin{matrix}\cos\\ \sin\end{matrix} (-\omega_r t)$$

$$+ \sum_{r=1}^{N} A_{rr} \begin{matrix}\cos\\ \sin\end{matrix} (0) \qquad \text{A6.7}$$

and

$$\sum_{m=1}^{N}\sum_{n=1}^{N} A_{mn} \begin{matrix}\cos\\ \sin\end{matrix} (\omega_m + \omega_n)t = \sum_{r=2}^{N+1}\sum_{q=1}^{r-1} A_{r-q,q} \begin{matrix}\cos\\ \sin\end{matrix} (\omega_r t)$$

$$+ \sum_{r=N+2}^{2N}\sum_{q=r-N}^{N} A_{r-q,q} \begin{matrix}\cos\\ \sin\end{matrix} (\omega_r t) \qquad \text{A6.8}$$

E(t) may be rewritten, after some manipulation,

$$2\,E(t) = \sum_{r=1}^{N} W_{rr} + \sum_{r=1}^{N-1}\sum_{q=1}^{N-r} (W_{q,r+q} + W_{r+q,q}) \cos\omega_r t$$

$$+ \sum_{r=1}^{N-1}\sum_{q=1}^{N-r} (X_{r+q,q} - X_{q,r+q}) \sin\omega_r t$$

$$+ \sum_{r=2}^{N+1}\sum_{q=1}^{r-1} Y_{r-q,q} \cos\omega_r t + Z_{r-q,q} \sin\omega_r t \qquad \text{A6.9}$$

$$+ \sum_{r=N+2}^{2N}\sum_{q=r-N}^{N} Y_{r-q,q} \cos\omega_r t + Z_{r-q,q} \sin\omega_r t$$

where

$$W_{mn} = \alpha_n\alpha'_m + \beta_n\beta'_m = a_n k_n (1-R_m) + b_n k_n b_m (1-R_m)$$

$$X_{mn} = \beta_n\alpha'_m - \alpha_n\beta'_m = b_n k_n a_m (1-R_m) - a_n k_n b_m (1-R_m)$$

$$Y_{mn} = \alpha_n\alpha'_m - \beta_n\beta'_m = a_n k_n a_m (1-R_m) - b_n k_n b_m (1-R_m)$$

$$Z_{mn} = \beta_n\alpha'_m - \alpha_n\beta'_m = b_n k_n a_m (1-R_m) + a_n k_n b_m (1-R_m)$$

For $1 < r < N - 1$ the first and last terms in A6.9 do not contribute so that for a particular frequency ω_r, the coefficients of $\cos(\omega_r t)$, A'_r and of $\sin(\omega_r t)$, B'_r may be written as:

$$A'_r = \sum_{q=1}^{n-r} (W_{r,r+q} + W_{r+q,r}) + \sum_{q=1}^{r-1} Y_{r-q,q} \qquad \text{A6.10}$$

$$B'_r = \sum_{q=1}^{n-r} (X_{r+q,q} - X_{q,r+q}) + \sum_{q=1}^{r-1} Z_{r-q,q} \qquad \text{A6.11}$$

The spectral density corresponding to the unwanted distortions in the wave record may thus be calculated at each frequency ω_r by evaluating the sums in A6.10 and A6.11 and summing their squares:

$$E^2(\omega_r) = A'^2_r + B'^2_r \qquad \text{A6.12}$$

In order to calculate the magnitude of $E^2(\omega_r)$ the author has treated three cases, the first corresponding to a realistic ship response function and a sea state with $H_s \simeq 1m$, the second to the same response functions and a sea state with $H_s \simeq 10m$, and the third corresponding to a fixed ship and $H_s \simeq 10m$. For each calculation the amplitudes of the sine and cosine coefficients, a_n and b_n were calculated assuming a Pierson-Moskowitz spectrum, using the equations

$$a_n = (S(\omega_n)\sigma f)^{\frac{1}{2}} \cos\Phi_n \qquad \text{A6.13}$$

$$a_n = (S(\omega_n)\sigma f)^{\frac{1}{2}} \sin\Phi_n \qquad \text{A6.14}$$

where $S(\omega_n)$ is the spectral density of Pierson-Moskowitz spectrum at angular frequency ω_n and the phase angles Φ_n were chosen at random in the range $0-2\pi$. In each case the underlying Pierson-Moskowitz spectrum had a peak frequency of 0.1 Hz, and was used to calculate 10 pairs of coefficients for frequencies in the range 0-0.3 Hz, allowing $E^2(\omega_q)$ to be calculated for $2 \leqslant q \leqslant 9$. Figure 6.1 shows the idealised chip response used in the first two cases; in the last case R_q was set to zero at all frequencies, so that the results of this calculation should correspond roughly to the calculations of van Aken and Bouws.

Figures A6.2 and A6.3 show the results of the calculations incorporating an idealised ship response function. In both cases the error spectrum is small in comparison with the assumed wave spectrum so that intermodulation effects may be neglected. In the third case (Figure A6.4) where a fixed pressure sensor was considered, the error spectrum is comparable with the wave spectrum above 0.2 Hz. This is in qualitative agreement with the calculations described by van Aken and Bouws.

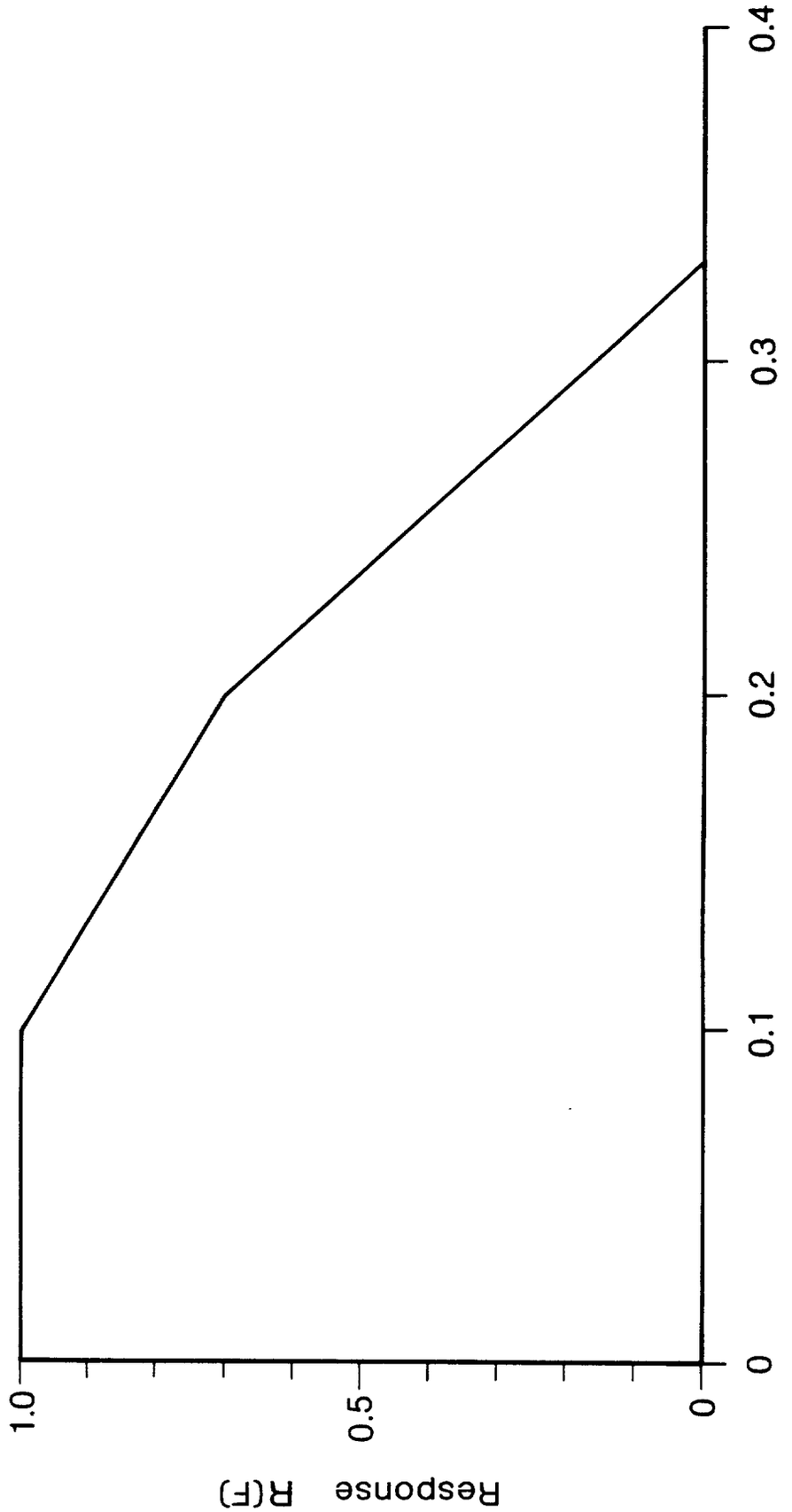

Fig A6.1 Idealised ship response used in calculations

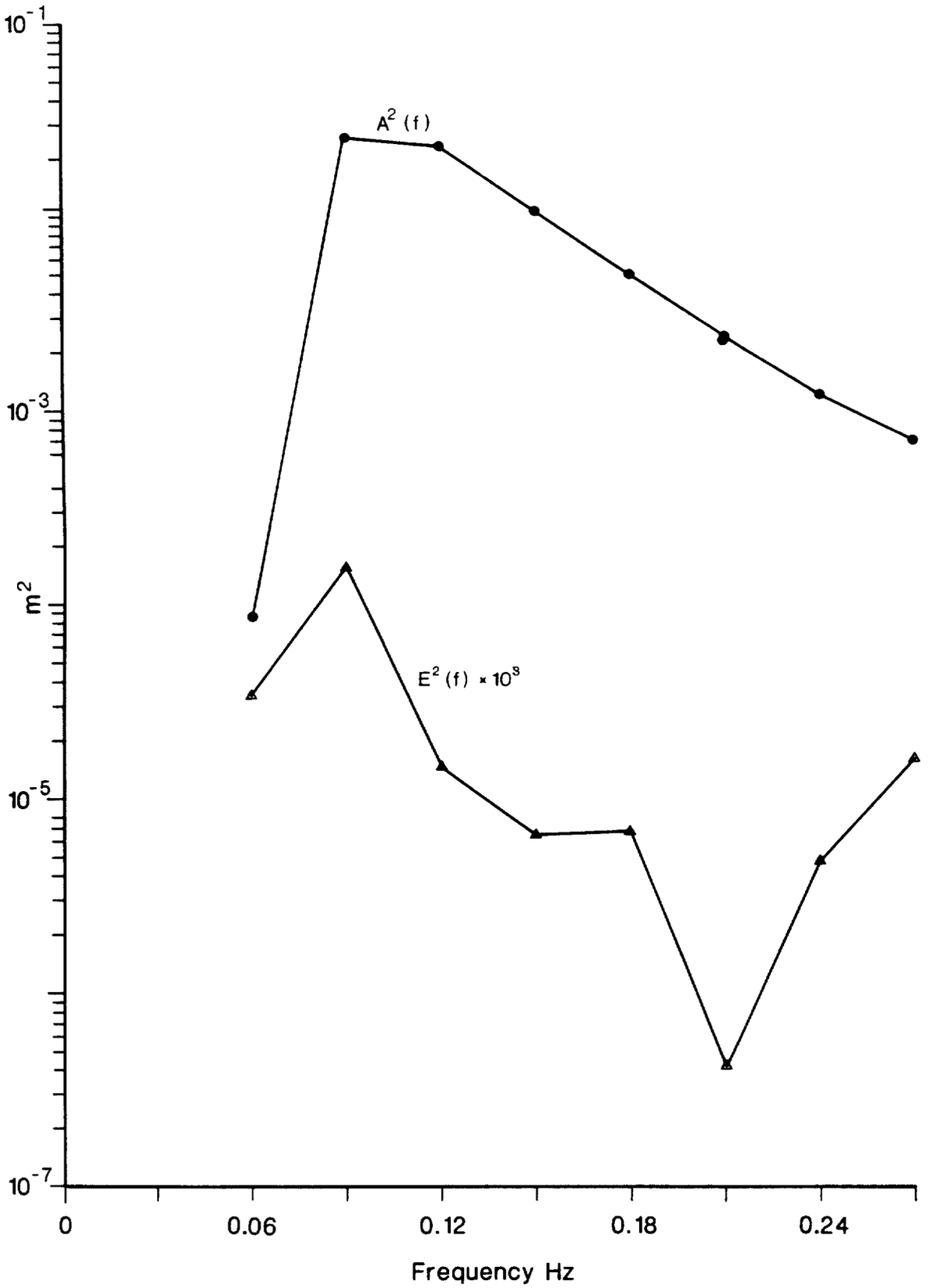

Fig A6.2 Component wave amplitudes (squared) and corresponding distortion amplitudes (squared) vs frequency

The calculations assumed an idealised ship response and Hs $\sim$ 1 m

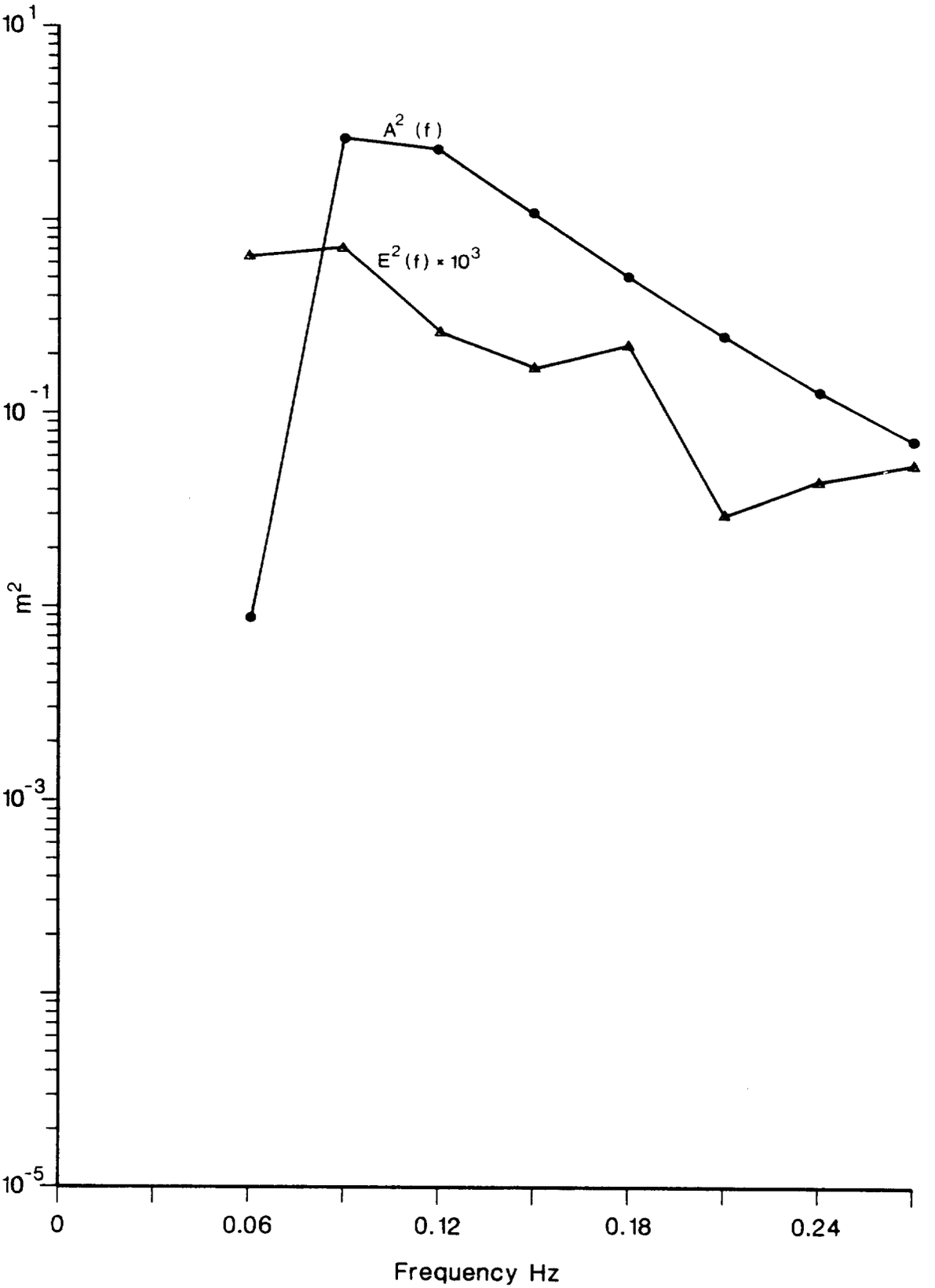

Fig A6.3 Component wave amplitudes (squared) and corresponding distortion amplitudes (square) vs frequency

The calculations assumed an idealised ship response and Hs ∿ 10 m

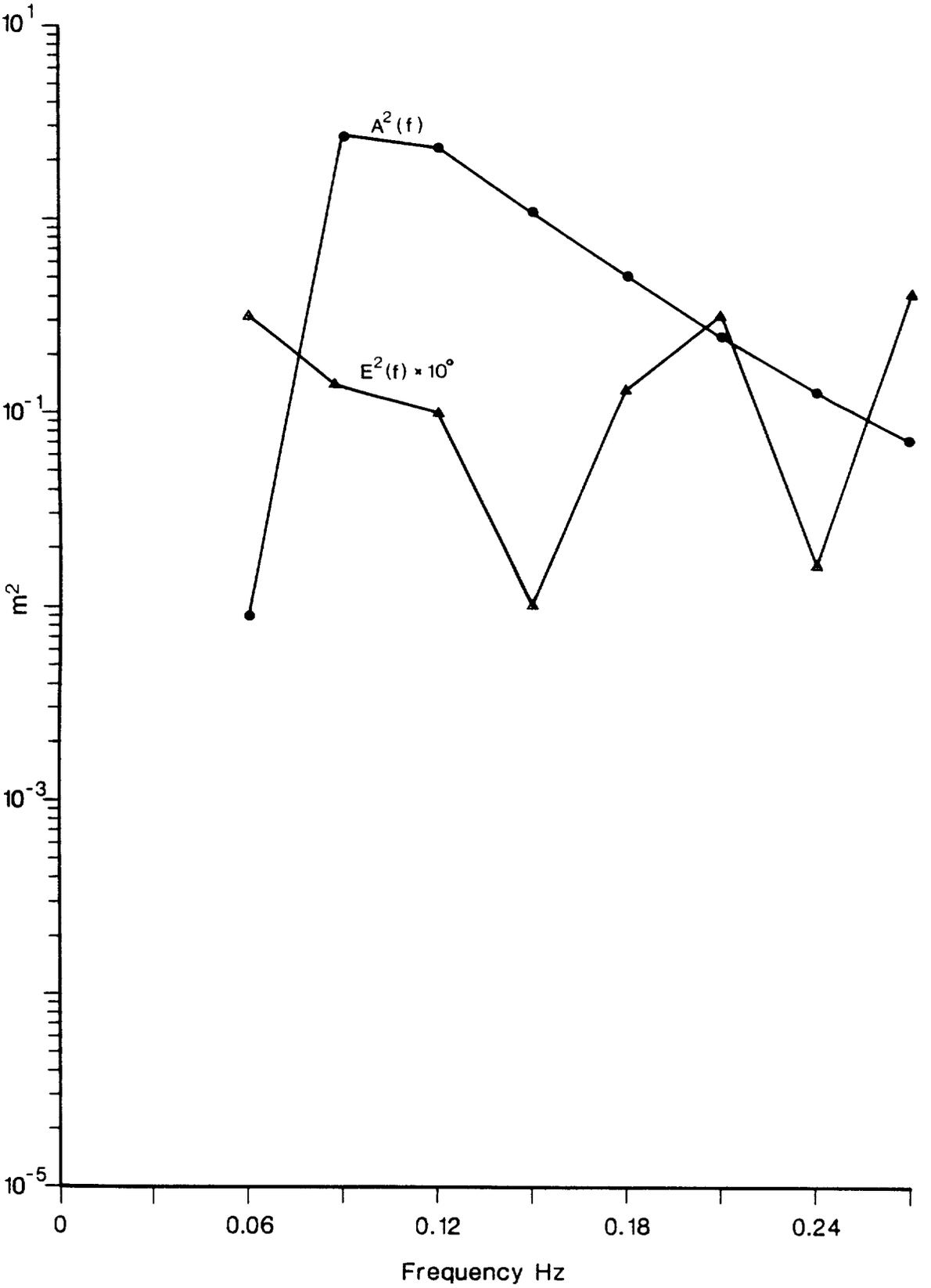

Fig A6.4 Component wave amplitudes (squared) and corresponding distortion amplitudes (squared) vs frequency.

The calculations assumed a fixed ship and Hs $\sim$ 10 m.
The error spectrum is of comparable size to the wave spectrum.

Nomenclature - Appendix 6

p	pressure
t	time
ρ	density of sea water
g	acceleration due to gravity
y	vertical co-ordinate
a_n, b_n	Fourier coefficients
ω	angular frequency
η	sea surface elevation
k_n	wave number at angular frequency ω_n (Wave number = 2π/wavelength)
R_m	ship heave response at angular frequency ω_m
$V(t)$	SBWR output
α_n, α'_n, β_n, β'_n, A_{mn}, W_{mn}, Y_{mn}, X_{mn}, Z_{mn}	coefficients
$E^2(\omega_r)$	spectral density of intermodulation products
ϕ	phase angle